COMPUTATIONAL SIMULATION OF SCRAMJET COMBUSTORS – A COMPARISON BETWEEN QUASI-ONE DIMENSIONAL AND 2-D NUMERICAL SIMULATIONS

BY

Chandraprakash Tourani

Submitted to the graduate degree program in Aerospace Engineering and the Graduate Faculty of the University Of Kansas School Of Engineering in partial fulfillment of the requirements for the degree of Master of Science.

Committee:

_____

Dr. Saeed Farokhi, Chairperson

_____

Dr. Ray Taghavi, Committee Member

_____

Dr. Shahriar Keshmiri, Committee Member

Date Defended: _____

The Thesis Committee for Chandraprakash Tourani certifies that this is the approved version of the following thesis:

COMPUTATIONAL SIMULATION OF SCRAMJET COMBUSTORS – A COMPARISON BETWEEN QUASI-ONE DIMENSIONAL AND 2-D NUMERICAL SIMULATIONS

Committee:

_____

Dr. Saeed Farokhi, Chairperson

_____

Dr. Ray Taghavi, Committee Member

_____

Dr. Shahriar Keshmiri, Committee Member

Date approved: _____

Abstract

1-D simulations based on the quasi-one-dimensional equations of fluid motion plus an ignition delay model and 2-D numerical simulations based on Reynolds-Averaged Navier-Stokes (RANS) equations have been performed for two different scramjet combustors. The combustor configurations at DLR and NASA's SCHOLAR Supersonic Combustor have been used as test cases for the 1-D and 2-D simulations. Comparisons between the published 3-D computational and experimental results and quasi-one-dimensional and 2-D simulations have been performed. The quasi-one dimensional modeling of NASA's SCHOLAR supersonic combustor captures the trends in Mach number, static pressure and static temperature for both cold flow and combustion case. The comparison with experimental result for combustion case reveals a close agreement with the pressure peak and the presence of an ignition delay. Thus, 1-D simulation very closely predicts the flow evolution within the combustor. On the other hand, for DLR supersonic combustor, due to the lack of oblique wave (i.e. shock waves and expansion waves) and shear dominated viscous flow simulation, 1-D model severely fails to predict the trend followed by the experimental result along the centerline of the combustor. However, the 1-D model is able to match the overall flow velocity achieved within the combustor downstream of the wedge at approximately six wedge chord lengths.

Acknowledgements

I would like to thank Dr. Saeed Farokhi, my graduate advisor, for his continued guidance and support during my research. It was his encouragement, which helped me churn out a research paper that has been accepted for an international level conference. I would like to thank my research committee members Dr. Ray Taghavi and Dr. Shahriar Keshmiri for their valuable inputs during my research. I show my sincere gratitude to Dr. S. Farokhi and Dr. R. Taghavi for providing me with financial support, as without their help it would have been financially very hard for my family alone to sustain my higher education. I am thankful to Dept. of Aerospace Engineering at University of Kansas for providing facilities for performing computational research. I would also like to thank Dr. Mark Ewing, Mrs. Amy Borton, and Mr. Tom Kurtz, for their support concerning any administrative task.

My family has and still plays a most important part in my life. I am so very thankful to my mother, Mrs. Anju Tourani, uncle, Dr. Harish Tourani, aunt, Mrs. Sunita Kishnani, and sister, Miss. Chandrakanta Tourani, for their moral support and inspiration, as coming down to US for higher education would have been impossible if it were not for them.

The journey from beginning to end during Master's education would have been very hard without friends and colleagues. There are so many people who in some way or the other have contributed towards my research. I very much thank my roommate and colleague, Mr. Anirudh Pochiraju for being there by my side, be it for research, inspiration or financial support and also for accompanying me during all the fun time. I thank Mr. Amool Raina, my roommate and colleague, for his support and concern during my higher education at KU. I thank my colleague, Mr. Sudarshan Loya, for being so patient while I kept bugging him with various queries concerning my research work. I would like to thank my very good friend and brother,

Mr. Saurabh Jain, for his support during tough emotional and nostalgic moments, and also for proof-reading this thesis document. I also thank my friend, Mr. Abhijit Mehta, for all the late night car rides back and forth to Eaton hall during my research work.

Last but not the least, I specially thank most prominent and supreme, my guru, Swami Abhedananda and Lord for showering their endless blessings by giving me strength, courage and support to sustain all hard times, and for gifting me with a beautiful and wonderful girl with whom I will be spending the rest of my life.

Table of Contents

List of Figures

List of Symbols

Symbol	Description	Units
a	Local speed of sound	m/sec
A_w	Duct wetted area	m^2
A	Duct cross sectional area	m^2
c_p	Specific heat at const. pressure	J/kg.K
D_h	Hydraulic diameter	m
f	Friction coefficient	-
F	Fluid impulse	N
h	Enthalpy per unit mass	J/kg
h_{pr}	Combustion enthalpy to form products from reactants	kJ/kg
H	Rate of energy transfer per unit mass flow rate	J/kg
$\dot{m}$	Mass flow rate	kg/sec
M	Mach number	-
p	Pressure	Pa
Q	External heat transfer per unit mass flow rate	J/kg
$\overline{R}$	Universal gas constant	J/kmol·K
s	Entropy per unit mass	J/kg·K
T	Static temperature	K
V	Gas speed	m/sec
W	Molecular weight	kg/kmol
W_x	Rate of external work per unit mass flow rate	J/kg
X	Drag force	N
ρ	Fluid density	kg/m^3
γ	Ratio of specific heats	-

Subscripts

0	Stagnation condition
g	Signifies injected gas
L	Signifies evaporated liquid

1 Introduction

During the conceptual design phase of a hypersonic vehicle, numerous performance estimates of the propulsion system configuration are required which make CFD simulations for each configuration time consuming to implement. Thus, there arises a need for computationally efficient methods to perform a quick estimation of scramjet propulsion system performance that accounts for the effect of propulsion system configuration. It is argued that the "*Quasi-one dimensional hypersonic propulsion models are one way of achieving this goal"* [2]**.** Therefore, in the present work, a model has been produced based on the system of quasi-one dimensional continuous gas dynamic equations as given by Shapiro [3] to perform 1-D simulation of a scramjet combustor with an ignition delay model.

For simulation purposes, two different scramjet combustors have been considered-namely scramjet combustion chamber at DLR and NASA's SCHOLAR Supersonic Combustor, which are different in their design, method of injection (wall injector and wedge shaped strut in the center) and the reacting flowfield pattern generated in them. 1-D simulation of both combustor configurations has been carried out using the quasi-one-dimensional model. Furthermore, 2-D numerical simulation using FLUENT has also been performed. For validation and assessment purposes, static pressure, static temperature and Mach number are compared between the computational models and experimental results. The weakness of the simplest approach, i.e., the quasi-one-dimensional flow, is shown to be consistent with the absence of oblique wave capability in 1-D modeling.

1.1 Historical Notes on Scramjet Engine Development

Throughout the aviation history, the propulsion devices have aimed at propelling vehicles faster and higher in the atmosphere, thereby extending the flight envelope. The engines have

traversed through the evolutionary path from propellers to turbo-jets, turbo-fans, ramjets and finally scramjets. The common attribute shared amongst all of the above mentioned propulsive devices is that they rely on the atmospheric air to achieve thrust, and are hence called air-breathing engines [4].

The strong driving force in the hypersonic industry is in finding a cheaper access to space with the ultimate goal of designing a launch vehicle for achieving single-stage to orbit or SSTO [4]. However, a vehicle must fly at hypersonic velocities, if it intends to reach orbit. Hence, from a cycle efficiency point of view, the air-breathing engines prove much superior to other chemical propulsive devices as they use oxygen from the atmospheric air [4]. This is significant from the systems perspective as it allows for a larger payload since the vehicle is not carrying an onboard fuel oxidizer [4].

The supersonic combustion air-breathing engines or scramjets have always been considered as a revolutionary engine technology, which aims to fly craft at high Mach range of 5 to 15 and seamlessly integrate air-to-space operations [5].

1.1.1 Scramjet Engine Developments in United States

The developmental history of scramjets engines in United States dates back to the early 1900's [5]. In 1940's theoretical studies were performed which helped to provide an understanding of high-velocity flow in ducts [6]. In late 1950's U.S.A.F., U.S. Navy and NASA began developing scramjet engines. In 1960's NASA performed several wind-tunnel tests on ramjet, scramjet and combined engines at Langley Research Center [7]. The first major project was called the Hypersonic Research Engine or HRE [7]. Also, numerous studies were performed over the concept of using scramjets for air-breathing launch vehicles. It was these studies that gave birth to the concept of airframe-integrated scramjet. Since then, various

hydrogen and hydro-carbon fueled scramjet engines have been developed under various programs [6]. In mid 1980's, these efforts finally culminated into nation's most influential hypersonics program called National Aerospace Plane (NASP), thus contributing to the modern scramjet development [8]. The NASP program was exclusively focused on achieving single-stage-to-orbit flight [8]. The target was to develop and fly a synergistically integrated low speed accelerator, consisting of ramjet and scramjet propulsion system [6]. This led to the development of X-30 (shown in Figure 1) [6]. At the core of X-30 was an airframe-integrated dual-mode ramjet/scramjet propulsion system powered by hydrogen fuel [7]. Mc Donnell Douglas and Rockwell International were responsible for the airframe and the Pratt & Whitney were responsible for producing the propulsion system [7].

Figure 1: NASA X-30 [6]

Further in mid 1990's McDonnell Douglas started conceptual design of a subscale model to perform flight testing at hypersonic speed [7]. This led to the more advanced US hypersonic program named as NASA Langley Hyper-X [5]. The NASP engine was significantly modified in terms of the scramjet flowpath so as to re-optimize it for engine operability and vehicle acceleration, accounting for scale, wall temperature effects, etc [9]. This program involved

flight-testing through the construction of X-43 vehicles. These Hyper-X engines went through extensive testing on the ground [7]. These tests were performed on the part of the aircraft called the DFX or "Dual Fuel Experimental" engine (as shown in Figure 2) and this was later replaced by the HXEM i.e. "Hyper-X Engine Module" (as shown in Figure 3) [7].

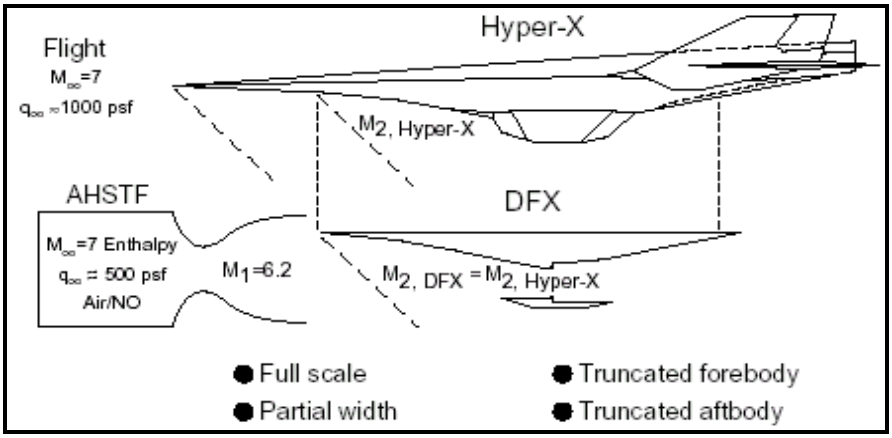

Figure 2: DFX Location on X-43 [7]

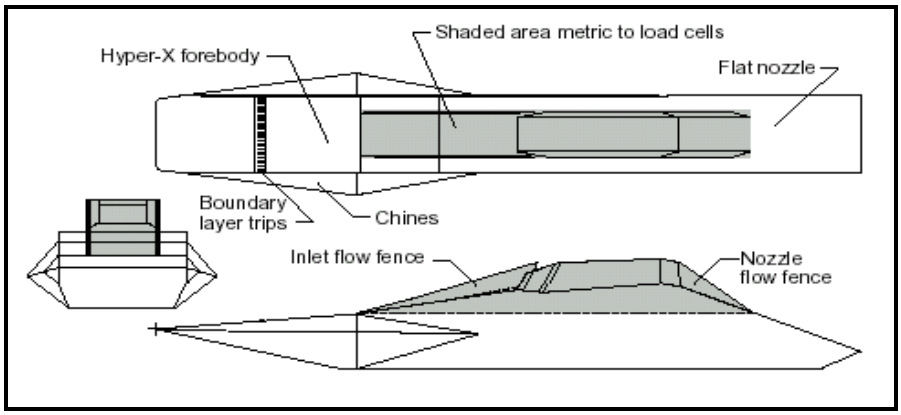

Figure 3: HXEM Location on X-43 [7]

In 2001, the first un-cooled hydrocarbon-fueled scramjet engine was ground-tested by U.S.A.F and Pratt & Whitney at simulated Mach number of 4.5-6.5 [6]. The same collaboration in the year 2003 demonstrated a scramjet constructed from nickel-based alloys and cooled by its JP7 jet fuel [6]. Also, in the same year, D.A.R.P.A, U.S. Navy, Boeing, Aerojet and John Hopkins University ground-tested a scramjet engine powered by JP10 jet fuel intended

specifically for hypersonic missiles [6]. On March 27th 2004, the first successful scramjet powered NASA X-43A craft flew for 11 seconds approaching the speed of Mach 7 [5]. There were other simultaneous hypersonic programs running along with the Hyper-X such as the Hypersonic Technology (HyTech) program [8]. Various critical technologies, such as inlet self-starting, integration for free-jet tests, fuel cooled structural panels, and combustor performance and operability over the Mach 4 to 8 range were demonstrated successfully by the HyTech program [8]. The HyTech program focused on a scramjet engine which ran on liquid-hydrocarbon as compared to most of the Hyper-X scramjet engine designs focusing on hydrogen as fuel [5]. The version "C" of NASA X-43 used the HyTech scramjet engine and was powered by kerosene [5].

The other U.S. scramjet advancement technology program consists of X-51A WaveRider, which is a consortium of the USAF, DARPA, NASA, Boeing and Pratt & Whitney Rocketdyne. The scramjet engine used in X-51A WaveRider (as shown in Figure 4) uses a 2-D design with the potential of propelling a missile to hypersonic speeds. It is cooled by its own hydrocarbon fuel JP 7 and is designated as SJX61 (as shown in Figure 5). The X-51A WaveRider successfully flew its first free-flight on 26 May 2010 and also achieved the longest duration flight of 200 seconds at speeds over Mach 5 [10].

Figure 4: X-51A WaveRider [11]

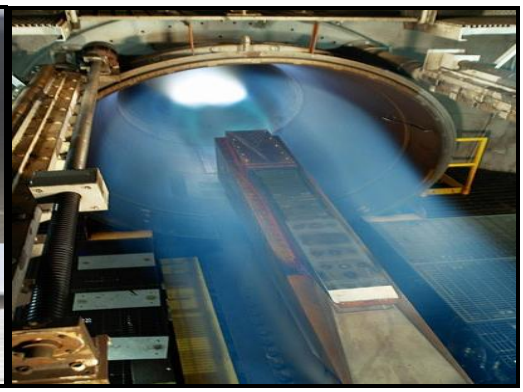

Figure 5: SJX61-2 Engine [11]

1.1.2 Other Scramjet Development Programs around the Globe

Hypersonic development programs are currently in progress in other nations too. In ***Australia***, the University of Queensland, Australia Centre for Hypersonics started a research project by the name of HyShot to demonstrate the possibility of supersonic combustion under flight conditions and compare the results of shock tunnel experiments [7]. The first launch of HyShot on October 23rd, 2001 was unsuccessful in demonstrating hypersonic combustion. However, the second launch on 30th July, 2002 successfully demonstrated scramjet combustion in flight at Mach 7.6 [7]. The triumph of the HyShot program spurred the highly successful Hypersonic Collaborative Australia/United States Experiment (HyCAUSE). The HyCAUSE team has been exploring alternate flowpath and injection designs [12].

Some system studies were performed in ***France*** concerning space launchers, so as to evaluate combined propulsion interest for space launchers [13]. The studies performed were concerning two-stage-to-orbit (TSTO) and single-stage-to-orbit vehicles. It was concluded that combined propulsion system didn't present any advantage if the flight Mach number range was limited to 6 to 6.5, so as to only permit sub-sonic combustion [13]. Hence it was decided to explore the domain of supersonic combustion. In the year 1992, this led to the establishment of French National Research and Technology Program for Advanced Hypersonic Propulsion (PREPHA) [13]. During the commencement of PREPHA, four concepts of combined propulsion systems were considered using slush hydrogen as fuel. The first two concepts consisted of twin-duct configuration formed by turbo-rocket-scramjet-rocket and turbojet-dual mode ramjet-rocket. The other two, used one-duct concept and were formed by rocket-dual mode ramjet-rocket and ejector dual mode ramjet-rocket [13].

"The French Aeronautics and Space Research Center (ONERA) and EADS Aerospatiale Matra Missiles (now in the new MBDA Missiles Systems European group and its "MBDA-F" French subsidiary) have been major contributors to the PREPHA Program" [13].

Since 1997, ONERA and DLR are the ones leading the Joint Air-breathing Propulsion for Hypersonic Application Research program or JAPHAR [13]. The goal of this program is to study hydrogen fueled dual mode ramjet with a flight Mach range of 4 to 8 along with defining a methodology for ground and flight performance demonstration [13]. Also, MBDA-F in a joint venture with Moscow Aviation Institute (MAI) is developing a dual-mode dual fuel ramjet, operating from Mach 3 to Mach 12 with a variable geometry [13].

In Germany, work has been carried out in cooperation with Russia on the testing issues of hypersonic flight and on scramjet flowpath technology at TsAGI (Jukowsky, Russia) [13].

1.2 Introduction to Ramjets and Scramjets

1.2.1 Ramjets

The ramjet engine works on the principal wherein the incoming supersonic flow is slowed down to subsonic velocity with a multiple oblique shock wave system, terminating into a normal shock. The fuel is then added to this subsonic flow and the combustion occurs. The combustion products are further accelerated through a converging-diverging nozzle having a narrow throat or a mechanical choke to supersonic speeds. This provides the necessary exhaust moment to accelerate the vehicle [4, 14]. A schematic of ramjet is shown in Figure 6.

The inlet of the ramjet uses large amount of turning to achieve the desired compression ratio. Most of the compression occurs on the external portion of the inlet with very little contraction, thus taking full advantage of the high dynamic pressure so as to convert it into the total pressure rise [15]. The inlets also contain boundary-layer bleeds so as to increase pressure

recovery and stabilize the shock boundary layer interactions and also to serve as a trap for the terminal shock system [15]. The subsonic flow within the ramjet combustor allows for efficient mixing and combustion near stoichiometric fuel to air ratios [15]. At Mach number less than 2.5, there is not enough dynamic pressure to achieve the required pressure rise due to ram effect, thus leading to inefficient combustion and low thrust [15]. At Mach number above 6, formation of normal shock begins at the lip of the inlet yielding to a poor total pressure recovery through the inlet and thus in turn causing the efficiency to drop [15].

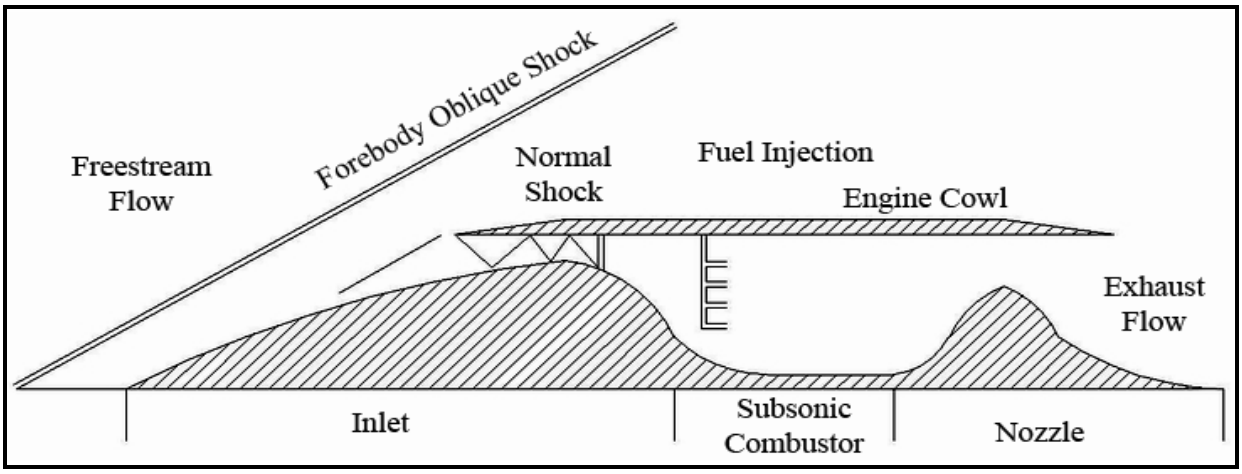

Figure 6: Schematic of Ramjet Engine [4]

1.2.2 Need for Supersonic Combustion or Scramjets

As the flight Mach number goes above the range of 3 to 6, the use of supersonic combustion provides higher specific impulse (as shown in Figure 7 [6]) [14]. The deceleration of airflow at such high velocity to subsonic conditions for efficient combustion, will result in high temperature and pressure [14]. These elevated temperatures are sufficient enough to melt down most of the known materials [16]. Also the increased temperatures can cause the dissociation of the combustion products, thus in-turn limiting the temperature rise and thereby reducing thermal efficiency [4]. The near-stagnation pressure resulting from slowing down high

speed supersonic flow to subsonic conditions can elevate the burner entry pressure [4]. As burner entry pressure is the highest pressure seen within a scramjet combustor, elevating this pressure will cause the mechanical and thermal loads to increase [4]. This will call for an increased weight so as to withstand the structural loads [4]. Thus, the structural integrity of the vehicle dictates the supersonic combustion past Mach 6 [14]. Hence, to obtain higher flight Mach numbers, the heat release due to combustion should take place at supersonic velocities [4]. This proves that supersonic combustion ramjet or scramjet is a necessary and efficient solution for hypersonic flight applications [4].

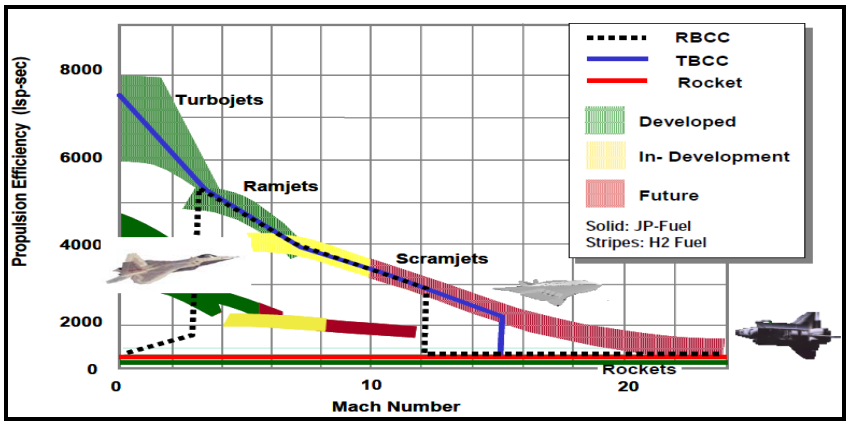

Figure 7: "Propulsive Efficiency and Operating Regimes of Variety of Flight Systems" [6]

1.2.3 Scramjets

In a supersonic combustion ramjet or scramjet, the flow is compressed and decelerated using a series of oblique shock waves [16]. A scramjet is a hypersonic air-breathing engine in which heat release due to combustion process, occurs in the supersonic flow relative to the engine [16]. Therefore, the flow velocity throughout the scramjet remains supersonic, thereby avoiding the need for mechanical chocking system [16]. Dugger and Billig were the first ones to report positive thrust results by performing supersonic combustion experiments [4].

The most integrated engine-vehicle design for an aircraft or a missile, wherein the engine occupies the entire lower surface of the vehicle is obtained using a scramjet engine [6]. As show in Figure 8, the scramjet propulsion system consists of following major engine components: the craft's forebody constituting an external inlet, internal inlet, isolator, combustor, internal nozzle, fuel supply subsystem, and the craft's aftbody forming an external nozzle [6].

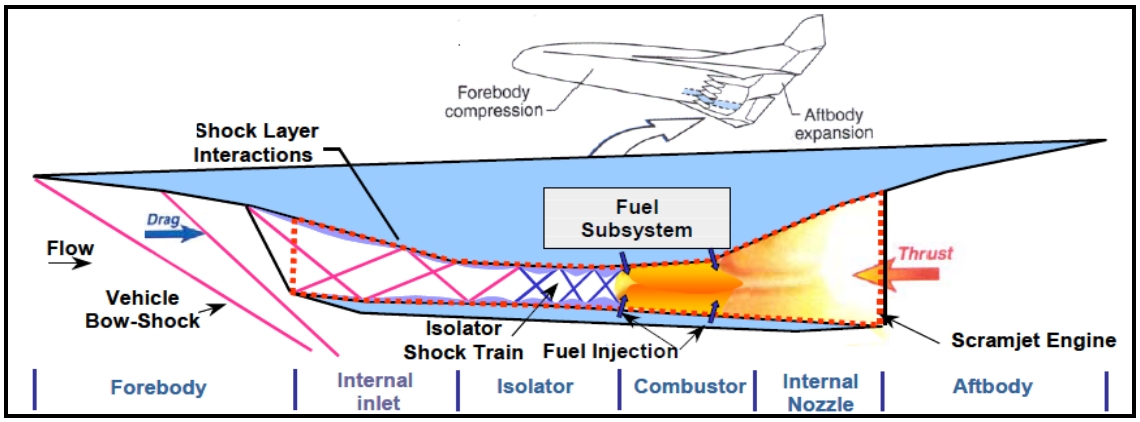

Figure 8: Integral Parts of a Scramjet Propulsion System [6]

1.2.3.1 Inlet Sub-system

In a scramjet propulsion system, the air induction system consists of vehicle's forebody and the internal inlet [6]. The task of the scramjet air induction system is to capture and compress air through a system of oblique shock waves or isentropic turning Mach waves. The forebody provides the required external compression to the incoming supersonic or hypersonic flow and contributes to the drag and moment of the vehicle. The final compression is provided by the internal inlet [6]. The design of the external and internal inlet is performed keeping in mind, the objective to achieve the required air mass capture and the aerodynamic contraction ratio. This results in maximum inlet efficiency [6]. The captured stream tube contains non-uniformities, due to the reflection of oblique shock waves thus causing shock-boundary layer

interaction and subsequent separation. These non-uniformities can influence the combustion process [6]. The figure 9 below shows the important flow physics of the forebody and internal inlet.

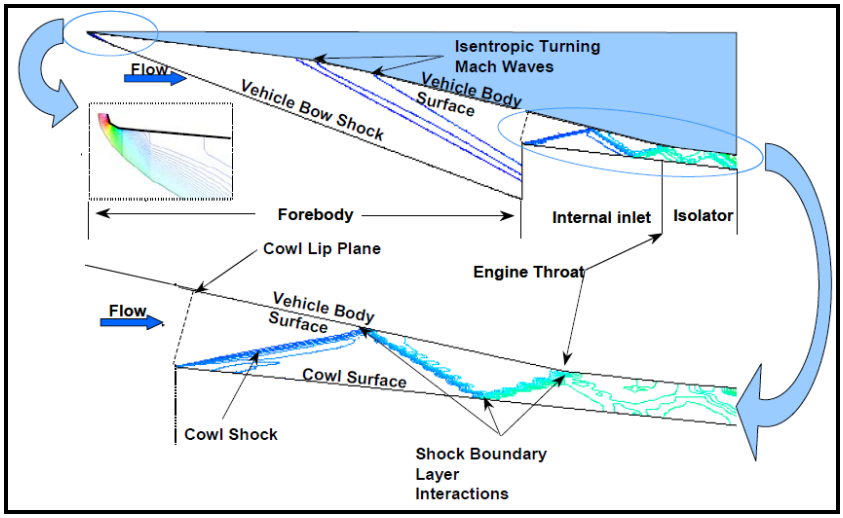

Figure 9: Important Forebody and Internal Inlet Flow Physics [6]

1.2.3.2 Isolator

In a scramjet combustor, when fuel is added to the supersonic freestream, the combustion process begins and is accompanied with pressure rise and boundary layer separation [6, 15]. In the presence of boundary-layer separation, the duct behaves like a supersonic diffuser, wherein with the downstream distance, the Mach number decreases and pressure increases [17]. The back pressure exists at the exit of the isolator. This back pressure can result from the release of chemical heat in the burner or the choking of downstream area as a result of the formation of thermal throat (as opposed to mechanical throat in ramjet engines) [17]. The back pressure can also be caused by the presence of fuel injector or due to the blockage by the presence of injected fuel [17].

The effect of the increased back pressure can propagate upstream through the subsonic region of the separated boundary-layer along the duct wall and result in the thickening of

boundary-layer [17]. In the presence of sufficient adverse pressure gradient, the boundary layer can separate from the wall, which in-turn causes a mismatch in pressure between the core stream and the separated boundary-layer [17]. This usually causes a series of shock and expansion waves collectively called as shock train or pre-combustion shock train within an isolator (as shown in Figure 10 [6]) [17]. The cross-sectional area of the isolator can be constant or diverging so as to accommodate the boundary layer separation [6].

Two types of shock trains exist within an isolator. At high Mach number and thinner inlet boundary-layers, the oblique shock train prevails. It consists of shock diamonds formed due to the repeated regular-reflection of oblique shocks and expansion waves [17]. The flow pattern and the observed static wall pressure distribution of an oblique shock train are shown in Figure 11 [17]. At low Mach numbers and thicker inlet boundary-layers, the normal shock train prevails. In these, the regular oblique shock diamonds may be replaced by Mach-reflections or lambda-shocks, wherein the normal shock wave bifurcates into oblique shock waves near the wall [16, 17]. The flow pattern and the observed static wall pressure distribution of a normal shock train are shown in Figure 12 [17]. The Mach number range between 2 to 3 is thought to be the dividing line between the occurrence of normal and oblique shock trains. The shock train occurring in this dividing range is called as "pseudoshocks" [16].

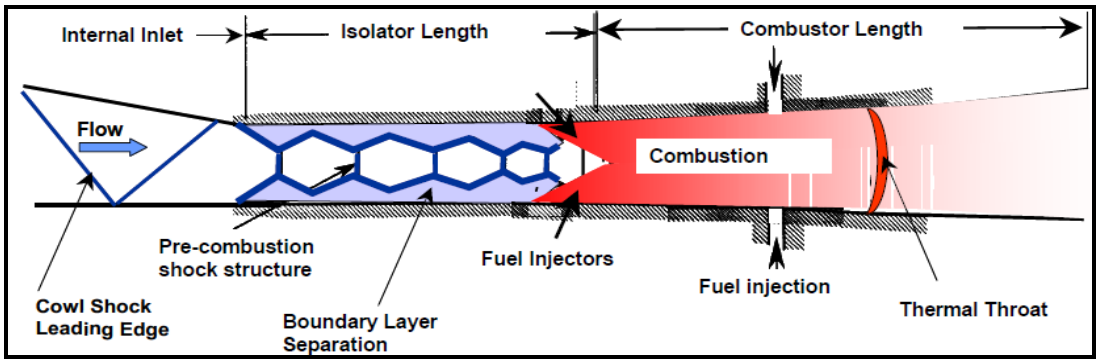

Figure 10: Details of Isolator and Combustor Flow Physics [6]

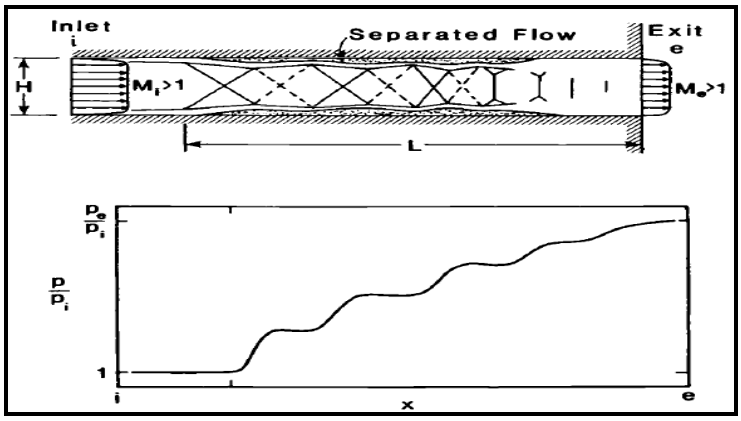

Figure 11: Flow Pattern and Static Wall Pressure Distribution of an Oblique Shock Train [16]

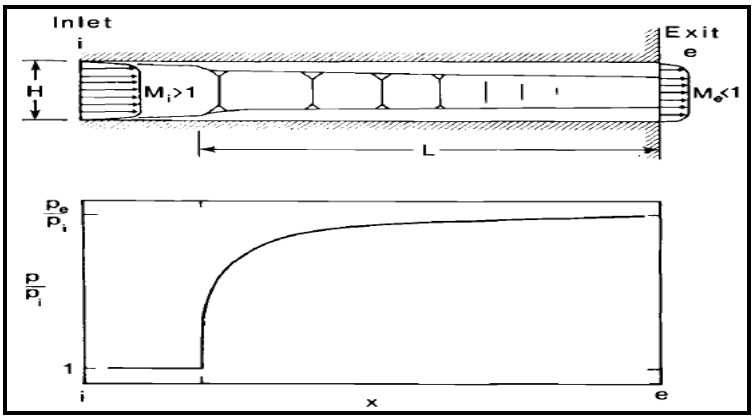

Figure 12: Flow Pattern and Static Wall Pressure Distribution of a Normal Shock Train [16]

The shock train allows the supersonic flow to adjust to the higher static backpressure as compared to the inlet static pressure, thus isolating the combustion process from the inlet compression process [6]. This helps in preventing an inlet surge or an unstart. The reason for inlet unstart is: too much of heat release due to combustion can cause the pre-combustion shock train to be pushed too far forward, through the isolator, into the inlet [15]. This would choke off the flow and result in a thermal blockage [15]. Thus a scramjet engine will typically operate above Mach 6, as high dynamic pressure at the inlet will prevent the pre-combustion shock train from protruding out through the inlet and eventually causing an inlet surge [15].

An optimal length of isolator module is required for housing the pre-combustion shock train, so as to prevent the inlet surge [18]. Thus, to optimize isolator's length over a broad range of scramjet operating conditions for a given scramjet flowpath geometry, knowing the location and structure of the shock train is very important [18]. The location and strength are governed by the flow conditions and the shock/boundary-layer interactions [18]. The location and structure of the shock wave can affect the flow properties entering the combustor and therefore are crucial parameters for the design of scramjet fueling schemes [18]. Waltrup and Billig developed a correlation for the length of the shock trains (given below as equation 1) [19]. The boundary layer momentum thickness, flow Mach number before the leading edge of the shock train and back pressure are identified as the most dominant parameters governing the length of the shock trains [18].

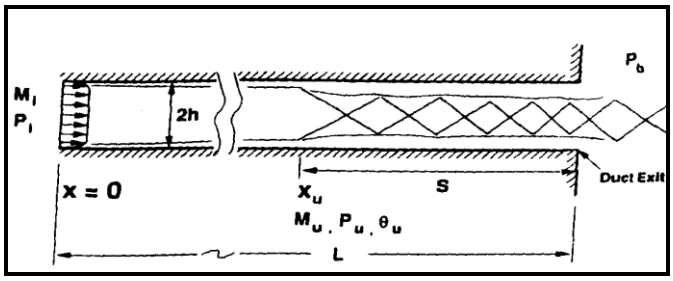

Figure 13: Schematic of a 2-D Constant Area Isolator [16]

$$\frac{\left(\frac{S}{D}\right)\bullet\left(M_a{}^2-1\right)\bullet \mathrm{Re}_\theta^{\frac{1}{4}}}{\left(\frac{\theta}{D}\right)^{\frac{1}{2}}}=50\bullet\left(\frac{P_b}{P_a}-1\right)+170\bullet\left(\frac{P_b}{P_a}-1\right)^2 \qquad (1)$$

Referring to Figure (13) and equation (1), **S** is the shock train length, **D** is the diameter of the duct, $\mathbf{M_a}$ is Mach number at shock leading edge, $\mathbf{Re_\Theta}$ is the Reynolds number based on boundary-layer momentum thickness, $\mathbf{\Theta}$ is boundary-layer momentum thickness and P_b/P_a is the pressure-ratio across the isolator [17].

1.2.3.3 Combustor

The combustor provides an efficient mixing of the fuel added to the incoming airstream from the isolator, within the available combustor length as shown in Figure 10 [6]. The fuel supply sub-system injects the fuel to the incoming airstream at appropriate locations and with the desired injection flow properties [6]. The flame holding and stabilization techniques are employed within the combustor, so as to obtain the heat release pattern for maximizing the engine thrust potential.

1.2.3.4 Expansion System

The expansion system is comprised of the internal nozzle and the vehicle's aftbody [6]. The function of the expansion system is to produce net thrust by accelerating the high temperature and high pressure combustion products exiting the combustor. The expansion system should be able to provide the required acceleration over the entire range of vehicle operation in a controlled and reliable manner, maximizing the performance of the scramjet propulsion system [16]. "The physical phenomena occurring within the scramjet expansion system include flow chemistry, boundary-layer effects, non-uniform flow properties produced due to shock wave and boundary-layer interactions and three-dimensional effects [6]. The design of the scramjet and ramjet exhaust systems is based on the method of characteristics technique for ordinary two-dimensional exhaust nozzles [16]. The expansion system design has a major effect on the flight dynamics of the vehicle due to its ability to influence vehicle pitching moment and lift [6]. The important expansion system flow physics are depicted below in Figure 14 [6].

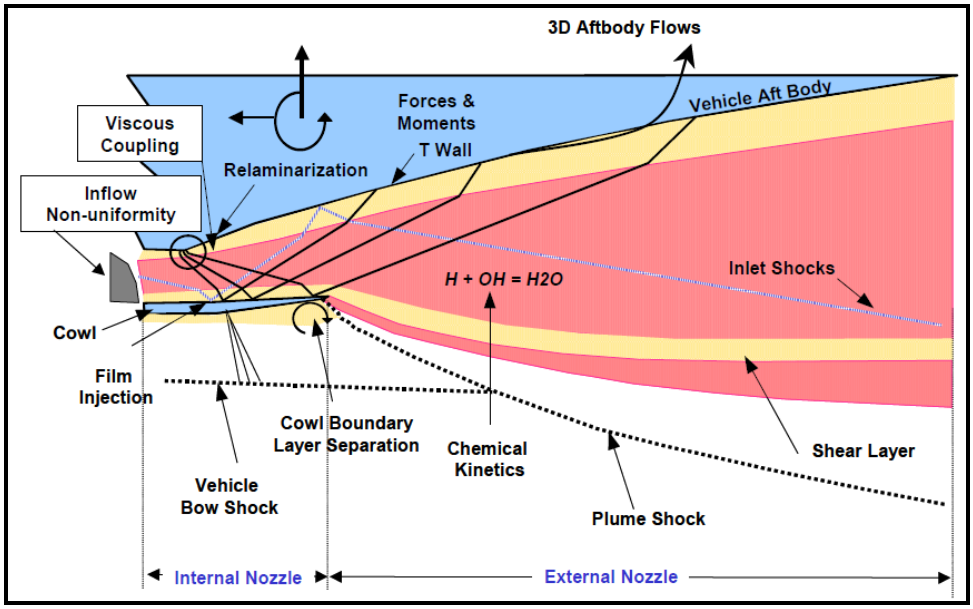

Figure 14: Details of the Scramjet Expansion System Flow Physics [6]

1.2.4 Dual-Mode Scramjet Engine

An air-breathing hypersonic vehicle has to cross the sub-sonic and supersonic speeds to achieve the hypersonic scramjet operating speeds. Thus, the hypersonic air-breathing vehicle needs to operate in multiple engine cycles and modes and this explains the need for dual–mode scramjet [6].

In the low speed regime from Mach number 0 to 3, the vehicle utilizes integrated propulsion cycles such as Turbine Based Combined Cycle (TBCC), where the ramjet or the scramjet can be integrated with a gas-turbine engine. Another choice for the low speed regime is Rocket Based Combined Cycle (RBCC), in which rockets are integrated with ramjet or scramjet engine [6].

In the flight speed regime between Mach numbers 3 to 6, the integrated hypersonic air-breathing scramjet propulsion system transitions from low speed propulsion cycle like TBCC or RBCC to dual-mode scramjet, operating in a ramjet mode [6]. In ramjet mode, a normal

shock train exists within the isolator thus creating a subsonic flow at the entrance of the combustor [6]. A dual-mode scramjet engine, while operating in the ramjet mode doesn't require physical throat for accelerating the combustion products supersonically through the expansion nozzle. This characteristic of a dual-mode scramjet engine provides an optimum cycle over a wider operating range of Mach numbers [6]. The required chocking of the flow is provided by means of a thermal throat, which is developed using a delicate balance between the heat release and the change in area of the combustor [20].

As the scramjet accelerates from Mach 3 to 8, there lies in between an inevitable range from Mach 5 to 7, within which a transition occurs from the ramjet mode to scramjet mode [6]. Within this transition region, both the characteristics of ramjet and scramjet mode exist. The pressure rise occurs due to combustion process and total temperature rise across the combustor begins to drop. This causes the pre-combustion shock train, typically an oblique shock train (whose strength is weaker than as required in case of dual-mode ramjet) to be pulled back in towards the combustor [6]. In this regime, the scramjet engine operates as a dual-mode scramjet, wherein a transition between both mixed characteristics of subsonic and supersonic combustion exist [6].

Further beyond Mach 7, the combustion products are no longer able to separate boundary layer and the dual-mode scramjet engine runs in scramjet mode [6]. In this mode, no pre-combustion shock exists within the isolator and the inlet shocks propagate through the entire engine [6]. The Figure 15 shown below highlights the transition of a dual-mode scramjet engine from ramjet mode to scramjet mode and also depicts how the isolator provides this seamless transition [6].

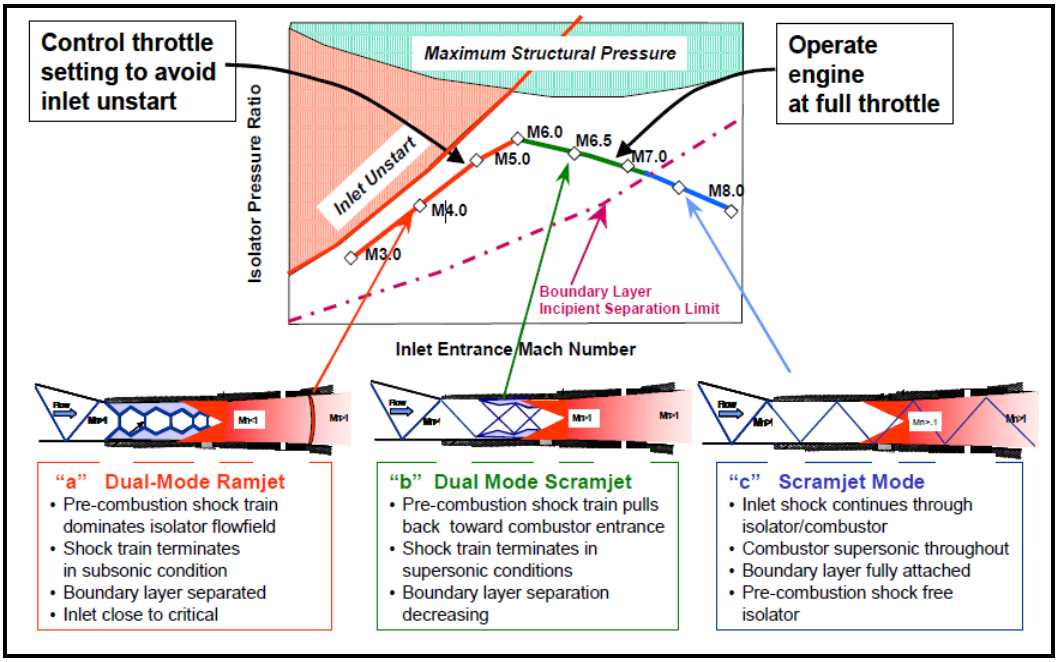

Figure 15: The Scramjet Operational Line and Isolator Physical Phenomena during Transition Mode [6]

1.2.5 Technological Challenges Encountered in Scramjet Propulsion System Design

The key technological challenges to be addressed for the successful design and operation of scramjet propulsion system are shown in Figure 16.

The technical issues concerning hypersonic scramjet propulsion system can be categorized in reference to engine components namely, air induction system i.e. inlet/isolator, combustor, nozzle, fuel sub-systems, structures and materials [8]. The requirement for mixing of fuel/air and cooling are far more stringent for scramjet propulsion system as compared to subsonic combustion engines. Also, losses due to shock waves and skin friction are amplified [4].

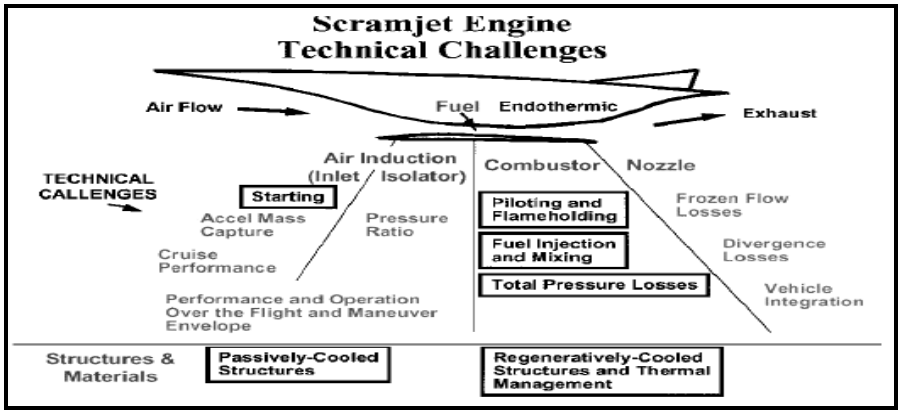

Figure 16: Scramjet Propulsion System Technical Challenges [8]

1.2.5.1 Inlet/ Isolator

Significant technical challenges concerning inlet/isolator for hypersonic air-breathing propulsion system are characterized as inlet starting, air mass capture, contraction ratio, thermodynamic efficiency, and pressure ratio [8]. For a supersonic inlet, the starting occurs when supersonic flow has been established within the internal compression portion of the inlet [8]. In the unstarted condition, strong shock waves appear ahead of the inlet cowling, causing the flow spillage and resulting in high drag and structural loads [8]. The thrust produced by the scramjet is directly proportional to the air mass flow rate processed by the engine which is governed by the amount of spillage [8]. The contraction ratio of the inlet is also governed by the starting condition. This poses a major challenge for fixed geometry scramjet flowpaths as there is a limit to the maximum contraction ratio [8]. The inlet design is dominated by the starting condition, mass capture and contraction ratio [8]. For a dual-mode fixed geometry scramjet design, the pressure ratio of the integrated inlet/isolator combination is of prime importance for operability [8]. Numerous design factors influence pressure-ratio of the integrated inlet/isolator combination, namely aspect ratio, sidewall configuration, inlet shock interactions, combustor fuel injectors, and boundary-layer characteristics around the perimeter of the isolator [8].

1.2.5.2 Combustor

Even though the geometric configuration of a scramjet engine is relatively simple as compared to a gas turbine engine, the flow physics encountered within the combustor of a scramjet engine is quite complex [21]. The reasons for the complexity of flow physics are the simultaneous injection of fuel from multiple injection ports with varied configuration, the mixing and combustion of that fuel downstream of the injectors [21]. In a scramjet engine, efficient combustion is required in supersonic regime within a combustor that is short enough to be compatible with practical engine sizes [22]. The efficient combustion depends on efficient injection techniques and complete burning without much pressure loss [22]. Billig [23] has listed some of the characteristics of hypersonic air-breathing vehicles which suggest that supersonic combustion processes are inherently mixing-limited [24].

At supersonic and hypersonic flight speeds, the residence time for the air entering through inlet, mixing with fuel and exiting the nozzle of the scramjet engine is of the order of a millisecond [21]. Therefore, the injected fuel should efficiently mix with air within tens of microseconds and react to release its energy in the combustor [21]. To a large extent, for given conditions, the efficiency and the effectiveness of fuel injection, drives the net heat release achieved in a scramjet combustor [22]. From the viewpoint of fuel injection process, two important aspects of concern are the degree of turbulent fuel mixing and its transport[22]. The degree of fuel penetration is measured by Injection effectiveness and the degree of turbulent fuel mixing and transport within the short residence time is measured by injection efficiency [22]. The supersonic combustion is governed by both mixing and chemical kinetics. In supersonic combustors, the shear losses can drastically reduce the engine performance, thus rendering the trade-off studies very complex for attaining high combustion efficiency [24].

Other factors that affect fuel-air mixing within a scramjet combustor are as following: The increased compressibility effect within a scramjet combustor reorganizes the turbulence field and modifies the development of turbulent structures. This results in reduced mixing layer growth rates and reduced mixing [24]. The chemical reaction occurring within a mixing layer and resulting in heat release causes the growth of mixing layer to retard in both subsonic and supersonic flow [24].

Another issue of concern during the design of combustor for scramjet engine is the aerodynamic heating of the combustor walls, which can affect the aerodynamic performance and durability of the combustor [5]. "At very high temperatures, the reactants may start to dissociate prior to combustion, which will result in lower levels of heat release than expected at standard temperature and pressure" [5].

1.2.5.3 Expansion Nozzle

The challenges in nozzle design are more focused on performance and efficiency rather than operability, as in case of inlet and combustor [8].

"The flowfield of the expansion nozzle is characterized by high velocities and high initial temperatures, significant divergence and skin friction losses, potential relaminarization of the flow, energy-bound chemical radicals that will not relax in a finite nozzle length, and excited vibrational states" [8]. "The favorable pressure gradient in the nozzle eliminates the concern with shock-boundary layer interaction and separation" [8]. For determining the overall scramjet cycle efficiency, the nozzle thrust coefficient is the most sensitive parameter [8]. The design of expansion system determines nozzle thrust vector and resulting pitching moments, which have a major effect on scramjet vehicle's system performance [8]. An excessive thrust vector

pointing in the wrong direction will require excessive trim from vehicle flight control surfaces thus, adding drag penalty [8].

1.2.5.4 Materials/Structures

The harsh conditions in which hypersonic vehicles and propulsion systems operate poses an extraordinary design challenge for the structural concepts [8]. The engine application represents a particularly challenging problem due to high thermal, mechanical, and acoustic loading along with an aggressive, corrosive mix of hot oxygen and fuel decomposition products [8]. Actively cooled structures are needed, otherwise the extremely high temperatures reached within a scramjet combustor will be sufficient enough to melt most metallic structural materials [8]. Materials used to manufacture flowpath components should be able to take form of lightweight wall panels and complex component shapes such as fuel injectors (as shown in Figure 17 [13]) [8]. Also, further development of thermo-structural design methods is needed along with developments in fabrication techniques for manufacturing actively cooled structures [8].

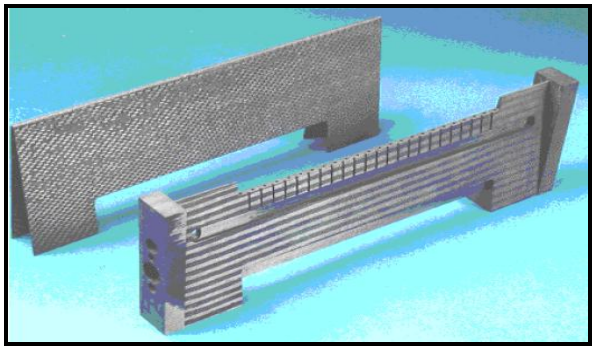

Figure 17: A Thermo-Structural Composite Injection Strut [25]

1.2.5.5 Fuels

For the future missions, the storable-fueled hypersonic vehicles are viewed as an important technology [24]. “Fuel is becoming an integrating factor of the complete high-speed vehicle

system" – E.T. Curran in [24]. One of the practical engine design challenges focusing fuels is the change in their behavior, due to the state change occurring with the rise in temperature as the fuel absorbs heat in the vehicle's cooling passage [24]. The use of fuel as a coolant causes the fuel to be partially reacted i.e. cracked or dehydrogenated before reaching the combustor. The cracking causes a hydrocarbon fuel to be divided into lighter hydrocarbons that burn more readily when injected into supersonic flow [10]. On the other hand cracking can lead to thermal and catalytic reactions in the fuel which can affect the reactivity of the fuel and in turn the combustion efficiency [24]. Also, the change in the state of fuel (such as high temperature for hydrocarbons) within the fuel lines as a coolant can result in coking or deposition, which would block or restrict the cooling passages resulting in a catastrophic failure [8].

1.2.5.6 Integration and Operability

The integration of the scramjet engine with the hypersonic vehicle, results in a propulsion system which is highly integrated from nose to tail and thus has a major shaping influence on the design of the vehicle [26]. The hypersonic vehicle due to highly integrated engine/airframe configuration and extensive flight envelope, involves many interdependent disciplines [26]. These disciplines are characterized with very large set of sensitive design variables belonging to a highly non-linear design space [26].

The integrated scramjet engine/vehicle configurations are also known as *Waveriders*. The scramjet engine's passage in a Waverider occupies the entire lower surface of the hypersonic vehicle's body [20]. In such a highly integrated engine/vehicle configuration, the mode of operation and heat supply largely dictates the aerodynamic characteristics and the optimal geometry of scramjet engine passage [20]. Therefore, a certain optimal geometry of the inlet

and combustor corresponds to a specific fuel-air equivalence ratio [20]. Variable engine geometry can also be used to adjust the airflow and heat release profile in the engine [8].

A dual-mode hypersonic air-breathing engine flies through dual ramjet, dual scramjet and scramjet mode to reach hypersonic velocities. Operation within a particular mode is based on the flight Mach number which in-turn governs fuel injection location thus altering the heat release profile. As mentioned in [10], "where fuel is injected is another critical aspect of making a scramjet practical". Injecting the fuel at the front (near the combustor inlet) gives more time for the fuel-air to mix and burn, but this poses an inlet surge risk due to backpressure from combustion blowing the shockwave system out of the inlet [10]. Therefore, at low flight Mach numbers, the fuel is injected towards the rear of the combustor [10]. As the vehicle accelerates to high flight Mach numbers, the fuel injection is staged forward near to the inlet of the combustor as the high dynamic pressure prevents the inlet surge [10].

There are various other parameters which affect the integration process for an optimal set of airframe and propulsion configuration. These are namely, specific impulse, contraction ratio, fuel, drag, lift-to-drag ratio, trim drag, volumetric efficiency, propellant fraction and thermal balance to size the overall system [20].

2 Literature Review

2.1 Hypersonic Air-breathing Propulsion Testing

One of the most important steps in the successful hypersonic air-breathing propulsion system design and development is the ground testing [16]. The aim of ground testing is to precisely evaluate highly instrumented articles under carefully controlled and realistic environmental conditions until they are ready to be flight tested [16]. Ground testing permits the comparison of performance, reliability and durability with the prescribed requirements, thus leading to improvements or the solution of an unexpected problem [16].

As compared to ground testing, the flight testing provides much more realistic environmental conditions which might be unobtainable through ground testing [16]. The ground testing, on the other hand, provides a greater control over the conditions of the quantity and quality of the instrumentation and data obtained along with safety and economy in comparison to flight testing [16]. Flight testing is performed using either a slave vehicle acting as a suitable platform for the propulsion device or on a parent vehicle [16].

The ground-test facilities can be divided into the ones used for research and development (R & D) and the other for testing and evaluation (T & E) [16]. Ground-test facilities for R & D purposes are used for understanding phenomena, developing and validating computational methods and for carrying out parametric studies on components and subcomponents [16]. They are characterized as highly instrumented and can generate high resolution data [16]. Testing and evaluation using ground-tests is used for evaluating the resulting vehicle design in terms of overall system performance, operability, and durability [16]. These are characterized as generally large scale and thus costly to build and operate. The emphasis in ground-test for T &

E purposes is on the measurement of global quantities near flight conditions, which have a very long lead time for acquisition [16].

2.1.1 Types of Ground-test Facilities

2.1.1.1 Continuous Flow Ground Testing Facility

The continuous flow ground-test is one of the prime testing methods for propulsion devices. It simulates the flight conditions in a full-scale continuous flow facility which is conceptually similar to a freejet test facility as shown in Figure 18 [16]. In the continuous flow ground test facility, the air is brought in from the nearby atmosphere and compressed, dried, and heated or cooled, as necessary, to duplicate the actual freestream stagnation conditions [16]. This air is then introduced into a test cell using a facility nozzle which is connected to the upstream plenum chamber. The facility nozzle brings the flow to the desired free stream Mach number, static pressure along with removing any combustion products using an exhauster system containing vacuum pumps and water spray cooling, so as to maintain the freestream static pressure downstream of the test article [16].

The continuous flow, full-scale testing is the most desirable ground test alternative as it allows the actually propulsion system concept to be tested as compared to its scaled-down or modified version [16]. It also enables the ability to perform long duration testing which allows the propulsion system to reach thermal and mechanical equilibrium [16]. This helps in precisely defining the configuration of propulsion system being tested and also for obtaining the testing conditions which are very similar to the ones found in flight [16].

These facilities are also used to test the integrated propulsion system response to transient throttle motions for demonstrating its operability within the desired flight envelope [16]. This is useful in predicting the integrated propulsion system's resistance to disruptive events as unstart

and flame-out and the authority of its control system [16]. One can also rapidly vary the test conditions and angle of attack in order to simulate the effect of transient maneuvers on the propulsion system [16].

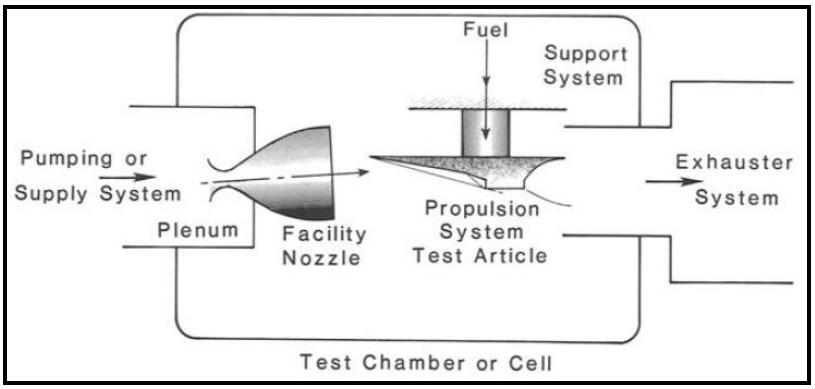

Figure 18: Schematic of air-breathing propulsion system freejet test facility [16]

The Aeropropulsion Systems Test Facility (ASTF) located at the U.S. Air Force Arnold Engineering Development Center (AEDC) in Tennessee (as shown in Figure 19), is a very advanced continuous flow ground test facility [16].

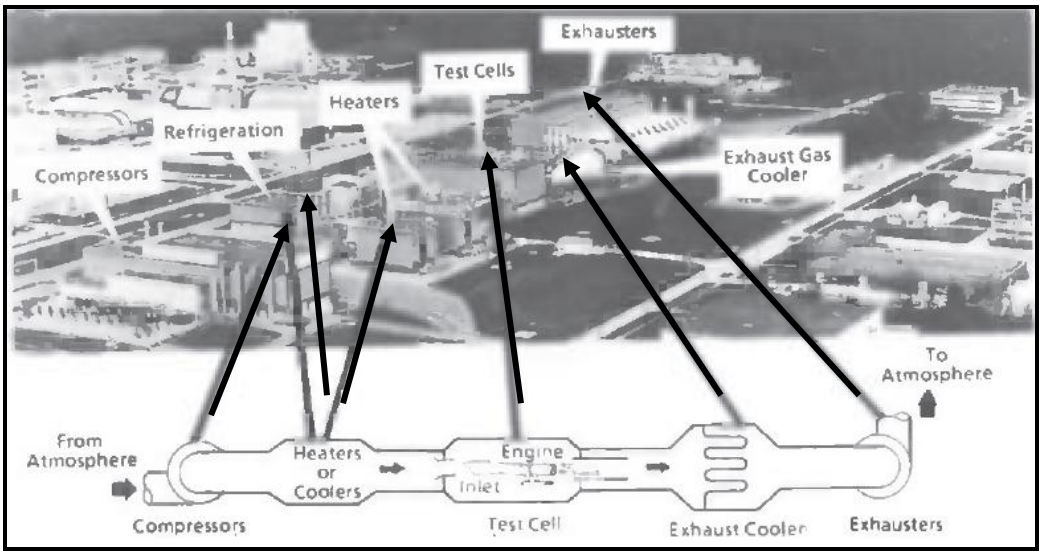

Figure 19: The Aeropropulsion Test Facility at the U.S.A.F. Arnold Engineering Development Center, Tennessee [16]

The performance characteristics of ASTF include full-scale testing of turbine engines which can generate thrust up to 100,000 lbf (444.8 kN) for a dynamic pressure between 500 to 2000 lbf/ft^2 and a freestream Mach number less than 3.8 [16].

2.1.1.2 Direct Connect or Semi-Direct Connect Testing Facility

The main advantage of using semi-direct connect testing facility as compared to continuous flow facility is that a lower stagnation pressure and less upstream flow is required for testing the same propulsion hardware [16]. This means that less power is needed for generating freestream flight condition for simulating full-scale ground tests and hence less costly [16]. The main disadvantage is that the combustor entry and external flowfields do not match the flight conditions to be simulated, even though the facility requires the same stagnation enthalpy to be provided [16]. The schematic of a semi-direct connect test facility is shown in Figure 20 [16].

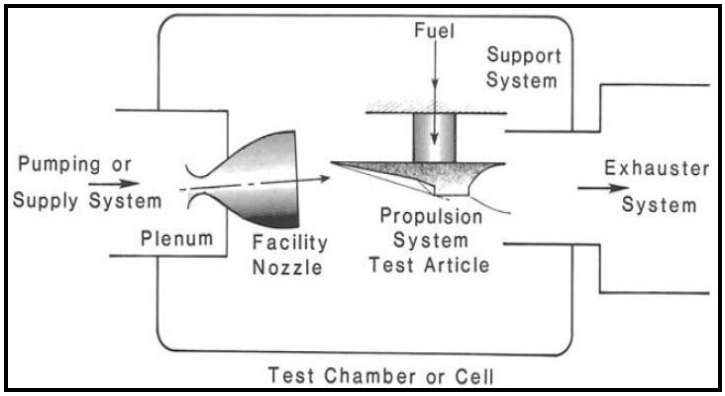

Figure 20: Schematic of a Semi-Direct Connect Test Facility [16]

In U.S., NASA Langley owns a Direct-Connect Supersonic Combustion Test Facility (DCSCTF) (shown in Figure 21) [27]. The size of the test cell is 16- by 16- by 52 ft [27]. The facility is used for assessing the mixing, ignition, flame-holding and combustion characteristics of ramjet or scramjet combustion models. This facility can provide following freestream test

conditions: stagnation pressure from 7.8 to 34 atm, stagnation temperature of 720 to 2000 K and simulated flight Mach number in the range of 3.5 to 7.5. The maximum run time of DCSCTF facility is 60 seconds. Further details on DCSCTF facility are given in [27].

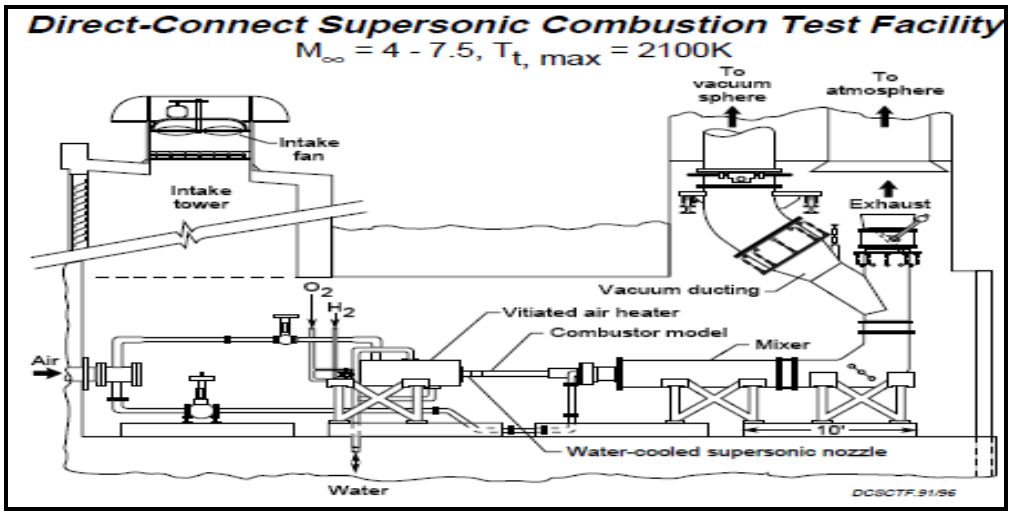

Figure 21: Direct-Connect Supersonic Combustion Test Facility, NASA Langley Research Center [28]

2.1.1.3 Short Duration Ground Testing

Short duration ground testing facility is also known as blowdown facility and is very similar to continuous flow ground testing [16]. In this facility, the air is slowly compressed and stored in high pressure vessels till the point it's ready and is then further heated through various means before reaching test cell [16]. The methods of heating air are namely thermal storage heater or pebble bed heater and vitiated heater [16]. In thermal storage heater or pebble bed heater, the air is passed through a lattice of heated bricks or pebbles for heating purposes [16]. The vitiated heater heats the air by burning it in a combustor which later replenishes the oxygen to obtain a test gas with same molar oxygen content as standard air [16]. The run times of this facility are of the order of a few seconds to a few minutes depending on the test condition [16]. These run times are long enough to approach aerothermodynamic equilibrium [16].

The Aerodynamic and Propulsion Test Unit (APTU) located at the AEDC is an advanced blowdown facility (shown in Figure 22) [16]. APTU is capable of providing test conditions for testing large test articles for a dynamic pressure of 1000 lbf/ft^2 (47.88 kN/m^2), stagnation pressure up to 135 atm and stagnation temperature up to 1800 K using alumina pebble-bed heater or 2500 K using vitiated heater [16]. This facility can provide freestream Mach numbers up to 6 using a pebble-bed heating and up to 8 with vitiated heating [16].

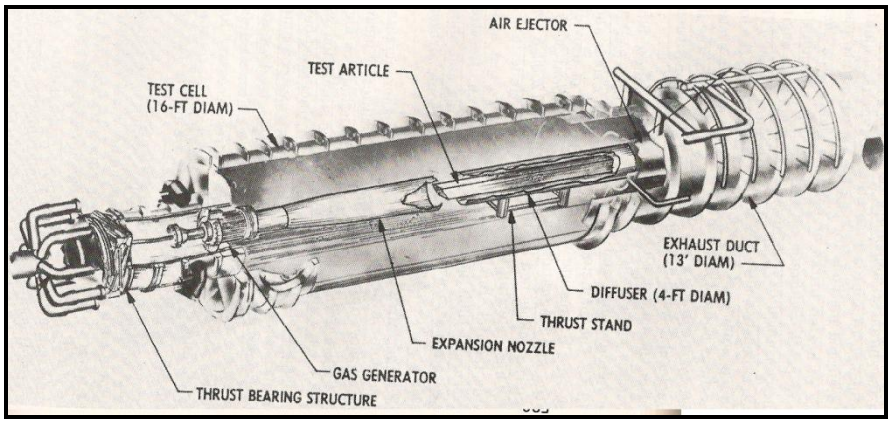

Figure 22: Advanced Blowdown Ground Test Facility APTU at U.S.A.F. AEDC [16]

Figure 23: DARPA's Falcon Combined-cycle Engine Technology (FaCET) scramjet test article in the APTU's Test Cell at AEDC [29]

Another blow down facility is the NASA's 8-Foot High Temperature Tunnel (8-Ft HTT) (as shown in Figure 24). True total enthalpy at hypersonic flight conditions can be obtained through this facility [27]. The facility has 26-foot diameter test section which can accommodate advanced large-scale, flight-weight aero-thermal, structural, and propulsion concepts. The range of flight conditions which can be obtained are: Mach number of 4, 5 and 7 through a range of altitudes from 47,000 to 120,000 ft, stagnation pressure from 3 to 136 atm, stagnation temperature from 900 K to 2000 K. The typical test duration obtained is around 60 seconds [27]. Further details about NASA's 8-Ft HTT can be found in [27]

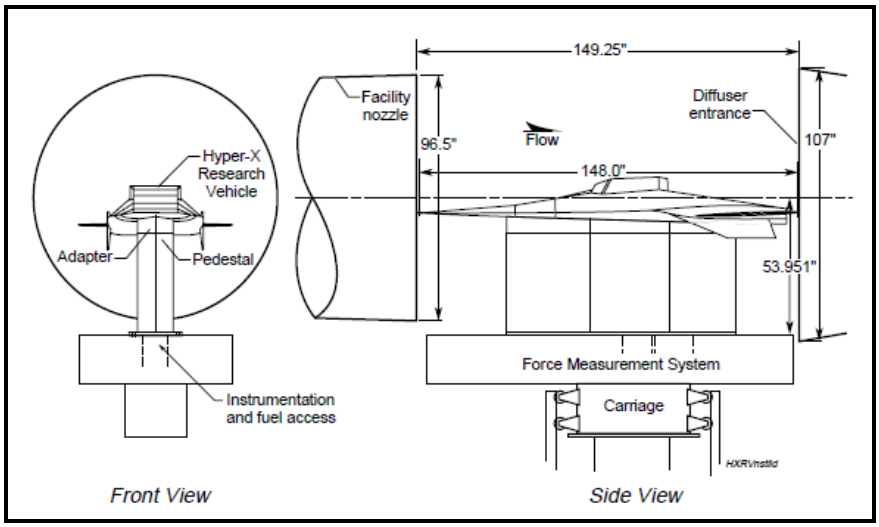

Figure 24: Hyper-X Research Vehicle in 8-Ft HTT [28]

2.1.1.3.1 Variants of Short Duration Ground Testing Facility

The first variant of short duration ground testing facility is one in which arc heater is used to produce further high stagnation temperature of the air up to 8889 K [16]. As the facilities cannot produce stagnation pressure higher than the current limit of 100 atm, the true aerothermodynamic simulation cannot be performed [16]. These facilities can be used to test materials and structures up to a freestream Mach number of around 15 which are characterized

by high stagnation temperatures [16]. The flow is contaminated by arc heaters due to the presence of molecular debris of sputtered electrode materials which causes the arc heaters to become less stable as mass flow rate increases [16]. The NASA Langley research center has an Arc-Heated Scramjet Test Facility (AHSTF) (as shown in Figure 25) which can provide simulated flight test conditions of Mach number 4.7 to 8, stagnation pressure up to 45 atm, stagnation temperatures from 800 K to 2600 K and maximum run time of 30 seconds at Mach 8 or 60 seconds at Mach 4.7 [27].

The second variant of short duration ground testing is obtained by replacing the upstream equipment with a liquid rocket engine [16]. The exhaust products from the rocket engine are similar to air in terms of oxygen concentration and molecular weight [16].

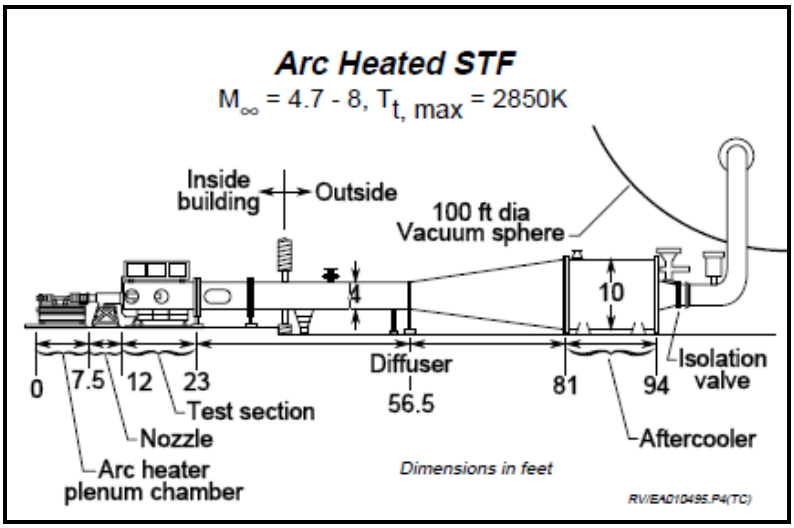

Figure 25: NASA Langley Research Center Arc-Heated Scramjet Test Facility [27]

2.1.1.4 Pulsed Flow Ground Testing Facility

These facilities are used for simulating freestream stagnation temperature conditions which are high enough to produce dissociation of the air or "real gas effects" in the regions where flow is brought to rest, like boundary layers, stagnation regions and separation zones [16]. The

need for simulating such high stagnation temperature flow arises because the real gas effects change the character of the chemistry in a complex way which needs to be discovered through testing [16]. The onset of the dissociation of air occurs around the stagnation temperatures of about 2500 K and freestream Mach number of about 8 for a constant dynamic pressure trajectory [16].

None of the present continuous or short duration ground testing facilities are capable of producing test conditions in which real gas effects can be simulated [16]. One of the short comings of pulse flow ground testing is the short duration of simulation which is of the order of fraction of milliseconds to milliseconds [16]. Even though the simulation period is very small, the flow the test article is considered to reach equilibrium based on the concept of passage time or fill time interval [16]. "The passage time or fill time concept considers that a flow comes to equilibrium in about the time it takes the average particle to traverse the region of interest" [16].

The pulse flow facilities operate on the principle of using the energy of a larger mass of gas by transferring it rapidly to a smaller mass, and then using the energy of the smaller mass by concentrating its release in space and time [16]. There are three types of pulse flow facilities namely, shock tunnel, free-piston shock tunnel and expansion tube [16].

2.1.1.4.1 Types of Pulsed Flow Ground Testing Facility

a. Shock Tunnel or Reflected Shock Tunnel (RST)

In a shock tunnel (as shown in Figure 26), the energy of the larger mass of high pressure driving gas is transmitted to a small mass of working gas by bursting the primary diaphragm (P) [16]. The bursting of diaphragm (P) causes a normal shock wave to propagate through the

working gas down the driven or shock tube [16]. This normal shock is reflected off the secondary diaphragm (S) which causes it to burst, allowing the highly compressed air behind the normal shock wave to escape through the facility nozzle [16]. The highly compressed air after passing through the test article is sent to a vacuum dump tank [16].

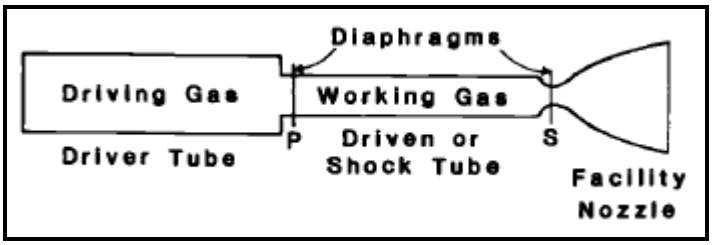

Figure 26: Schematic of Shock Tunnel or Reflected Shock Tunnel [16]

b. Free-piston Shock Tunnel (FPST)

In a free-piston shock tunnel (as shown in Figure 27), the driver is a piston that slides freely within the compression tube [30]. The piston is driven through the force of a highly compressed driving gas in the gas reservoir. The compression tube is generally filled with light gas typically helium at a low pressure with respect to the gas in the reservoir [30]. A heavy metal diaphragm (P) separates the compression tube and shock tube. The shock tube is usually filled with air as a test gas and is separated from the facility nozzle by a second diaphragm (s) made out of a very thin and light material [30]. To start the tunnel, a force is applied on the piston by the high pressure gas in the gas reservoir which causes it to traverse through the compression tube, pressurizing the light gas inside it. When the pressure within the compression tube reaches a certain level, it will result in the rupture of diaphragm (P) which will initiate a normal shock wave to propagate through the shock tube [30]. The shock wave compresses the test gas within the shock tube as it propagates until the point where it hits the secondary diaphragm (S), ruptures it, reflects back and propagates in the opposite direction.

This compresses the test gas second time, causing a further increase in the temperature and pressure [30]. In AEDC FPST facility, test gas can achieve a high pressure up to 2000 atm and high temperature of 10,000 K [30]. This hot, high-pressure mass of gas is then expanded through the facility nozzle which flows over the test article. The FPST tunnel is used to simulate high freestream Mach numbers that are characterized by high stagnation enthalpy. The major short coming of FPST facility is the duration of test period which is typically just a few milliseconds [30].

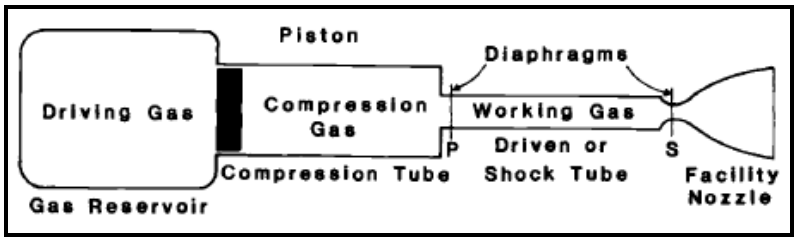

Figure 27: Schematic of a Free-Piston Shock Tunnel [16]

c. Shock Expansion Tunnel (SET)

The shock expansion tunnel consists of three chambers (as shown in Figure 28), filled with gases at different pressure and separated initially by diaphragms [31]. After the primary diaphragm (P) is burst, the high-pressure, heated, low molecular weight driver gas (typically hydrogen or helium) is released, causing a primary shock of moderate strength to move through the working gas [31]. When the normal shock wave reaches the secondary diaphragm (S), it bursts, sending a normal shock wave down the acceleration tube, causing the working gas to accelerate into acceleration tube which is maintained at nearly vacuum state [31]. The expansion of the compressed working gas into the nearly vacuum acceleration tube causes it to cool and accelerate to very high velocities thus rendering any need for a facility nozzle. The velocity obtained for simulation purposes is primarily dependent on the molecular weight,

pressure of the driver gas and the vacuum level of the acceleration tube [31]. The testing begins when the mass of air has passed through the test article and it ends with the arrival of tail of the expansion fan created due to the bursting of second diaphragm (S) [16]. In the SET, the working gas flow never stagnates, thus reducing the extent of dissociation [16]. Different simulation conditions can be obtained by varying the initial filling pressure within the three chambers of the SET [16]. The only disadvantage is that the test durations obtained are very short [31].

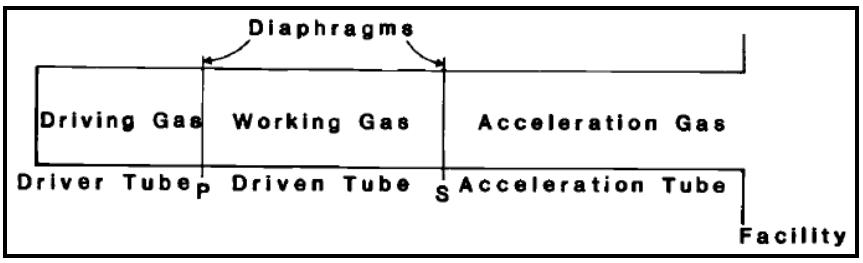

Figure 28: Schematic of a Shock Expansion Tunnel (SET) [16]

The Hypersonic Pulse Facility (HYPULSE) at NASA Langley Research Center (as shown in Figure 29) is a dual-mode shock tunnel which can be configured as both reflected shock tunnel (RST) and shock expansion tunnel (SET) [27]. In the RST mode, the facility can simulate test conditions for atmospheric flight speeds up to Mach 10. The HYPULSE facility recently has been used in the RST mode for testing and evaluation of the Mach 10 engine flowpath of the X-43 A (Hyper-X) [27]. In the SET mode, the facility can generate test conditions to simulate hypervelocity flight regime from Mach 12 to near orbital for the aerothermodynamic studies of aeroheating and planetary re-entry [24]. Further details about the HYPULSE facility are given in [27].

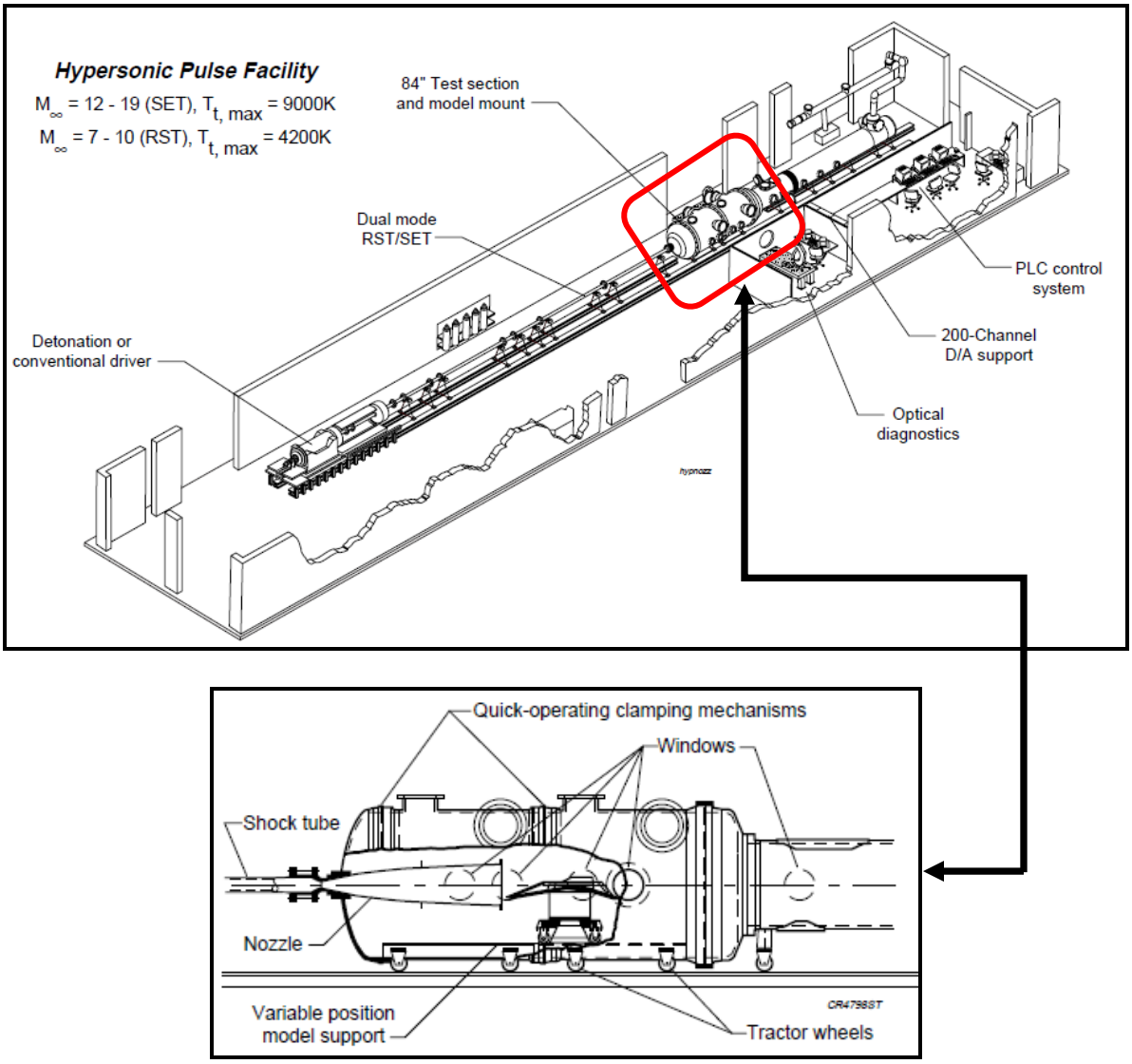

Figure 29: HYPULSE Facility, NASA Langley Research Center [28]

2.2 Nonintrusive Diagnostic Techniques for Scramjet Research & Development

The reactive flow encountered within scramjet combustors is very complex and difficult to model theoretically [32]. This reactive flow is characterized as turbulent, three-dimensional, reacting (multi-species), separated and in some cases, multi-phase [32]. For determining the performance parameters in supersonic combustion flows within a scramjet combustor, various stream properties namely, fuel mixing, extent of reaction, gas temperature, gas pressure, gas

velocity and concentration of major and minor species, need to be assessed [33]. To help enhanced the understanding of turbulent combustion, instantaneous 2-D visualizations and simultaneous measurements of different physical quantities is required at a high frequency as compared to measurement of one given quantity at a given point and at a given instant [33]. This will lead to improved modeling of turbulent mixing mechanisms and the interaction between turbulence and combustion [34].

In the ground tests for scramjet combustors, various methods are used for measuring performance and operability such as, thrust stand for thrust, pressure transducers for wall pressure, pitot tubes for stream velocity, thermocouples for temperature and temperature sensitive paints for heat flux or calorimeter for total heat release [35, 36]. As the above mentioned measurement methods are limited to points where the flow comes in contact with the wall, they do not provide any information about the flowfield or the reaction zone within the flowpath [36]. Also, the in-stream measurements are hard to obtain using above mentioned methods as perturbing the flow will cause tremendous flow disturbance. Hence need arises for non-intrusive measurement methods [36].

Laser based optical diagnostic techniques with high spatial and temporal resolution aids to explore detailed features of the combustion zone such as, "reaction zone structure, spatial uniformity of the flame, extent of flame propagation across or around the flowpath, static temperature and distribution of certain chemical species" [35].

2.2.1 Types of Non-Intrusive Diagnostic Techniques

Light based on refractive index and the phase-shift phenomenon can be used as a sensor for obtaining information about the distribution of concentration or temperature in a substance [37]. Along with the phase-shift, the phenomenon of scattering can also be used for obtaining

information concerning the chemical and physical conditions in a gas or a liquid. The different types of light scattering phenomena that occur are namely, Raman scattering, Rayleigh scattering and Fluorescence [37].

2.2.1.1 Rayleigh scattering

When a laser light impinges upon a molecule, it interacts with the electron cloud and bonds of that molecule, thus exciting the electron within the molecule to a highly unstable virtual level by absorbing the photon for moment. The electron afterwards immediately returns back to its ground state by emitting a photon. If the emitted photon has same energy or frequency and wavelength as compared to the incident photons of light, Rayleigh scattering will be observed [37]. Rayleigh scattering is characterized as being elastic in nature as the energy of the incident and emitted photos are same. As Rayleigh scattering is proportional to the total density of the flow and is not species specific, the amount of scattered light increases with the increase in the density of the flow being sampled. Thus the flow temperature can be deduced from the density if the species within the flow being sampled are known [36]. The Rayleigh scattering method is very sensitive to background sources of scattered light as the frequency and wavelength of the incident and radiated light (photon) are same. For performing measurements accurately, the particles causing the scattering should have less than one-tenth of a diameter of the incident light wavelength. “It’s due to this reason the Rayleigh scattering measurements are limited to non-reacting flow as the scattering cross-section is greatly affected by the density variation between the reactants, products and combustion intermediaries”. “Rayleigh scattering can be used for measuring temperature, density and gas velocity in high-speed flows” [36].

2.2.1.2 Raman Scattering or Raman Effect

Based on the above mentioned definition of scattering phenomenon, if the energy of the emitted photon, after the molecule is struck by an incident light, is higher or lower than that of the incident photon, Raman scattering occurs [36]. This shift in the energy or frequency between the incident and the scattered photon is termed as *Raman Shift* and is exactly equal to the difference between the initial and final energy state of the scattered photon [37]. The Raman shift or the frequency shift effect is characteristic of specie's own energetic structure. This relates a specific frequency shift effect to a specific molecule [37]. *Raman Spectroscopy* is a non-intrusive method based on the phenomenon of Raman scattering or Raman Shift and is used for measuring species concentration, concentration ratios and temperature of molecules. Raman-spectroscopy non-intrusive measurement technique can be applied to any transparent medium regardless of its physical state but is limited to liquid and gaseous medium in case of heat and mass transfer applications [37].

There are two types of Raman scattering, *Stokes* and *Anti-Stokes* scattering [38]. After scattering, if the final energy state of the molecule is higher than the initial state or the photon is emitted at a frequency lower than the incident photon, the frequency shift is termed as Stokes Shift [39]. This phenomenon is called Stokes Scattering [38]. If the final energy state of the molecule after scattering is lower than the initial state or the frequency of the emitted photon is higher than the incident photon, the frequency shift is termed as Anti-Stokes Shift and the phenomenon is called Anti-Stokes scattering [39]. Raman scattering signals even though weaker than Rayleigh scattering are insensitive to background scattering sources, as the scattered signal is shifted in frequency with respect to the incident light source [36].

2.2.1.3 Coherent Anti-Stokes Raman Spectroscopy (CARS)

In case of Raman scattering, the signals emitted are based on spontaneous transition of individual molecules and are spread in all directions giving them an incoherent nature [40]. "The total Raman signal collected from a sample is an incoherent addition of the signal from individual molecules" [40]. Detecting such widespread signals requires large light collection angles and very high powered lasers limiting the practical application of Raman scattering for propulsion devices [32].

The Coherent Anti-Stokes Raman Spectroscopy (CARS) is a nonlinear (i.e. scattered signal is not linearly related to the input laser intensity [41]) optical measurement technique based on Raman spectroscopy and can be used for simultaneous measurements of temperature and species concentration within combustion flows [32]. As compared to incoherent signals from Raman scattering, CARS signals rely on coherently driven transition and therefore total CARS signal comes from a coherent addition of the signal from individual molecules [40]. "CARS measurement technique is relatively well-understood and is thus a suitable probe for ground-based testing of practical air vehicle propulsion systems" [32].

In basic sense, CARS process is composed of three laser beams interacting with the sampling medium and producing fourth beam which is detected and analyzed [29]. The spectrum of this fourth beam contains information concerning temperature and composition of the gas [29]. Using CARS, properties of the sampling medium can be acquired at a very fast time resolution of the order of 10 ns and with good spatial resolution [32]. The three beams in CARS process are namely, pump beam at frequency $\boldsymbol{\omega}$ (p), stokes beam at frequency $\boldsymbol{\omega}$(s) and a probe beam at frequency $\boldsymbol{\omega}$ (pr). These beams interact with the sampling medium based on the non-linear properties of the system, to generate a coherent Anti-Stokes optical signal at the

frequency [**ω** (pr) + **ω** (p) - **ω** (s)] [42, 43]. The generated anti-stokes optical signal's strength can be greatly enhanced if the frequency difference between the pump and the stokes beam [i.e. **ω** (p) - **ω** (s)] is close to the Raman resonance or the Raman active vibrational frequency of the particle or molecule of interest within the medium [43]. The anti-stokes signal, generated during CARS process is like a coherent laser beam, which can be easily distinguished and separated from incident beams and collected with 90 percent efficiency [44]. This is in contrast to the signals obtained from Raman scattering which are incoherent and spread in all direction. Therefore, only a small portion of the total scattered signals can be collected [45]. CARS has been used to obtain static temperature measurements for supersonic combustions tests in the Direct-Connect Supersonic Combustion Test Facility (DCSCTF) at NASA Langley Research Center [28].

2.2.1.4 Laser Induced Fluorescence (LIF)

In combustion chemistry, the number of molecules playing significant role never exceeds 100 ppm [34]. At such low densities, Raman process is inappropriate for producing strong enough signal which can be detected and analyzed [34]. An alternative approach lies in utilizing the ability of the atoms and molecules to fluoresce [41]. The fluorescence scattering technique includes species selectivity provided by Raman scattering along with using exciting laser tuned to induce resonance in the molecule of interest. This enhances the scattering cross-section and therefore amplifies the signal strength by many orders of magnitude [45].

Fluorescence denotes the radiation emitted when an atom or molecule drops down after a spontaneous emission of photon from a higher energy level to a lower one [45]. The fluorescence occurs between the energy states having same electronic spin states [34]. Various

methods can be used for causing the atom of molecule to fluoresce but lasers are the preferred choice because of their ability to reach high temporal, spatial and spectral resolutions [41]. The lifetime of an atom or molecule demonstrating fluorescence is typically 10^{-10} and 10^{-5} seconds. Fluorescence is induced at a wavelength longer than the excitation wavelength and resonance fluorescence is induced at a wavelength equal to the excitation wavelength [41].

Laser-Induced Fluorescence (LIF) is a non-intrusive diagnostic technique used for measuring local concentrations in mass transfer processes or in chemical reactions along with temperature monitoring and instantaneous full-field velocity, pressure and density map [37, 41]. LIF consists of optical components for imaging the fluorescence light emitted after the molecule or atom has been electronically excited using a sheet of laser beam [46]. The wavelength of the laser is tuned to induce resonance in the substance or specie of interest, such as OH-radical in hydrogen combustion. LIF allows for a direct two-dimensional mapping of the species concentration and temperature with high spatial resolution, high temporal resolution and high sensitivity [45, 46].

The LIF set up (as shown in Figure 30) works by expanding and deforming the laser beam into a thin light sheet which travels through a narrow quartz-window into the reaction zone. It is in this thin light sheet of approximately 5 cm in height and less than 0.7 mm in thickness, where the fluorescence is produced. The fluorescence observed is captured in the direction perpendicular to the laser sheet using an imaging CCD-camera. The signal of camera is processed and transformed into pseudocolor pictures. Large quart-windows are required to get a good view of fluorescence area and the parts where no optical observations are required have to be painted black in color, so as prevent the damping of light scattering in reaction zone [37]. LIF has been used for point measurement in flames and in supersonic low pressure streams for

mixing studies. Also, in past few years, after the introduction of intensified 2-D charge couple device (CCD) detector arrays, LIF has primarily been used for flame and flow field imaging [45].

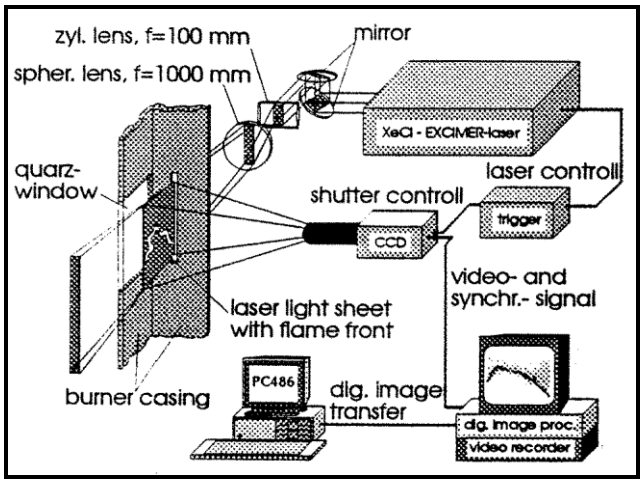

Figure 30: Optical System setup for Laser-Induced Fluorescence [37]

2.2.1.5 Planar Laser-Induced Fluorescence (PLIF)

The 2-D image obtained using LIF technique provides valuable information about structural and physical processes governing fluid dynamics. In most of the practical situations, a lot more information is desirable, such as multispecies measurements, for fully describing the thermodynamic parameters of the observed volume of interest. Also needed is an understanding of the correlations between different species' concentrations and their local variations. "The PLIF technique offers an advantage by easily combining itself with the other two-dimensional imaging techniques based on incoherent scattering processes such as Raman, Rayleigh, etc" [34].

"The planar laser-induced fluorescence (PLIF) working on the same principle as LIF technique and combining itself with other measurement techniques, allows for the imaging of scalar properties such as species concentration, temperature, velocity, pressure and density

shown in [34, 47]. For e.g. as shown in Figure 31, PLIF has been used in conjunction with Particle Image Velocimetry (PIV) measurements, for obtaining both temperature and velocity measurements for performing mixing or heat transfer studies at the scalar transport level [48]. PLIF too is a non-intrusive diagnostic technique with high spatial and temporal resolution used for probing harsh environments such as turbulent flames [34]. In PLIF, the fluorescence image captured by the CCD-camera can provide information regarding the structure of flow and combustion process which can influence combustor design. The image of the laser sheet interacting with the sampling medium and causing fluorescence provides instantaneous flowfield properties over a large number of points that are spatially resolved. A detailed study regarding the large scale and small scale turbulent structures occurring in both non-reactive and reactive flows can be performed based on the image obtained [34].

The use of PLIF for diagnostics requires good understanding of the physical and spectral behavior of fluorescence molecules. The selection of these molecules is governed by the type of physical process that needs to be investigated in the flowfield [34].

Fluorescent tracers are used to gain deep understanding of the complex physical processes such as flow generation, fuel injection and spray formation, mixing, ignition and combustion process occurring within a scramjet combustor. There are two types of fluorescent tracers namely, flame front tracers and fuel tracers [34].

The flame front of the reaction zone is a thin region of high local release rates, within which most of the combustion reaction takes place, converting fuel and oxidizer to combustion products. The high local release rates can be used as indicators of the flame front. The flame front in the non-premixed and premixed flame separates fuel and oxidizer and burned and

unburned gases, respectively. The OH radical is commonly used as flame front indicator or tracer [34].

Fuel tracers are used for flow visualization and for obtaining information about the fuel concentration distribution. If the fuel contains molecules that do not fluoresce, then tracer molecules are added which have very similar properties to that of fuel itself [34]

PLIF techniques have been employed, using OH-radical as a tracer, to study flame structure within a hydrocarbon fueled direct-connect supersonic combustion test facility [35].

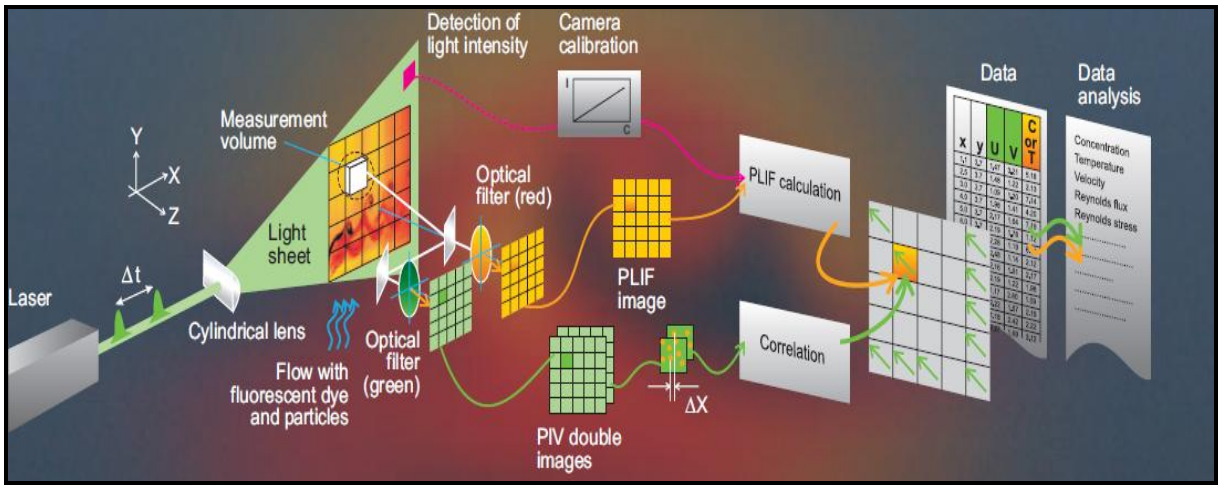

Figure 31: Working of PLIF Technique along with PIV Measurements [48]

2.2.1.6 Various Other Types of Non-Intrusive Diagnostic Techniques

The other types of non-intrusive diagnostic techniques are Laser Doppler Velocimetry (LDV) and Particle Image Velocimetry (PIV). These techniques are used for measuring the velocity of particles in the flow field [41]. The velocity range that can be measured is from zero to supersonic [49]. LDV technique has high spatial and temporal accuracy which makes it as a reference for comparing velocity measurements [41]. In LDV, simultaneous measurements can be obtained for all three velocity vectors along with flow reversal [49]. Further details about the LDV technique are given in [49]. The PIV with the use of CCD-camera can provide

instantaneous 3-D real-time velocity maps [50]. As compared to LDV, the PIV technique is fundamentally 2-D and its spatial resolution is much lower. The in depth details about PIV technique can be found in [41, 50].

2.3 Fuel Injection, Ignition, Flame-Holding and Mixing Enhancement Techniques

At such high flight speeds, the atmospheric air takes on an average about a millisecond to travel through the scramjet flow path from inlet to the nozzle exit. Therefore, it's required that the injected fuel and air mix at both macro and micro scales within tenth of millisecond and burn completely to produce maximum energy possible within the available combustor length [21]. With the combustor Mach number increasing, new methods of fuel injection are required, as conventional methods depending upon natural convective and diffusive processes to mix fuel and air lead to a decrease in overall efficiency and thrust. "To a large extent, for given conditions, the net heat release achieved in a scramjet combustor is driven by the efficiency and effectiveness of the fuel injection" [22]. Various fuel injection and flame holding methods have been developed and tested [20]. A trade-off exists between mixing effectiveness and pressure drop caused by the injection scheme within the scramjet combustor which governs the thrust available at the nozzle exit. Two most important aspects of fuel injection process are the degree of turbulent fuel penetration and fuel-air mixing and transport [22].

There are several key characteristics that a fuel injection scheme should possess for it to be efficient. The fuel injector and the injection process should result in minimum total pressure losses, so as to obtain maximum thrust. The injection scheme must produce rapid mixing and combustion of fuel and air thus minimizing combustor's length and weight [21]. This will result in a lighter craft having more payload carrying capacity. The injection process must provide a uniform fuel distribution profile at combustor's exit or nozzle's inlet resulting in an

efficient nozzle expansion. At flight speeds above Mach 10, the angle of injection should more or less be aligned with the freestream flow direction, as the fuel momentum would constitute a significant portion of the engine thrust. The fuel injector should have a provision for flame-holding, thus providing a stable piloting source for the downstream ignition. The injector design must not cause severe local flow disturbance as it would lead to increased frictional losses and hot spots, thus generating a need for severe wall cooling [21].

2.3.1 Passive Mixing Devices

Two most common approaches for fuel injection within a scramjet combustor are wall injection and in-stream injection [21]. Penetration depth of injected fuel is measured in terms of momentum flux ratio, which is ratio of jet-to-freestream momentum flux [22]. It was found by Schetz and Billing [51], that when fuel injection pressure is matched with that of surrounding or to the effective backpressure in the combustor, optimum penetration of fuel jet was achieved. The fuel-air mixing efficiency is defined by Mao, et al [52], as "that fraction of the least available reactant that would react if the fuel– air mixture were brought to a chemical equilibrium without additional local or global mixing" [22]. For the combustion process, adequate large-scale mixing of fuel-air and flame-holding is required for initiating and sustaining reaction between them [53]. For accelerating the rate of reaction, enhanced molecular level mixing is required [53]. In reactive mixing layers, the large scale mixing is governed by large-scale coherent turbulent structures, which control the mixing layer evolution [53]. Molecular level mixing is governed by fine-scale turbulent structures which are produced during the development of the mixing layer [53]. Commonly employed passive mixing devices are the ones having geometrical configuration such as ramps, struts, pylons and cavities. Out of these intrusive devices, the ramps, struts and pylons greatly enhance mixing but at the same

time require continuous cooling due to the formation of hotspots by the virtue of separated recirculation zone acting as a flame-holder.

2.3.1.1 Wall Injection

Wall injection is the simplest technique for fuel injection. Fuel can be injected at various angles through a hole or an array of holes in the wall. Various injector nozzle geometries have been designed and experimentally tested. Bayley, et al [54], has performed an experiment by injecting fuel at various angles to the supersonic stream and analyzing the injectant penetration and mixing. The simplest form of wall injection is transverse injection technique. The transverse injection of jets provides a rapid near-field mixing of fuel-air along with good fuel penetration. The interaction of jet with the oncoming flow produces a bow shock and a highly three-dimensional flow field. The formation of bow shock causes the upstream and the downstream flow near the wall to separate. These regions of reversed flow act as the radical production and flame-holding regions [21]. The normal injection of fuel, due to the bow shock formation causes significant loss in total pressure, leading to reduced scramjet cycle efficiency [55]. A perspective view of the normally injected fuel interaction with the mainstream is shown in Figure 32 [56].

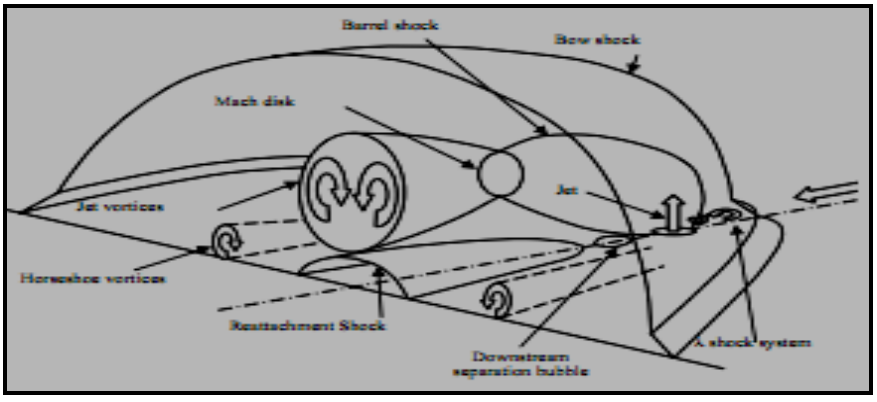

Figure 32: Normal Fuel Injection [56]

The fuel is injected through wall using either circular or non-circular orifices. According to [57], small-aspect-ratio elliptic nozzles showed better large-scale and small-scale mixing characteristics as compared to circular cross-section nozzle jet. Gutmark, et al [53] experimentally studied tapered slot nozzle which is a derivative of elliptical nozzle. "It consists of a conical contraction region that leads into the elliptic outlet" [53]. Tapered slot nozzle jet was found to have a higher turbulence in fuel jet core as compared to circular and elliptical nozzle jets [53]. Due to the change in the nozzle cross-section shape from conical section to the slot outlet, change in the flow direction occurred, resulting in the flow acquiring angular momentum, thereby generating axial vorticity [53]. The placement, number and sweep angle of holes also play a major role in the resulting mixing characteristics of the emerging fuel jets.

Various numerical and experimental studies have been performed on fuel injection through orifices with sharp leading edges, such as diamond or wedge shaped orifice [58-60]. Timioka, et al [58], performed experimental studies of the plume formed by sonic injection from a diamond-shaped orifice into a Mach 3 crossflow. It was concluded that, at lower jet-to-freestream dynamic pressure ratio, the fuel jet penetration was higher from a diamond-shaped orifice as compared to an equivalent circular injector. At high dynamic pressure ratios, the performance of diamond-shaped and equivalent circular injector were same [58]. Also, adding sweepback and a moderate yaw angle to the sweepback, greatly enhanced the penetration depth obtained using diamond-shaped injector, which is unlikely in the case of a circular injector [58]. Hirano, et al [59] studied fuel injection from various orifice shapes, namely, circular, diamond, wedge, arrowhead, rectangular and stringer. Following conclusions were drawn: mixing efficiency is higher in case of sharp leading edge injectors as compared to blunt leading edge injectors. The smaller the half angle of the wedge shaped injector, the larger is the fuel

penetration height. Based on the use of genetic algorithm, stringer shaped injector was proposed (shown in Figure 33), for reducing total pressure loss by preventing plume diffusion. Approximately 60 percent gain was obtained in penetration height with the use of stringer shaped injector as compared to circular injector but the penetration performance was obtained only at low jet-to-freestream dynamic pressure ratio unlike circular nozzle injector [59]. Kobayashi, et al [60] performed studies examining the effects of igniter torch flow on the near-field flow structure of a diamond-port flush wall injector in a supersonic crossflow. It was concluded that, diamond-shaped injector port geometry could be "tailored for improving mixing and producing an additional secondary flow structure with gasdynamic flame-holding potential", such that an igniter torch could be used without adversely affecting the tailored flow structure [60].

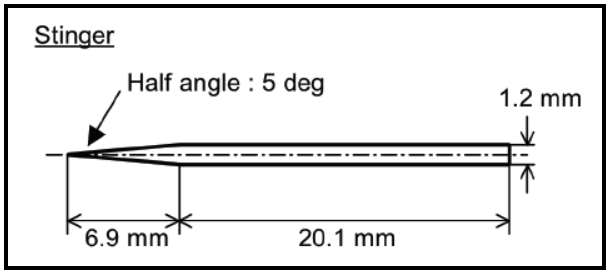

Figure 33: Stringer Shaped Injector Configuration [59]

2.3.1.2 Ramp Injection

Combustion can be achieved through wall injection in very short distances as the separated region upstream and downstream of the injector acts as flame holder. Wall injection, on the other hand causes significant total pressure losses, therefore, interest was turned to parallel or nearly parallel injection schemes as they result in lower total pressure loss [55]. The parallel injection schemes have lower combustion efficiency due to poor mixing at supersonic speeds, but as per Dimotakis [61], the mixing efficiency can be enhanced using parallel injection

scheme if it were accompanied with generation of axial vorticity [55]. These axial streamwise vortices produce turbulent fluctuations perpendicular to the flow, thus breaking down large 2-D flow structures into small turbulent vortices which enhance diffusion and mixing [62]. Wall injection techniques comprising of wedge-shaped geometrical structures, such as ramps or Hypermixers, can be used for inducing axial vorticity into the flowfield. The supersonic flow over a ramp or a hypermixer produces both expansion and shock waves leading to the generation of counter-rotating streamwise vortices (as shown in Figure 34) by the virtue of baroclinic torque. The baroclinic torque is generated when the pressure and density gradients are not aligned parallel to each other [55].

The fuel is injected from the base of the ramp, which also serves as a flame-holding and stabilization zone, thereby providing a stable piloting source for the downstream combustion through a radical pool buildup [21]. Stouffer, et al [63], tested expansion and compression ramp configurations (as shown in Figure 35-a) for determining the effects on supersonic combustion and heat transfer. It was concluded that expansion ramps, due to the improved local, small-scale mixing near the fuel injection port, produced higher combustion efficiencies. The overall mixing performance of expansion ramps was lower than compression ramps [64]. Further, the testing was performed at NASA Langley by adding a ‘sweep’ to the ramp fuel injectors for controlling shock and expansion waves (as shown in Figure 35-b) [64]. It was found that sweep enhanced spillage, thereby improving the vorticity generation as compared to unswept ramp configuration [22]. Also, swept ramp configuration demonstrated higher combustion efficiencies by lowering the shock angle [64].

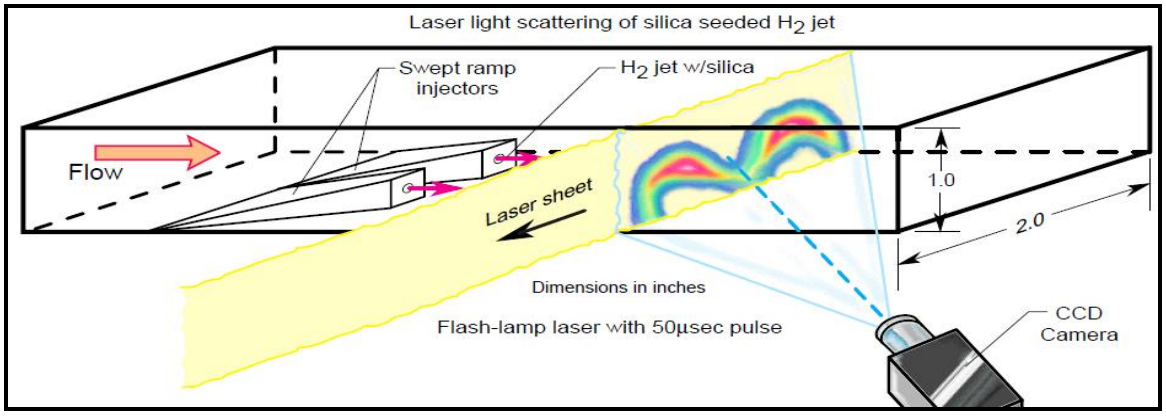

Figure 34: Ramp fuel injectors inducing a pair of counter-rotating streamwise vortices [28]

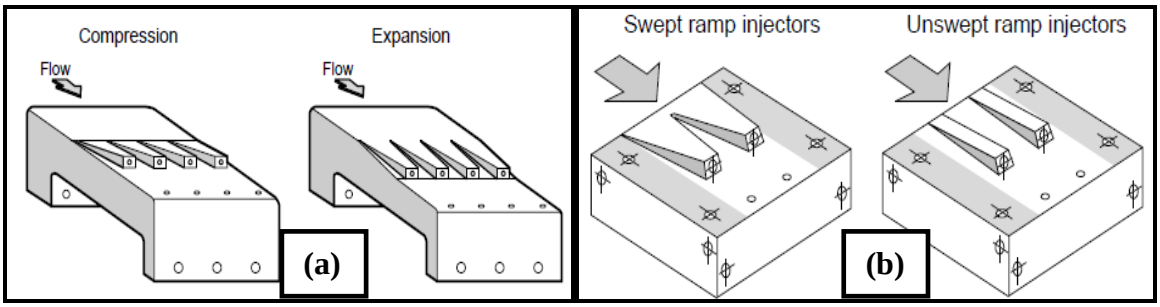

Figure 35: (a) Compression and Expansion [63]; (b) Swept and Unswept Ramp Fuel Injectors [28]

Another type of ramp injector configuration is the cantilevered ramp injector [65] (as shown in Figure 36). Cantilevered ramp injector derived from a conventional ramp injector, is "thought to embody both the characteristics of conventional ramp injector and that of low angled wall injector" [65]. The presence of two shock waves (A and B) further increases the baroclinic effect as compared to a conventional ramp injector, which in-turn increases the pressure gradient at the fuel-air interface, thereby generating strong longitudinal vortices enhancing large scale mixing efficiency [65]. Also, strong vortices (M and N), present behind the bluff-body further enhance the mixing process along with providing a flame-holding zone, similar to a low angled wall injection [65]. A numerical study has been performed by Sislian and Schumacher [66] comparing conventional and cantilevered ramp injectors. The following

inferences were drawn: mixing efficiency of cantilevered ramp injector for the considered flow conditions was 45 percent higher than that of conventional ramp at an expense of 20 percent total pressure loss, higher than conventional ramp [66].

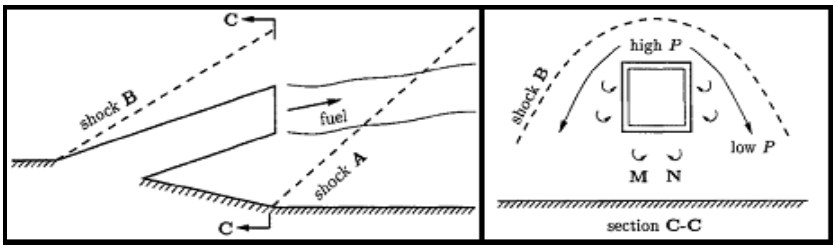

Figure 36: Schematic of Cantilevered Ramp Injector [65]

2.3.1.3 Struts Injector

Low angled wall injection or ramp injection techniques require high fuel injection pressure for gaining deep fuel penetration within the core of the crossflow [62]. Instead the struts can be used for injecting fuel directly into the core of mainstream with lower injection pressures [62]. A strut spans across the entire width or height of the combustor and attaches to both the combustor walls [62]. Apart from injecting fuel into the core of the mainflow, a strut injector promotes uniform spreading of the fuel in the lateral direction [67]. "The large scale structures present in the wake of the strut injector enhance macro-mixing" [67]. Also, the shock emanating from the leading edge of the strut reflects from the combustor walls and is useful for enhancing the mixing via baroclinic torque mechanism [67]. Another advantage of strut injector is the presence of recirculation region at the base of the strut which acts as a flame-holding zone [67]. In-stream injection from a strut results in a slower mixing as compared to the transverse injection. Therefore, approaches such as non-circular injector orifices, tabs and ramps can be used for increasing the mixing efficiency of the strut injector [21]. Desikan and Kurian [67] performed numerical and experimental analysis of various types of strut-based fuel

injectors (as shown in Figure 37), namely, plane strut (C-1), ramp-strut (C-2), straight castellated (C-3) and tapered castellated (C-4). They concluded that castellated injectors performed better compared to the other two injectors [67]. Tapered castellated strut injector outperformed all the other injectors with the enhanced mixing capability due to the increased vorticity strength produced by the tapered castellated portion [67]. Also, ramp-strut performed better as compared to the plain strut injector [67].

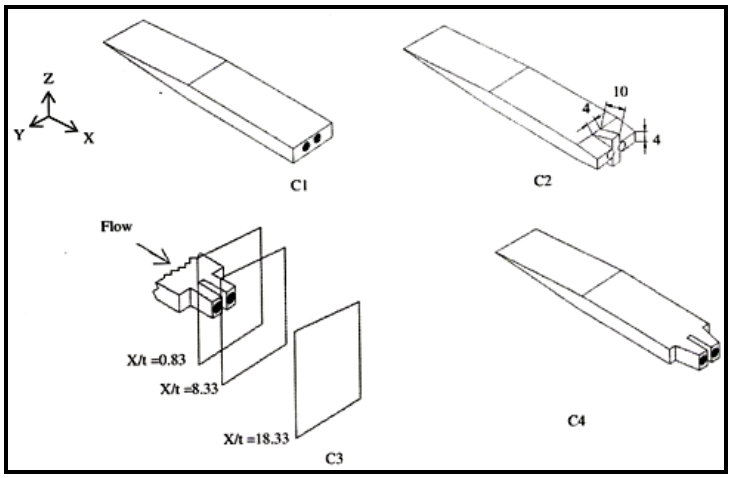

Figure 37: Different types of Strut-based Fuel Injectors [67]

2.3.1.4 Pylon Injectors

Pylon injectors like strut injectors are used for injecting the fuel within the core of the mainflow with lower injection pressures [62]. Injecting the fuel within the core of mainflow, aids to utilize the fuel momentum for gaining higher thrust output from the propulsion system. For optimized flight trajectories of scramjet-integrated aircrafts, higher equivalence ratios close to unity are required [68]. Such high equivalence ratios can be obtained by achieving a satisfactory fuel distribution across the combustor with the use of pylons [68]. The pylons rapidly form homogeneous fuel-air mixture across the whole flow cross section thereby providing compact reaction zones resulting in an efficient scramjet combustor [68]. Gruenig, et

al [68] experimentally tested various pylon injector configurations (shown in Figure 38). It was concluded that to obtain a homogeneous fuel distribution across the whole combustor's cross section, several fuel jets are preferred to single-jet injection [68]. Thus, pylon B had mixing and combustion efficiency far better as compared to the rest of the pylon configurations [68]. Also, the slot shaped injectors (C and D) resulted in higher mixing efficiencies than the circular-port pylon injector (A) [68].

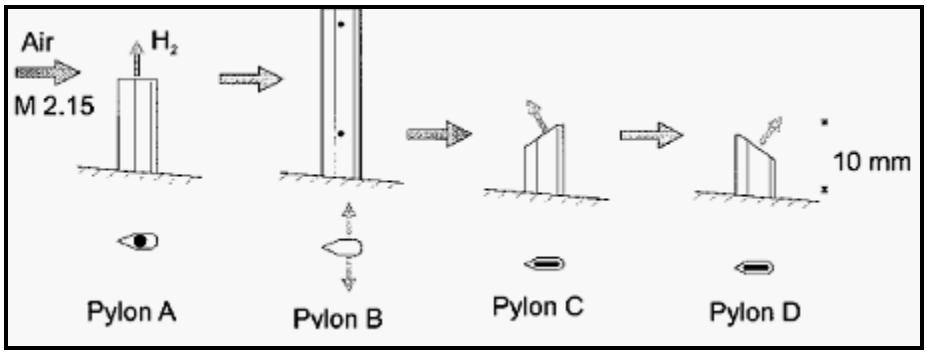

Figure 38: Various Pylon Fuel Injector Configurations [68]

2.3.1.5 Aero-ramp or Aerodynamic Ramp Injector with Plasma Torch Igniter

The birth of the "Aerodynamic Ramp" or "Aero-ramp" concept is credited to Dr. J.A. Schetz [69]. The idea behind the concept of aero-ramp injector was to come up with an injector design incorporating the features of both swept ramp and flush-wall injectors. As known, the swept ramp injector design provides efficient mixing enhancement by inducing strong streamwise axial vortices but at the expense of pressure losses and a requirement for thermal protection due to the creation of hotspots at the injector site. On the other hand, wall injection results in reduced pressure losses as compared to the swept ramp configuration but, at the same time provides poor mixing of fuel-air streams. Experiments were performed by Jacobsen, et al [70] on a three-holed flush wall injector array. The studies confirmed that the interference effects due to multi-hole injection result in mixing enhancement as compared to a single wall

injector. Moreover, it was found that increasing the toe-in angle of the exterior injector holes greatly enhanced mixing efficiency and core penetration by creating additional vorticity [70]. Thus, the aero-ramp injector incorporates swept ramp and flush wall injector effects so as to "cause the mainstream flow to go up and spill over the sides of the interaction region to induce helpful vortical structures" [69]. This negates the use of an intrusive physical structure within the high enthalpy flow, thereby, minimizing pressure and drag losses and the need for thermal protection. Fuller, et al [71], performed an experimental investigation to compare conventional swept ramp and aerodynamic ramp configuration. The aerodynamic ramp injector (as shown in Figure 39-b) used, consisted of nine flush-wall injectors arranged to produce strong, counter-rotating, streamwise vortices, which entrain air into the injectant stream and aid mixing [71]. The results showed that aero-ramp injector exhibited a significant increase in penetration with the increase in jet momentum, where as swept-ramp showed no noticeable change [71]. The aero-ramp also demonstrated a high near-field mixing efficiency as compared to swept-ramp, but the far-field mixing at high jet momentum were comparable for both injector configurations [71]. It was finally concluded that aero-ramp injector suffered losses lesser as compared to swept ramp configuration. These merits of aero-ramp configuration assert further parametric optimization studies to be carried out [71]. Schetz, et al [69], performed both computational and experimental investigation to parametrically study the effect of pitch, toe-in angle and hole spacing on previously mentioned nine-holed flush-wall aero-ramp injector configuration and confirmed that the mixing efficiency results obtained were exactly as anticipated. One very important deduction based on the study performed was the presence of both subsonic and reverse flow regions within the wakes of the first and second rows of injectors [69]. These

regions hold the potential for flame-holding, thus providing a fuel injection and flame-holding design which can negate the need for physical flame-holding devices such as cavities [69].

Jacobsen, et al [72] commented that the "sheltered channel" created within the wake of the aero-ramp injector jets as noticed by Schetz, et al [69] could be incorporated with plasma torch igniter. This sheltered channel could act as a suitable region for flame initiation and rapid spreading into the jet plume [72].

Weinberg [73] discussed that magnetically rotated plasma jets could be used for generating radicals at high temperatures for flame stabilization and high intensity combustion. Magnetically rotated plasma jets ensure uniform heating of the gas through which the arc traverses [74]. It also allows the control of downstream mixing rate within the combustor to be controlled by varying the degree of swirl and turbulence, which can be imparted to the gas by the arc rotation [74]. Harrison and Weinberg [74] performed experiments which convincingly demonstrated that "a small amount of electrical power supplied to a small volume of gas could be used to generate combustion-enhancing radicals and enhance a flame. The flame enhancement was identified to occur due to an early attack on the fuel by the plasma jet and higher concentration of combustion species [74]. Various gases could be used as feedstock for plasma torch igniter such as, nitrogen, argon, oxygen, and etc. It was noted by Weinberg "that the effectiveness of a particular plasma feedstock gas depends upon the application for which it is intended".

Kimura, et al [75], performed feasibility study on the use of plasma jet in supersonic air streams for stabilizing flame and promoting combustion of fuel jet. The conclusions were drawn that the performance of plasma jet is dependent upon its position [75]. The feedstock gases used are hydrogen and nitrogen, where nitrogen proves superior based on the input of

electrical power required [75]. Warris and Weinberg [76], asserted the application of plasma torch for high-speed flow combustors by noting that "plasma torches with choked orifices cannot be blown out, as the combustor conditions cannot propagate into the arc chamber". Kato and Kimura [77] performed numerical simulations which concluded that plasma torch can be used for flame stabilization within a scramjet combustor thus revoking the need for a step flame-holder. Also, the plasma jet injection slit when located downstream of the fuel injection slit required less input power than otherwise [77].

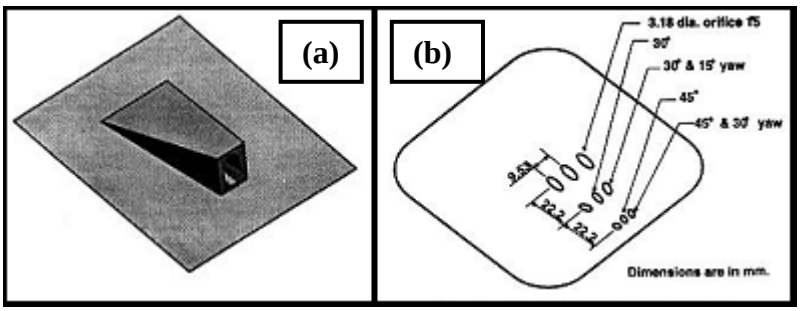

Figure 39: (a) Swept Ramp Injector; (b) Aerodynamic Ramp Injector [71]

2.3.1.6 Cavity

The efficient mixing of fuel and air alone does not directly initiate a combustion process [78]. Ignition and flame-holding are other two important factors governing the initiation of a combustion process. "Ignition is considered accomplished when sufficient free radicals are formed to initiate the reaction system, even though no appreciable heat has been released" [78]. Once ignition has been established, combustion efficiency is then governed by the mixing efficiency of fuel-air [78]. The primary role of the flame-holder is to provide sufficient residence time, act as a continuous source of radicals required for establishing ignition within the shortest distance and further sustain continuous combustion [78]. One of the commonly used integrated fuel injection and flame-holding techniques is cavity flame holders. The recirculation region within the cavity forms a hot pool of radicals which act as a piloting source

for initiating and maintaining sustained combustion process along with increasing the residence time of the fuel-air mixture entering in it [78].

Cavity flows can be subdivided into two categories, namely open cavity flow (Figure 40-a) and closed cavity flow (Figure 40-b). The type of flow prevailing within a cavity is primarily controlled by the length-to-depth ratio (L/D) of the cavity [78]. In both types of flow, a shear layer separates from the upstream lip of the cavity and reattaches to the downstream lip [78]. For L/D < 7-10, open cavity flow exists, as the upper shear layer reattaches to the downstream lip of the cavity thus permitting oscillations within the cavity [78]. For L/D > 10-13, closed cavity flow exists, as the free shear layer reattaches to the lower wall thereby isolating the recirculation zones [78]. Due to this phenomenon, the pressure at the aft wall of the cavity increases and pressure at the front lip of the cavity decreases causing large drag losses [78].

The critical L/D ratio which triggers the transition from open to closed cavity flow depends upon boundary-layer thickness at the leading edge of the cavity, mainstream Mach number and the cavity width [78]. The open cavity flows due to lower drag penalties prove to be good for flame-holding [78]. The ignition and flame-holding capability depends upon the flow prevailing within the cavity which in-turn is dependent upon the length and depth of the cavity [78]. The depth of the cavity governs the residence time required to initiate an ignition and the length governs the volume of radicals needed to sustain the combustion process farther downstream [78]. A cavity is characterized by having strong internal oscillations due to free shear layer impingement [78]. These oscillations result in an unstable cavity emitting shock waves that can be used to enhance mixing and ignition [78]. An unstable cavity on the other hand cannot be used for continuous flame-holding region [78]. For the purposes of flame-holding, the shear layer can be stabilized so as to result in a stable cavity that can sustain

continuous and stable combustion [78]. The stabilization can be attained by incorporating an oblique rear wall (shown in Figure 41-a) [78]. Stabilized cavity can then also improve mixing when a fuel jet injected upstream (shown in Figure 41-b) interacts with the strong trailing-edge shock of the cavity [78]. The oblique shock wave – jet interaction by the virtue of baroclinic torque enhances the molecular level mixing, which leads to higher jet spreading rate due to the shear layer growth which in-turn enhances the combustion efficiency [78].

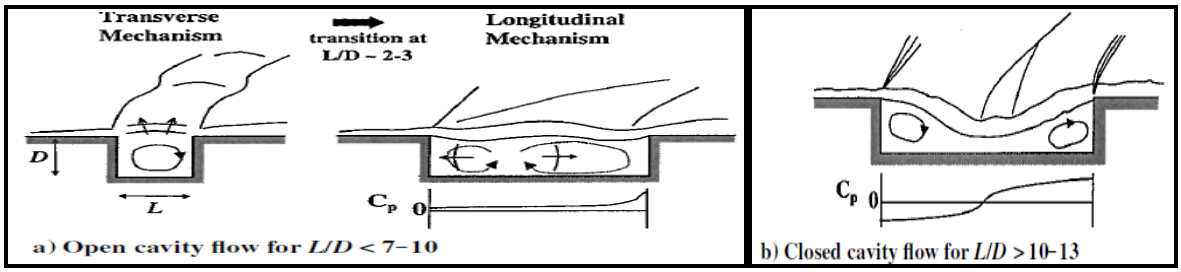

Figure 40: Types of Cavity Flowfield based on L/D ratio in Supersonic Flow [78]

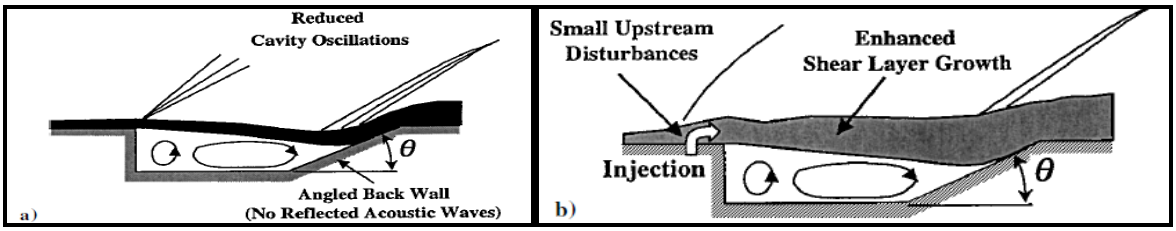

Figure 41: Concepts for stabilizing the cavity oscillations: (a) Angled rear wall and (b) Small disturbance produced upstream by a secondary jet [78]

2.3.2 Active Mixing Devices

Active mixing devices are the ones whose dynamic involvement in mixing enhancement can be controlled.

2.3.2.1 Pulsed Injector

Epstein and Kutschenreuter [79] were the ones who devised pulse injection concept. They determined that at extremely high flight Mach numbers and pressures of the mainflow entering the combustor, conventional continuous fuel injection method achieves only minimal

penetration into the mainflow resulting in poor mixing characteristics [79]. In a pulsed injector on the other hand, fuel is usually injected into the mainstream as a succession of pulses at elevated flow rates and pressure, for promoting fuel-air mixing [79]. Fuel is usually injected through a number of injectors simultaneously, such that the interaction of the multiple fuel pulses enhances fuel-air mixing [79]. The duty cycle and flow rate of these fuel pulses can be controlled to achieve equivalence ratio of unity [79]. Another beneficial effect of pulsed fuel injection concept is that the combustor operation process always remains in a transient state and never achieves steady state condition [79]. This transient condition of the combustor not only helps to further enhance fuel-air mixing, but also disperses the heat load within the combustor, thus simplifying combustor wall cooling requirements [79]. The Epstein and Kutschenreuter concept of pulsed fuel injector is shown in Figure 42, where the injector plate consists of a four-by-eight matrix of fuel injectors, out of which eight are simultaneously fired so as to generate fuel pulses [79].

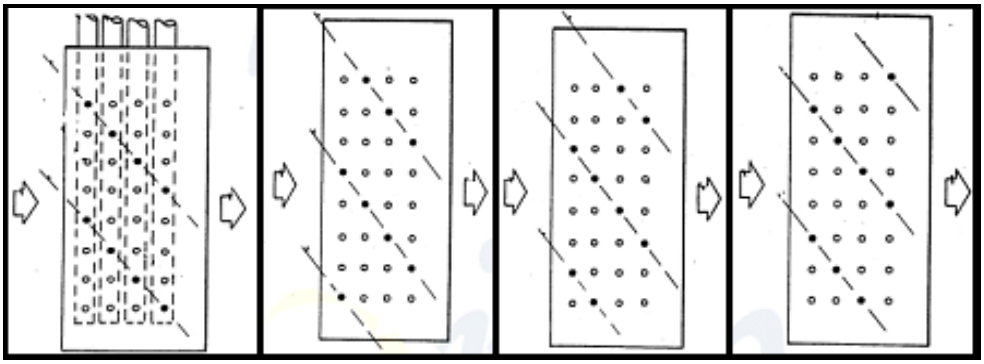

Figure 42: Schematic of the Pulsed Fuel Injection concept [79]

3 Quasi-One Dimensional Simulation

In this section, a system of generalized one dimensional continuous flow equations is developed to perform quasi-one dimensional simulation of a scramjet combustor.

The physical effects of interest in a scramjet combustor are the effects of area variation, wall friction, drag of internal bodies (e.g. strut injector, pylon injector), external heat exchange for non-adiabatic, i.e., cooled walls, chemical reaction, change of phase, e.g., evaporation of fuel and condensation of water, injection and mixing of secondary and main stream and changes in molecular weight and specific heat caused by combustion, evaporation and secondary injection.

The governing equations are derived based on the following simplifying assumptions:

i. The flow is quasi-one dimensional, i.e. the axis of the duct serves as the primary flow direction where the flow is assumed to be uniform in each plane normal to the axis, i.e., the primary flow direction
ii. The flow is steady
iii. The medium is a perfect gas, which obeys Boyle's and Charles' laws concerning mixture of gases.
iv. The gas is thermally-perfect that means the specific heats (and their ratio) vary with temperature and gas composition.

3.1 Physical Definition and Equations

The combustor or the duct is divided into thin slabs along its length. Within these sections, following phenomena are considered to occur: gaseous and liquid mass injection with evaporation of liquid stream, area variation, energy exchange in the form of external heat

transfer and shaft power as well as internal chemical reaction due to combustion, drag of a submersed body, change in gaseous composition due to secondary mass injections and chemical reaction. An excellent description of the flow model is derived in Shapiro [3].

(a) Equation of State

The fluid in the main stream is assumed to be a perfect gas with the equation of state:

$$p = \frac{\rho \bar{R} T}{W} \tag{2}$$

The logarithmic derivative of the perfect gas law is:

$$\frac{dp}{p} = \frac{d\rho}{\rho} + \frac{dT}{T} - \frac{dW}{W} \tag{3}$$

The molecular weight, W is that of the main stream flow. The change in molecular weight is due to secondary mass injections, vitiated inlet main stream flow and a change in species concentration due to combustion.

(b) Speed of Sound and Mach number

The speed of sound in a perfect gas follows:

$$a^2 = \gamma \bar{R} T / W \tag{4}$$

The logarithmic derivative of equation 4 is:

$$\frac{da}{a} = \frac{1}{2}\left(\frac{d\gamma}{\gamma} + \frac{dT}{T} + \frac{dW}{W} \right) \tag{5}$$

Based on the definition of Mach number and speed of sound, i.e., equation 4, the logarithmic derivative of Mach number is expressed as:

$$\frac{dM^2}{M^2} = \frac{dV^2}{V^2} + \frac{dW}{W} - \frac{d\gamma}{\gamma} - \frac{dT}{T} \tag{6}$$

(c) Equation of Continuity

The conversation of mass in a uniform steady flow is governed by:

$$\dot{m} = \rho A V \tag{7}$$

In equation 7, $\dot{m}$ is the mass flow rate of the main stream. The formulation in the quasi-one-dimensional method allows for the injection of gaseous and liquid streams in the main flow. The injection process is modeled by terms like $d\dot{m}_g / dx$, which introduces a change in gaseous flow rate in the primary flow direction, or by $d\dot{m}_L / dx$ which identifies the change of liquid flow rate along the duct. Perfect mixing of the injected flow and the mainstream is also assumed in quasi-one-dimensional flow modeling.

Writing continuity equation 7 in logarithmic differential form, we get:

$$\frac{d\dot{m}}{\dot{m}} = \frac{d\rho}{\rho} + \frac{dA}{A} + \frac{dV}{V} \tag{8}$$

In equation 8, $d\dot{m}$ indicates the change in the mass flow rate in the main stream due to injection of gaseous and evaporated liquid, i.e.,

$$d\dot{m} = d\dot{m}_L + d\dot{m}_g \tag{9}$$

Again in equation 8, *dA* refers to the change in the cross-sectional area of the duct along an infinitesimal duct length *dx*. This area variation represents the primary duct geometry and not the injection cross sectional areas where the secondary mass injections take place.

(d) Conservation of Energy

The law of conservation of energy applied to an infinitesimal section of the duct, neglecting gravitational effects, may be expressed as:

$$\frac{dT}{T}+\frac{\gamma-1}{2}M^2\frac{dV^2}{V^2}=\frac{dQ-dW_x+dH}{c_pT} \qquad (10)$$

The terms on the right-hand-side of equation 10 are the driver terms that cause a change in fluid total enthalpy. These terms account for an external heat exchange, dQ, mechanical work exchange, dW_x and the contribution of secondary injection in chemical reaction and phase change, dH. The latter term is expressed as:

$$dH=dh_{pr}-\left[\bar{c}_{pg}(T-T_{0g})+\frac{V^2}{2}\right]\frac{d\dot{m}_g}{\dot{m}}-\left[h_L-h_V+\frac{V^2-V_L^2}{2}\right]\frac{d\dot{m}_L}{\dot{m}} \qquad (11)$$

The term dh_{pr} on the RHS of equation 11 accounts for the enthalpy change in an infinitesimal control volume, due to a chemical reaction that forms products from known reactants. The term dh_{pr} is computed per unit mass of the main gas stream. However, the chemical reaction is not spontaneous and is a complex process that depends on the type of fuel, the mixing effectiveness of fuel and air, evaporation of liquid fuel and reaction rates of the species in the combustible mixture of gases. Here, the quasi-one-dimensional model needs an empirical input that depicts a heat release profile downstream of the injection ports in the scramjet combustor. The heat release profile may be expressed as combustion efficiency that is empirically derived for different fuels. Combustion efficiency data implicitly accounts for: (a) effects of fuel-to-air ratio, (b) method of fuel injection, which impacts the quality of fuel penetration, (c) ignition delay, (d) chemical kinetics and (e) mixing level achieved between reactants [80]. In the present report, gaseous injection of hydrogen as fuel is considered.

The flowfield enthalpies are calculated based on the specific heat of the main stream flow, which is a mixture of various individual species of perfect gas. In the present quasi-one

dimensional model, a simplified combustion model that assumes chemical equilibrium of a limited number of major species like O_2, N_2 and H_2O is considered [81].

The specific heat of individual species or gases used to compute specific heat of the main stream flow is calculated using molar specific heat polynomials as given in [82]. These polynomials consider individual gases to be thermally perfect.

(e) Conservation of Momentum

The viscous momentum equation for a quasi-one dimensional flow with injection is:

$$\frac{dp}{p}+\frac{\gamma M^2}{2}\frac{dV^2}{V^2}+\frac{\gamma M^2}{2}\left(4f\frac{dx}{D_h}+\frac{dX}{\frac{\gamma}{2}pAM^2}\right)+\gamma M^2(1-y)\frac{d\dot{m}}{\dot{m}}=0 \qquad (12)$$

The last term in the above expression is the contribution of angular injection of secondary streams to momentum, namely,

$$(1-y)\frac{d\dot{m}}{\dot{m}}=(1-y_g)\frac{d\dot{m}_g}{\dot{m}}+(1-y_L)\frac{d\dot{m}_L}{\dot{m}} \qquad (13\text{-a})$$

Where

$$y_g=\frac{V_g}{V} \quad and \quad y_L=\frac{V_L}{V} \qquad (13\text{-b})$$

In equation 13(a), the terms y_g y_g and y_L y_L account for the angle of injection. Skin friction coefficient for the wall, *f*, is taken from Anderson [83]. From the definition of hydraulic diameter, we relate the duct wetted area and flow cross sectional area as:

$$\frac{dA_w}{A}=4\frac{dx}{D} \qquad (14)$$

(f) Equation for Impulse Function

$$\frac{dF}{F} = \frac{dA}{A} + \frac{dp}{p} + \frac{\gamma M^2}{1+\gamma M^2}\frac{dM^2}{M^2} + \frac{\gamma M^2}{1+\gamma M^2}\frac{d\gamma}{\gamma} \tag{15}$$

An increase of impulse function in the streamwise direction indicates a force that is exerted on the (internal) walls of the duct by the main stream, which acts in the opposite direction to the flow, i.e., in the drag direction.

(g) Entropy Variation

The entropy variation in a perfect gas with no chemical reaction is expressed as:

$$\frac{ds}{c_p} = \frac{dT}{T} - \frac{\gamma - 1}{\gamma}\frac{dp}{p} \tag{16}$$

Using the above equations, fourteen differential variables can be grouped into six independent and eight dependent variables. The dependent and independent variables are then connected to each other through influence coefficients. Shapiro [3] has a list of these influence coefficients in Table 8.1 of chapter 8. For the sake of brevity, we will not include the table of influence coefficients in this report.

4 2-D Computational Fluid Dynamic Simulations

Computational Fluid Dynamics (CFD) is a computational tool specifically developed with the purpose to solve the complex fluid dynamics problems. It uses numerical methods and algorithms mostly finite volume method to get approximate solution to various fluid problems, for example fluid flow in an engine. Over the years, the continuous development and software implementation of CFD codes has led to the solution of myriad of fluid dynamic problems along with proving its worth as an invaluable tool for design and analysis in high speed propulsion devices [84].

CFD plays several roles serving as an engineering tool for the detailed design and analysis of hypersonic propulsion system. The flowfield measurements obtained from ground testing fail to properly provide a detailed analysis and visualization of the flow field. As for the intrusive measurements, they can only provide data for the points where flow touches the boundaries, such as wall static pressure using pressure transducers. The optical non-intrusive diagnostic techniques even though better than intrusive measurement techniques can only provide the flowfield visualization and flow properties at discrete points. CFD overcomes these shortcomings by providing a detailed visualization of the entire flow field. In addition, CFD is used for performing parametric studies during the conceptual design phase of hypersonic propulsion system. CFD techniques are also used for assessing the effects of the ground-test facility on the simulation [24].

4.1 Governing Equations

Computational Fluid Dynamics is based on the fundamental conservation laws governing fluid flow, i.e., conservation of mass, momentum and energy. The equations representing chemically reacting single phase flows are Navier-Stokes equations coupled with species mass

continuity equations. The specie mass continuity equation is for (n-1) species, where (n) is the total number of species considered in the reaction.

$$\frac{\partial \rho}{\partial t} + \frac{\partial (\rho u_j)}{\partial x_j} = 0 \tag{17}$$

$$\frac{\partial (\rho u_i)}{\partial t} + \frac{\partial}{\partial x_j}\left(\rho u_i u_j + \partial_{ij} P - \tau_{ij}\right) = 0 \tag{18}$$

$$\frac{\partial (\rho E)}{\partial t} + \frac{\partial}{\partial x_j}\left(\rho H u_j + q_j - \tau_{ij} u_i\right) = 0 \tag{19}$$

$$\frac{\partial (\rho X_m)}{\partial t} + \frac{\partial}{\partial x_j}\left(\rho X_m u_j + \rho X_m V_j\right) = \dot{w}_m \tag{20}$$

In the above given equations 17 to 20, ρ is the density, P is the pressure, u_i is the velocity, E is the total energy which is equal to the sum of total internal energy and kinetic energy, H is total enthalpy which is equal to the sum of total internal energy and pressure-volume work, τ_{ij} is the stress tensor, q_j is the heat flux vector and X_m, V_j and $\dot{w}_m$ are mass fraction, mass diffusion velocity, and mass production rate, respectively of species "m" [84].

4.2 Turbulence Modeling

A turbulent reactive flow as present within a scramjet combustor is characterized by having fluctuations in the flow field varying in space and time [85]. Turbulent flow process is a highly three-dimensional, unsteady and has an infinite number of scales. "Turbulence occurs when the inertial forces in a fluid grow higher as compared to viscous forces". The occurrence of turbulence causes the transported properties such as momentum, energy and species concentration to fluctuate [85]. These fluctuations can be of small-scale in nature with a high frequency of occurrence, making them very hard and computationally expensive to simulate

using exact form of governing equations. Therefore, the exact forms of governing equations are modified by applying Reynolds-averaging or time-averaging and thereby removing the need for simulating small-scale turbulent fluctuations. The resulting set of modified equations is known as the Reynolds-averaged Navier-Stokes (RANS) equations. The RANS equations due to modification contain additional unknown variables that need to be assessed. Turbulence models are used for determining these unknowns in terms of known quantities and thus providing a "closure" for the unknown variables. The choice of turbulence model depends upon several factors such as, the flow physics that needs to be simulated, level of accuracy required and the computational resources available [85].

The Reynolds averaging is performed by decomposing flow variables into the mean or time-averaged component and fluctuating component. The governing RANS equations are obtained by substituting the above decomposed form of flow variables into the instantaneous or exact form of equation from 17 to 20 and are given in [85].

For turbulence modeling in this thesis, Realizable k-ε, two-equation model has been used. The two transport equations are for turbulent kinetic energy (k) and turbulence dissipation rate (ε). The solution of these transport equations helps determine turbulent velocity and length scales independently. The Realizable k-ε model is an improvement over the standard k-ε model as it simulates the turbulent flow physics more realistically as compared to standard k-ε or RNG k-ε, hence the word "realizable" is used for defining the model [85]. As given in [85], Realizable k-ε model accurately simulates the spreading of both planar and round jets. It also provides superior performance for simulating flows involving rotation, boundary layer separations under strong adverse pressure gradients (as in the presence of shock waves), and recirculation. Studies performed have shown Realizable k-ε to outperform standard and RNG

k-ε for simulating separated flows and flows with complex secondary flow structures, such as present within a scramjet combustor. The Realizable k-ε model provides reasonable compromise between accuracy and robustness for simulating supersonic flows. The transport equations for Realizable k-ε model are given in [85]. For the research working concerning this thesis, the commercial CFD code – "FLUENT" has been used for performing numerical simulations.

4.3 Combustion Modeling

The combustion modeling has been performed using the commercial code – "FLUENT" as a platform. Generalized finite-rate approach has been followed, where the transport equations for species mass fraction are solved. The reaction rates appearing in the source terms in the species transport equations are computed from Arrhenius rate parameters. The reaction modeling has been performed using laminar finite-rate model, wherein the effect of turbulent fluctuations is ignored, and reaction rates are determined by Arrhenius parameters [85]. Combustion chemistry has been simulated using global one-step reaction mechanism. The Arrhenius rate parameters, governing the rate of reaction progress have been taken from [86]. The global one-step reaction mechanism is non-reversible. The equations for laminar finite-rate model are given in [85] for the calculation of chemical source terms occurring within the transport equations for species mass fraction.

4.4 Physical Model

The combustor geometry of the Scramjet Combustion Chamber at DLR is the same as given by Oevermann [1] and is shown in Figure 43. Vitiated air enters through the inlet, with hydrogen injected parallel to the air stream through 15 holes, each with a diameter of 1mm at the base of the wedge, as shown. The upper combustor wall has a 3 degree divergence angle so

as to prevent thermal choking of the duct due to the heat released by the combustion. The inlet conditions for the vitiated air and for the hydrogen injection are taken from Oevermann [1].

The inlet stagnation temperature and pressure for the vitiated air is 612 K and 7.825 bar respectively. The hydrogen injection conditions are adjusted so as to obtain a sonic injection with a mass flow rate to maintain the equivalence ratio of 0.0125 [87]. The temperature and pressure are high enough to produce auto-ignition of the hydrogen-air mixture.

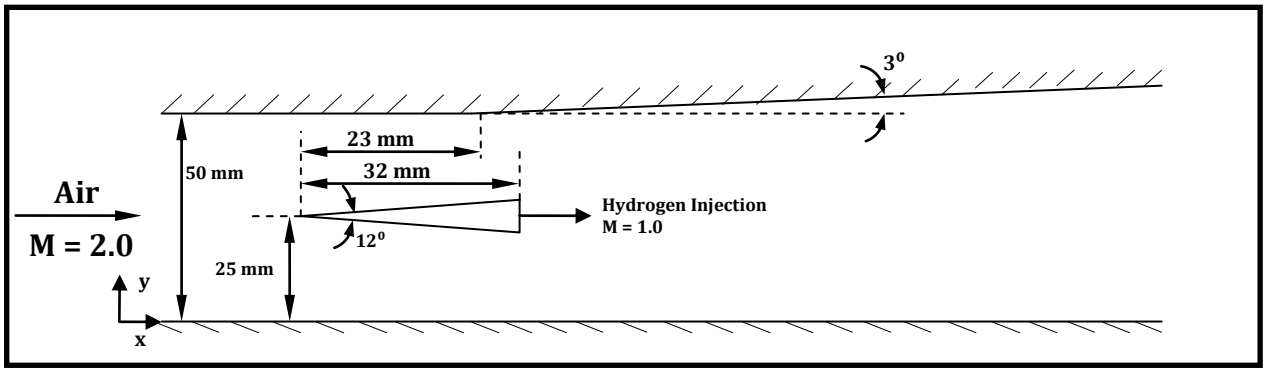

Figure 43: Scramjet Combustion Chamber at DLR [1]

NASA's SCHOLAR supersonic combustor's geometrical and constructional details are described by Rodriguez [88] and shown in Figure 44. The combustor consists of a constant area isolator section from left to right, ending in a small outward step at the top wall. There are five pilot fuel injector holes located ahead of the step and the main fuel injector located just downstream of the start of 3 degree divergence, as shown in Figure 44.

The stagnation conditions at the entrance of the duct are 0.765 ± 0.008 MPa and 1,827 ± 75 K for pressure and temperature, respectively. The inlet air stream Mach number is 1.989 ± 0.005 with static pressure and temperature of 100 ± 1.5 kPa and 1,187 ± 60 K respectively. The hydrogen fuel is injected at a Mach number of 2.5. The stagnation conditions for the injector are 3.44 ± 0.07 MPa and 302 ± 4 K. The resulting equivalence ratio is 0.99 ± 0.04 [88]. The

static pressure and temperature at the injector exit are 0.202 MPa and 133 K respectively [89]. Temperatures are high enough to cause auto-ignition of hydrogen-air mixtures.

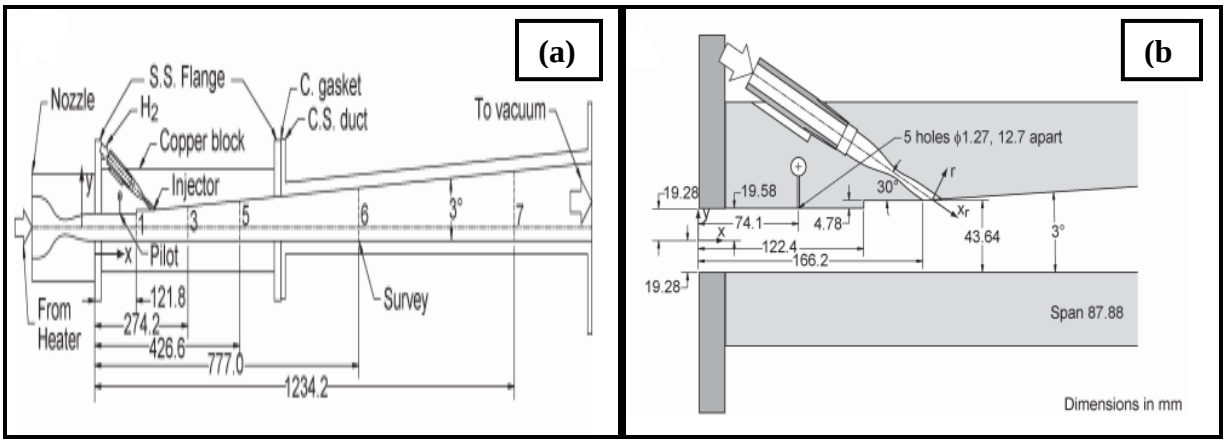

Figure 44: Fig. 2 Layout of NASA's Scholar scramjet combustor: (a) nozzle and complete combustor, (b) detailed view of the main injector region (all dimensions are in mm) [90]

4.5 Numerical Simulation and Boundary Conditions

The 2-D viscous numerical simulations for both combustor configurations have been performed using the commercial CFD code - FLUENT.

For DLR scramjet combustor, which employs a triangular wedge shaped strut injector; two different 2-D structured meshes consisting of 43500 and 87,000 (as shown in Figure 45) cells are constructed for performing simulations and to check for grid independence of the obtained results. The grid packing near the wall region is used to resolve the turbulent boundary layer for the wall function formulation. Also, the grid packing scheme is used in the wake region to resolve the mixing and diffusion effects of hydrogen effectively [87]. Density based on second order finite volume discretization method using explicit solver has been employed. The governing equations in FLUENT are the Reynolds-averaged Navier-Stokes, turbulence model and species continuity equations. The realizable k-ε turbulence model is used with default values of constants like turbulent Prandtl and Schmidt numbers. Turbulence and chemistry

interaction model chosen is laminar finite-rate with the hydrogen-air reaction being simulated using one step global reaction model. The Arrhenius parameters governing the reaction rate for one step global reaction mechanism have been taken from Hsu and Jemcov [86]. The turbulence at the combustor inlet and at the exit of the injector is specified using k and ε. The properties of hydrogen-air mixture have been calculated using mass-averaged mixing laws for mixture of perfect gases. For individual fluids, properties like viscosity and specific heat capacities are calculated using Sutherland's law and 5^{th} order polynomial function of temperature, respectively. Wall surfaces have been considered adiabatic with no slip condition and standard wall functions have been used. Near wall mesh has been chosen so that wall y^+ values are less than 100. This is an acceptable value for turbulent calculations with standard wall functions [87]. The complete flow domain within the combustor has been initialized using the prescribed inlet conditions from experimental data.

As the flow within the computational domain is supersonic, hence all the variables at the outlet boundary are calculated from the extrapolation of interior domain values. Also, grid adaptation was used based on pressure gradients, so as to capture the shocks and the boundary layer separation due to shock impingement by refinement of the near wall mesh.

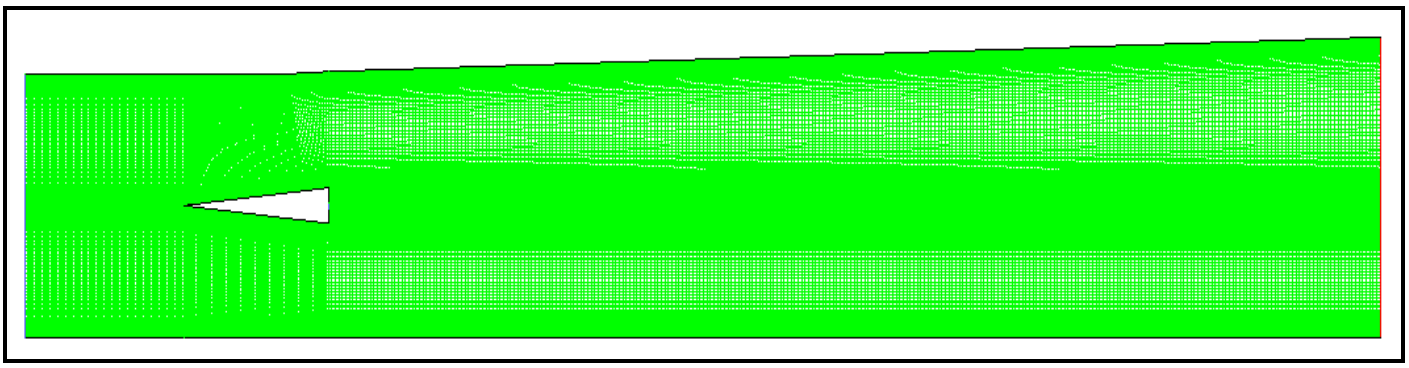

Figure 45: Structured Mesh for DLR Scramjet Combustor consisting of 87000 Cells

For the second combustor case i.e. NASA's SCHOLAR Supersonic Combustor; two different 2-D structured meshes consisting of 87,350 and 174,700 (as shown in Figure 46) cells are constructed for performing simulations and to check for the grid independence of the obtained results. The grid has been made dense near the wall region for properly resolving turbulent boundary layer formulation with wall function. Most of the numerical modeling parameters and boundary conditions are same as used in the above case except the following: a) Turbulent Prandtl and Schmidt numbers both are equal to 1.0 [88]. b) Wall surfaces have been considered as non-adiabatic with no slip, where wall temperatures for copper and carbon-steel sections have been maintained at 400 K and 700 K respectively. c) For turbulence modeling, Realizable k-ε with non-equilibrium wall functions has been used. Near wall mesh has been chosen so that wall y^+ values are between 30 and 300, based on the requirement of using non-equilibrium wall function [85], d) Turbulence at the inlet of the combustor is specified using turbulence intensity and turbulent viscosity ratio equal to 2 percent and 200, respectively [88]. e) Turbulence at the outlet of the hydrogen injector is specified using turbulence intensity of 2.75 percent and hydraulic diameter of 7.6 mm and calculated based on the relations given in reference [85].

The convergence criteria chosen for obtaining 2-D numerical solution for the above mentioned two test cases is based on: a) residuals of the flow properties are less than 10^{-4} or no change in the residual value is observed for around 2000 iterations, b) the profile of wall static pressure becomes invariant with iterations and c) global mass balance is obtained between inlets and outlets.

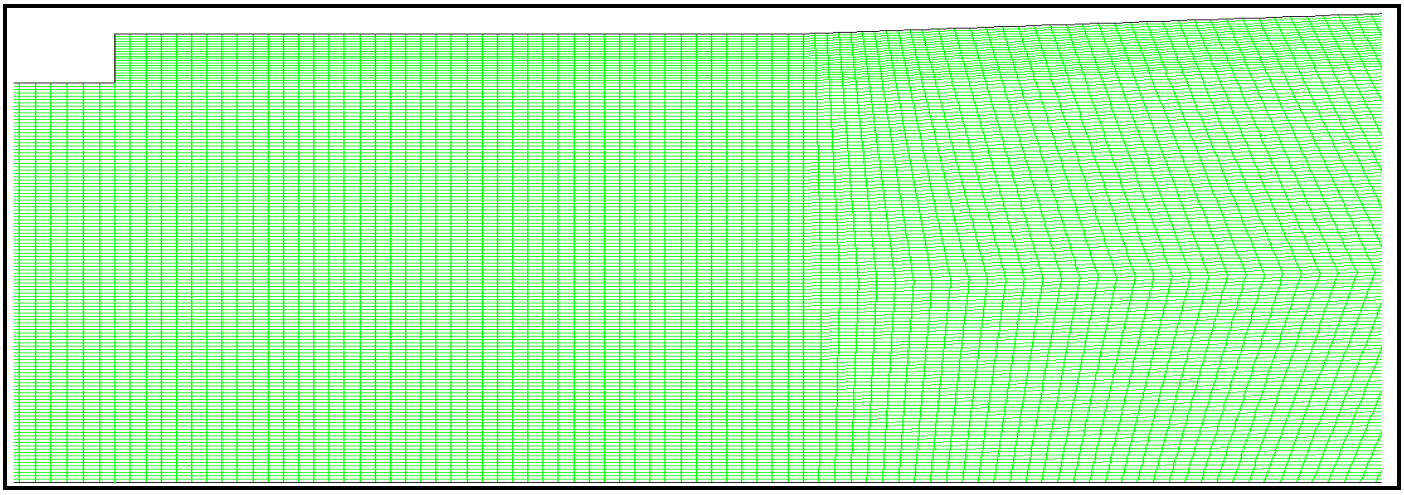

Figure 46: Close view of the step region in NASA's Scholar Combustor's mesh domain consisting of 174,700 cells for highlighting the regions which employ grid packing.

5 Results and Discussion

5.1 Test Case 1: NASA's Scholar Scramjet Combustor

In this section, results have been presented for computational simulations of NASA's Scholar supersonic combustor. The 2-D numerical simulation has been performed using FLUENT as a platform for only "Cold Flow" or "Fuel OFF" case. The 1-D simulation has been performed for both cold flow i.e. "Fuel-OFF" and combustion i.e. "Fuel-ON" case. Finally, comparisons have been drawn between 1-D and 2-D computational and experimental results for static pressure, static temperature and Mach number variation along the length of the combustor.

Grid independence study has been performed for NASA Scholar scramjet combustor by constructing two different 2-D structured meshes consisting of 87,350 (Mesh 1) and 174,700 (Mesh 2) cells. 2-D numerical Simulations have been performed for "Cold Flow" case (i.e. without fuel injection and combustion) and the results obtained for static pressure along the combustor centerline are compared to check for grid independence. Based on the results, the difference between the values of the centerline static pressure for Mesh 2 along the combustor's length with respect to Mesh 1 is of the order of 10^{-4}. The 2-D FLUENT simulation results presented in the next section 5.1.1 are based on the 2-D structured mesh consisting of 174700 cells.

5.1.1 Simulation Results

- **Cold Flow or "Fuel OFF" Simulation:**

Results for cold flow or "Fuel OFF" condition have been presented for Mach number in Figure 47-48, static pressure in Figure 49-50 and static temperature in Figure 51-52.

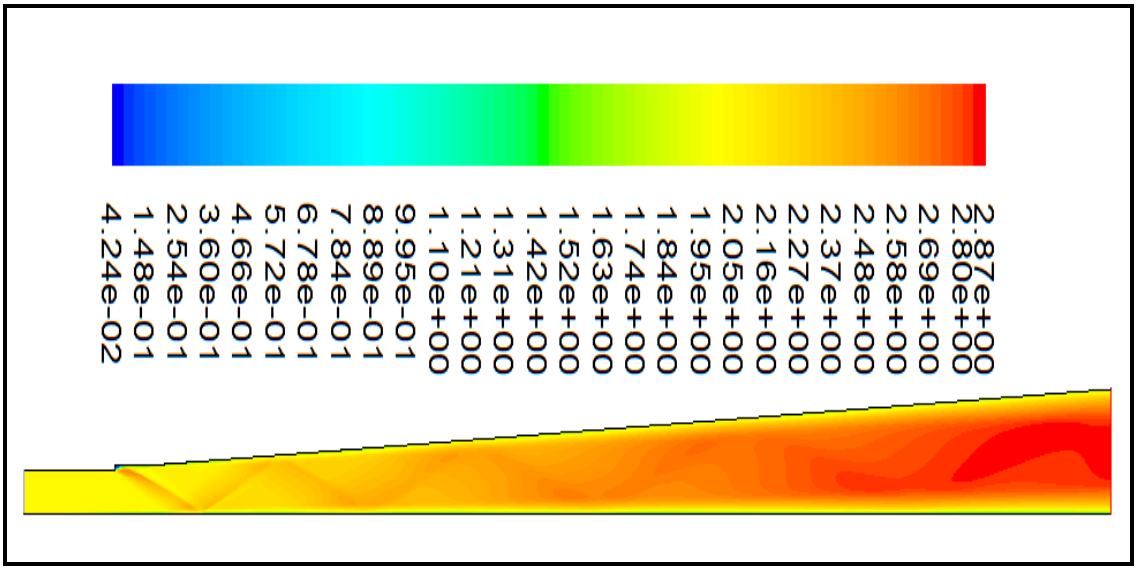

Figure 47: Mach number Contours for 2-D Cold Flow Simulation

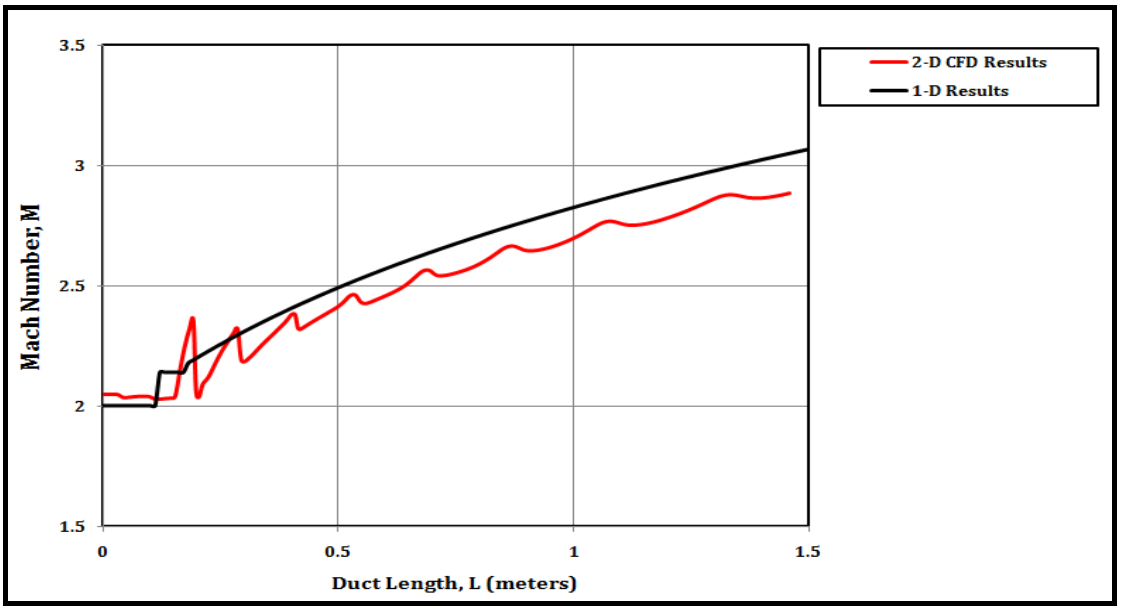

Figure 48: Mach number comparison for "Fuel OFF" case

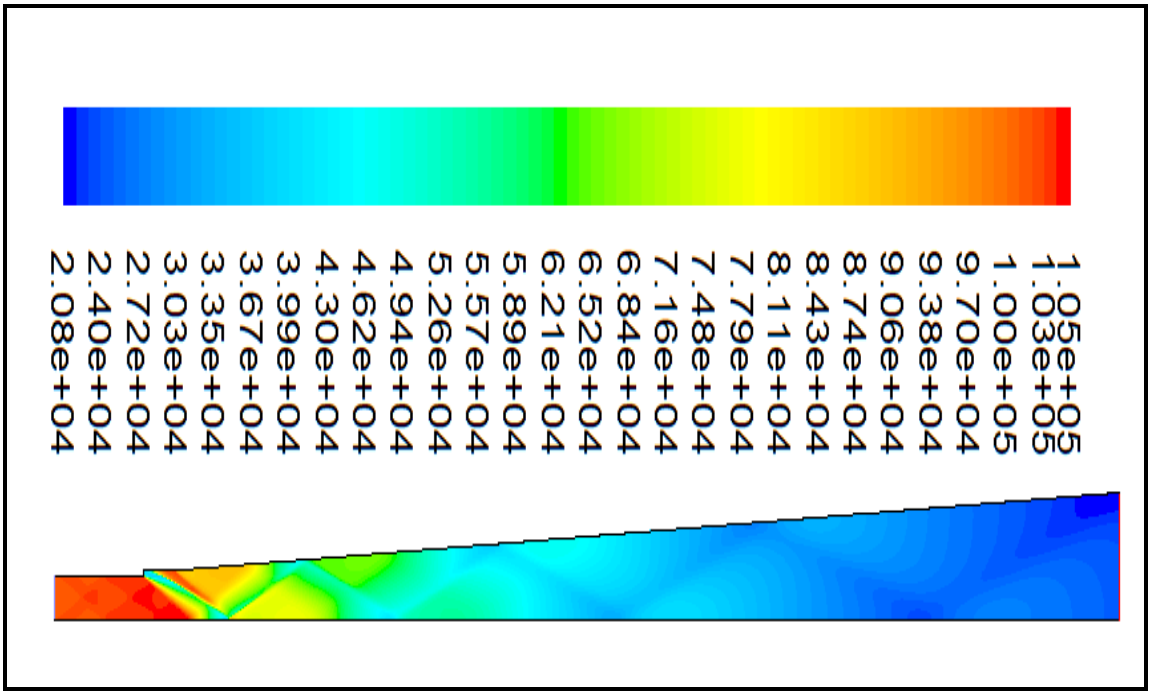

Figure 49: Static Pressure (Pascal) Contours for 2-D Cold Flow Simulation

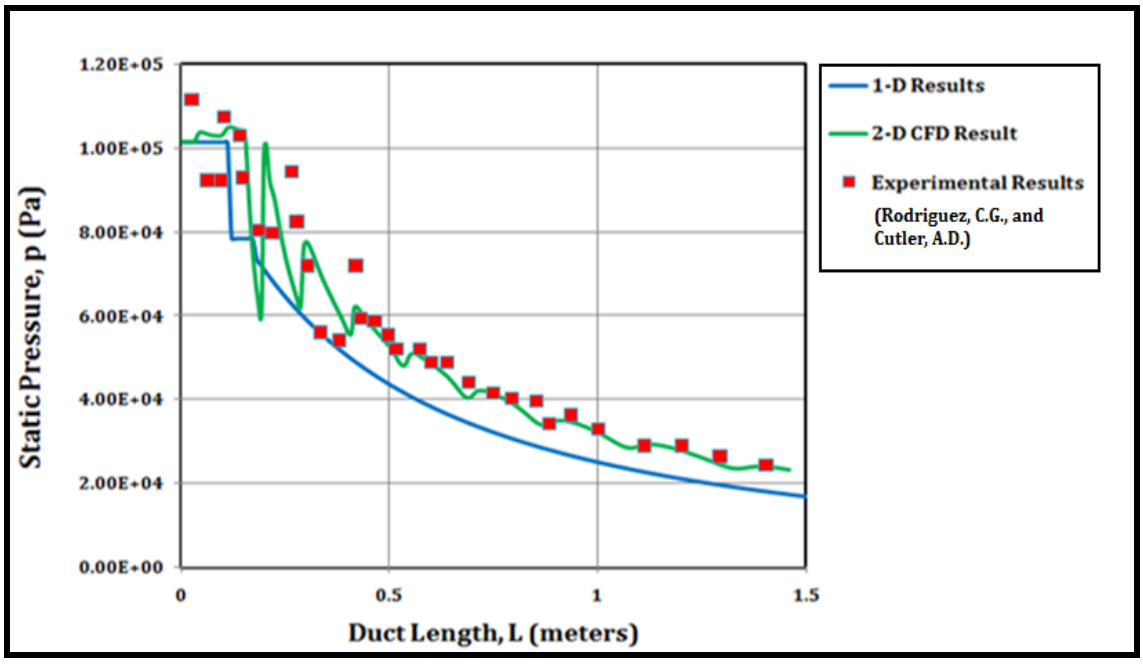

Figure 50: Static pressure comparison for "Fuel OFF" case

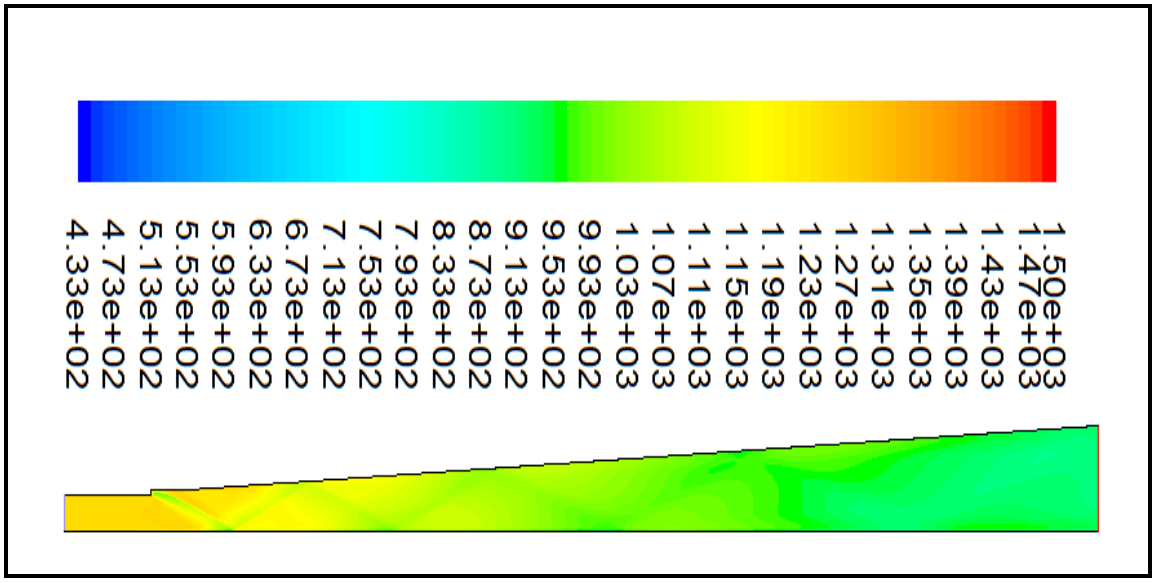

Figure 51: Static Temperature (Kelvin) Contours for 2-D Cold Flow Simulation

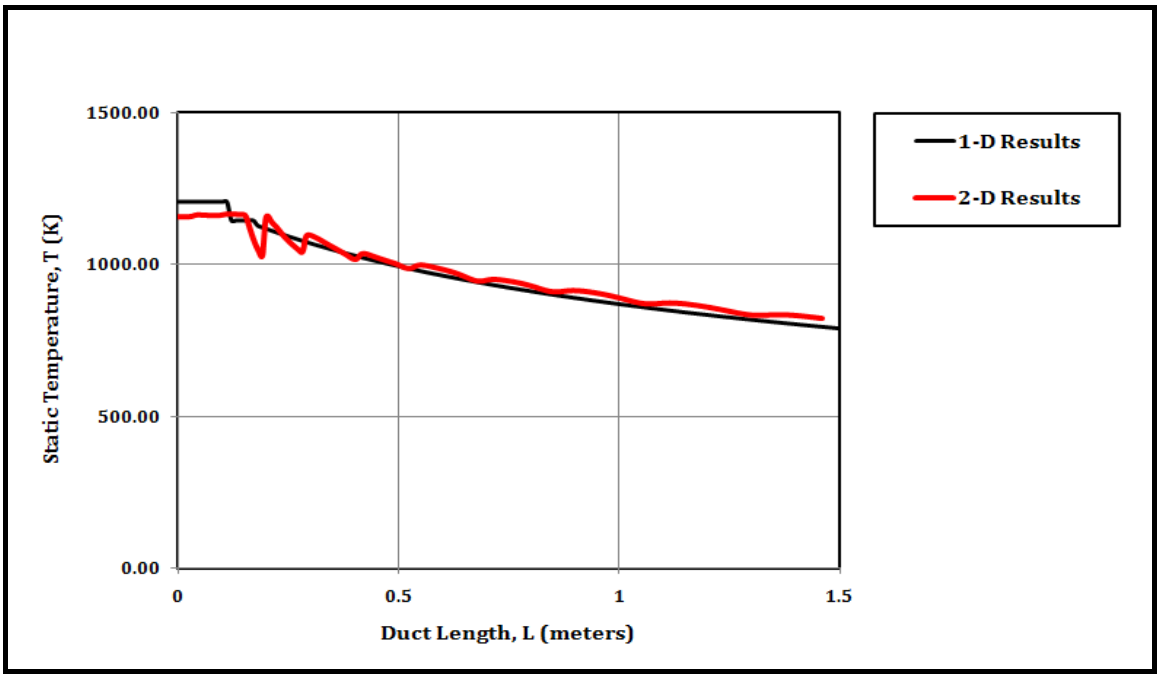

Figure 52: Static temperature comparison for "Fuel OFF" case

The 2-D contour plots for flow variables as obtained from FLUENT for the Cold Flow case have been presented for Mach number, static pressure and static temperature in Figure 47, 49 and 51, respectively. From these contour plots, the occurrence of following physical

phenomena can be seen: 1) Generation of Prandtl-Meyer (P-M) expansion fans centered at the corner of the step on the upper wall of the combustor. 2) Generation of oblique shock wave as the flow, after passing through the P-M expansion fans turns back into the mainstream flow direction, so as to align with respect to the upper wall just after the step. 3) The oblique shock and the P-M waves, both impinge on the bottom wall of the combustor. After impinging, the strength of the oblique shock diminishes and it is not reflected back, whereas, the P-M waves propagate downstream through multiple reflections from the upper and lower wall of the combustor, diminishing in strength after each reflection. 4) As seen in Figure 47-48, Mach number increases downstream along the combustor length due to the presence of a diverging duct and multiple P-M wave reflections. 5) The static pressure (as shown in Figure 49-50) and temperature (as shown in Figure 51-52) decrease along the combustor length due to the presence of the multiple reflections of P-M waves.

The 2-D viscous computational results, in Figures 48, 50 and 52, show the jumps in flow variables across oblique shocks, expansion waves and reflections of these waves from the walls that are created in supersonic flow. The quasi-one-dimensional model cannot capture oblique waves and thus show a smooth variation in flow parameters. In the Mach distribution case, i.e., Fig. 48, the trend is clearly captured, but the Mach number is over-estimated by the 1-D model. In Figure 50, a comparison is shown between 1-D, 2-D computations and experimental results for static pressure. A close agreement between the 2-D and the experimental results is shown in Fig. 50. However, the 1-D simulation can only predict the static pressure trend and under-estimates both experimental and 2-D results. The lack of oblique shock model (and to a lesser extent the lack of recirculation zone) in quasi-one-dimensional flow modeling is deemed responsible for the behavior of the over-estimating Mach number and under-estimating the

static pressure evolution along the duct axis. Static temperature comparison between 1-D and 2-D is shown in Fig. 52. The agreement in static temperature between the quasi-one-dimensional model (with no shock waves) and 2-D viscous computation (with shock waves) is very close and is consistent with the adiabatic nature of shock flows. We also note from the experimental and 2-D simulation results that the strength of the reflected waves continues to diminish in the flow direction, as expected.

- **Combustion or "Fuel ON" Case:**

Results for "Fuel ON" or combustion case have been presented below for static pressure in Fig. 53, static temperature in Fig. 54 and Mach number in Fig. 55.

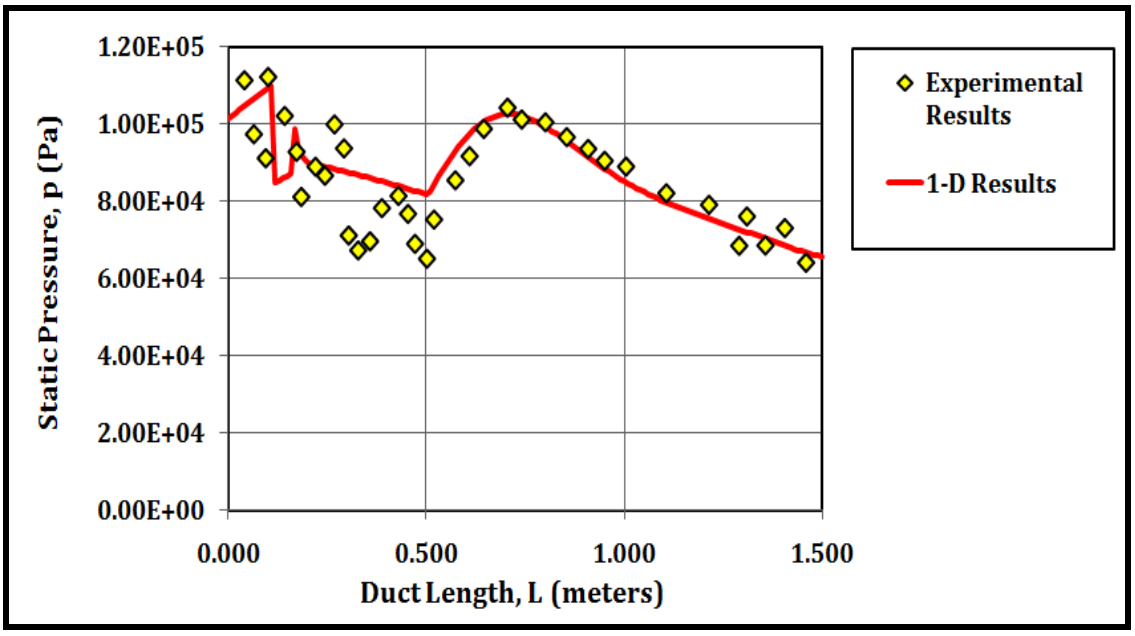

Figure 53: Static pressure comparison for "Fuel ON" case

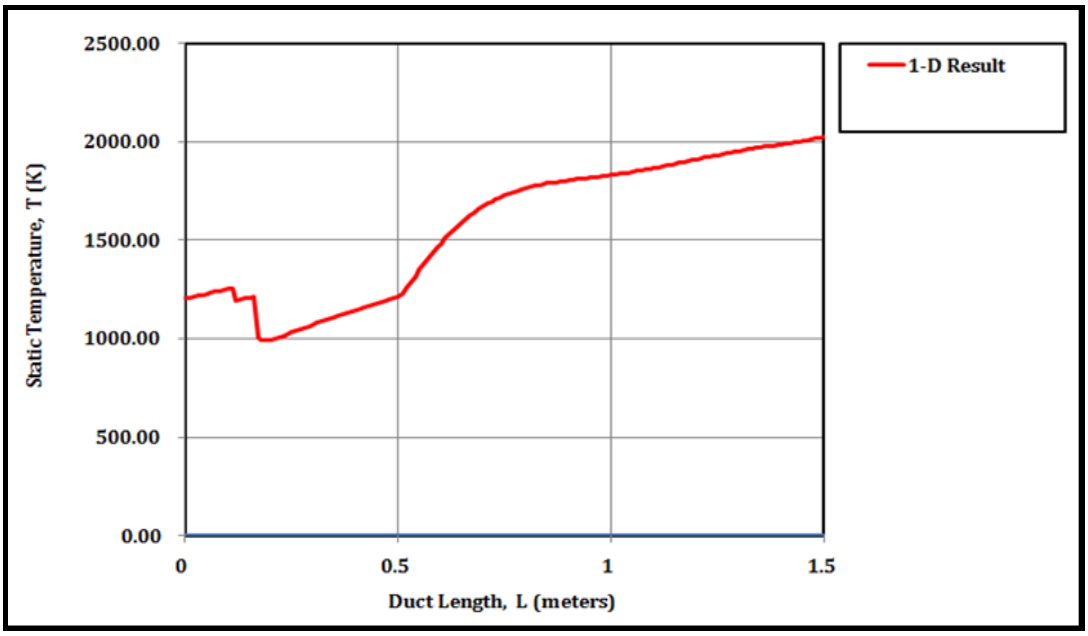

Figure 54: Static temperature distribution for "Fuel ON" case

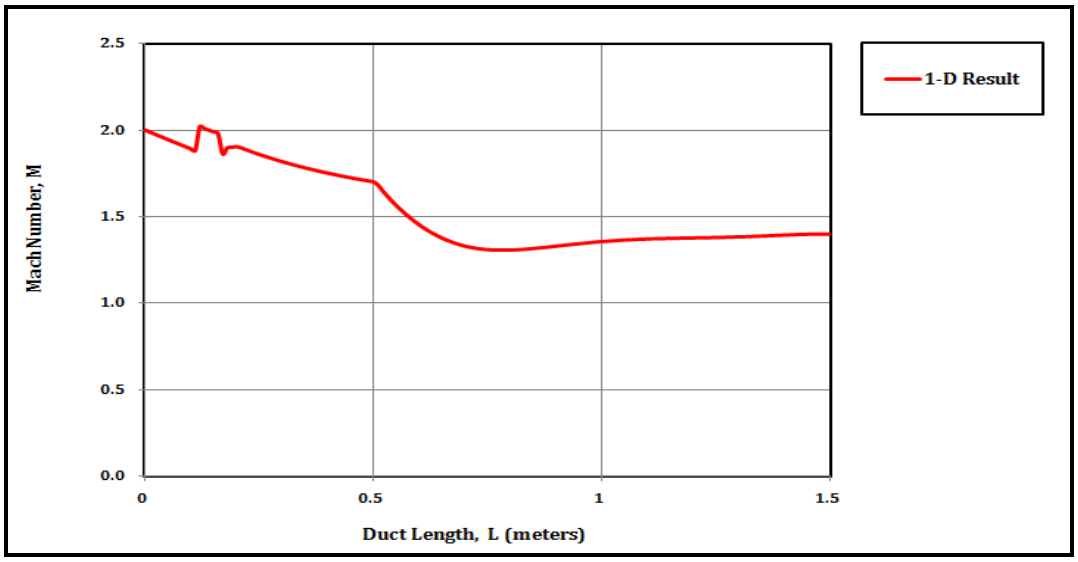

Figure 55: Mach number distribution for "Fuel ON" case

By examining Fig. 53, we conclude that 1-D simulation has clearly captured the static pressure trend and the pressure peak along the combustor length in fuel-on case. The quasi one-dimensional model due to the lack of oblique wave (i.e., shocks and expansion waves) simulation, does not capture the jumps as present in the experimental static pressure result. We

also note the phenomenon of ignition delay as shown by static pressure rise in experimental results (see Fig. 53). Figures 54 and 55 show the static temperature and Mach distribution as predicted in 1-D simulation. Although experimental results are not available in this case, we expect the 1-D simualtion to predict the correct trends, with a better match in static temperature and a very close match in Mach number.

5.2 Test Case 2: DLR Supersonic Combustion Chamber

In this section, results have been presented for computational simulations of DLR supersonic combustion chamber. The 2-D numerical simulations have been performed using FLUENT as a platform for three cases, namely, cold flow, cold flow with fuel injection and cold flow accompanied with fuel injection and combustion. The 1-D simulation has been performed for combustion case. Finally, comparisons have been drawn between 1-D and 2-D computational and experimental results for static pressure and centerline axial velocity variation along the length of the combustor.

Grid independence study has been performed for DLR scramjet combustor by constructing two different 2-D structured meshes consisting of 43,500 (Mesh 1) and 87,000 (Mesh 2) cells. Simulations are performed for: (1) “Cold Flow” (i.e. without fuel injection and combustion), (2) Cold flow with fuel injection and (3) Cold flow with fuel injection and combustion. The static pressure variation along the combustor bottom wall is used for comparing the results of Mesh 1 and Mesh 2, so as to check for grid independence. Based on the results for the above three cases, the difference between the values of the static pressure along the combustor bottom wall for Mesh 2 and Mesh 1 is of the order of 10^{-4}. The 2-D FLUENT simulation results presented in the next section for the above mentioned three cases are based on the 2-D structured mesh consisting of 87,000 cells.

5.2.1 Simulation Results

- **Cold Flow Simulation:**

The Figures 56–58, as shown below, are 2-D contours plots for Mach number, static pressure and static temperature, respectively, as obtained from FLUENT for cold flow simulation case.

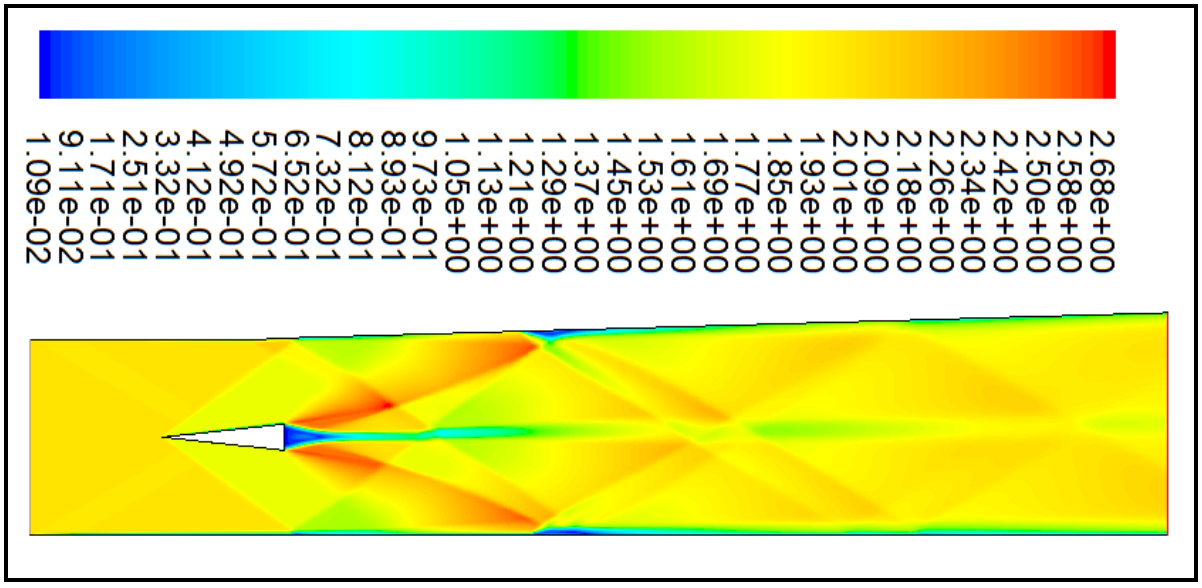

Figure 56: Mach number Contours for 2-D Cold Flow Simulation

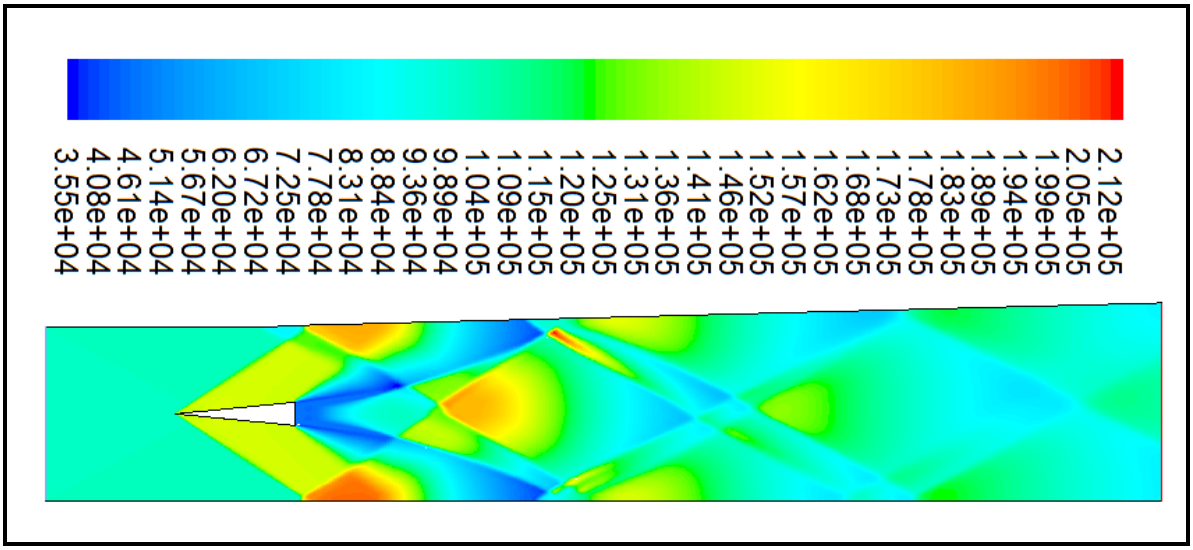

Figure 57: Static Pressure (Pascal) Contours for 2-D Cold Flow Simulation

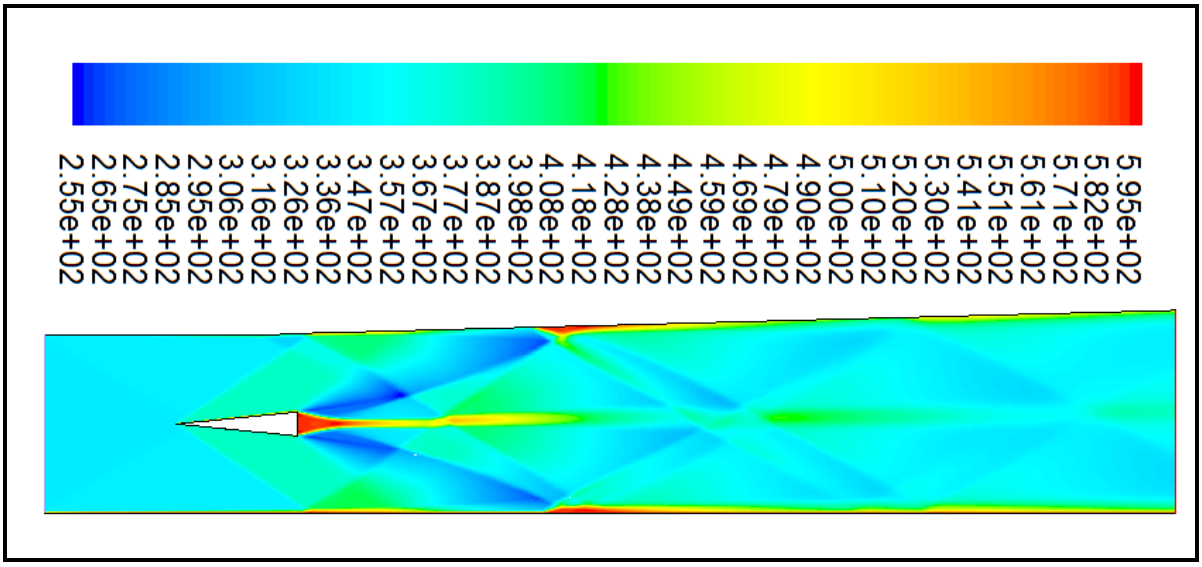

Figure 58: Static Temperature (Kelvin) Contours for 2-D Cold Flow Simulation

Referring to Figure 56-58, the occurrence of following physical phenomena can be observed: (1) an oblique shock wave, generated due to the presence of a wedge in the supersonic mainstream flow. (2) The boundary layer on the wedge separates in the presence of an adverse pressure gradient due to formation of an oblique shock at the tip of the wedge. (3) The separating boundary layer over the wedge forms a shear layer between the wake and the fast main flow, which persists almost through the whole computational domain. (4) The oblique shock generated from the tip of the wedge, reflects from the top and bottom walls of the combustor. Due to the divergence angle of 3 degrees on the upper wall, the oblique shock reflected from the upper wall is weaker in strength and hits the wake a bit further downstream than the one reflecting from the bottom wall. This gives a slightly asymmetrical shape to the wake. (5) The oblique shock wave generated from the tip of the wedge propagates downstream through multiple reflections from the edge of the shear layer as well as upper and lower walls, thereby generating shock diamond patterns. (6) The Prandtl-Meyer expansion fans can be clearly seen to originate at the base of the wedge which results in partially curved

recompression shocks which get reflected off the combustor walls. (7) The shocks reflecting from the combustor walls at certain locations can been seen to strongly affect the boundary layers, thereby causing the boundary layers to thicken and also producing a rise in wall temperatures. (8) The expansion fans originating at the base of the wedge cause the flow over the wedge to deflect downward towards the wake region along the combustor centerline. (9) A triangular shaped subsonic recirculation region is present at the base of the wedge. Fuel is injected into this subsonic recirculation region which serves as a flame holder and flame stabilization zone. (10) The velocity in the wake region accelerates from subsonic to supersonic speeds further downstream within the combustor.

- **Cold Flow with Fuel Injection:**

Cold flow with fuel injection simulation is performed so as to investigate the effect of injecting inert hydrogen into the main flow stream. The simulation for cold flow with fuel injection is restarted from the converged solution obtained for cold flow case, as this saves additional computational time and also provides starting guess for the simulation of the reacting case.

The Figures 59-61, as shown below, are 2-D contours plots for Mach number, static pressure and static temperature, respectively, as obtained from FLUENT for cold flow with fuel injection simulation case.

The flow phenomena for cold flow with fuel injection, as shown in Figures 59-61, has following differences with respect to the cold flow case: (1) The hydrogen filled recirculation zone is longer and wider than in cold flow case, (2) the expansion fans originating at the corners of the wedge are not as strong as in the cold flow case due to the presence of hydrogen

and (3) the recompression shocks are now weaker and affected by hydrogen-rich wake, giving them a straighter shape than observed in cold flow case.

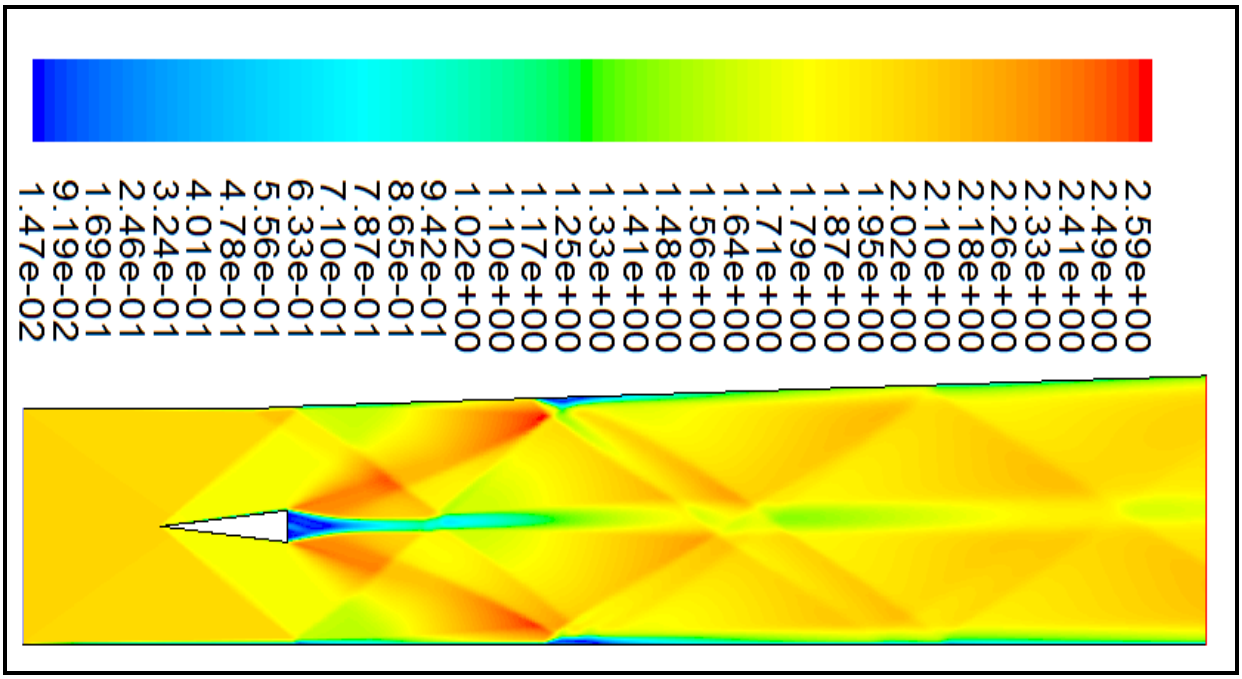

Figure 59: Mach number Contours for 2-D Cold Flow with Fuel Injection Simulation

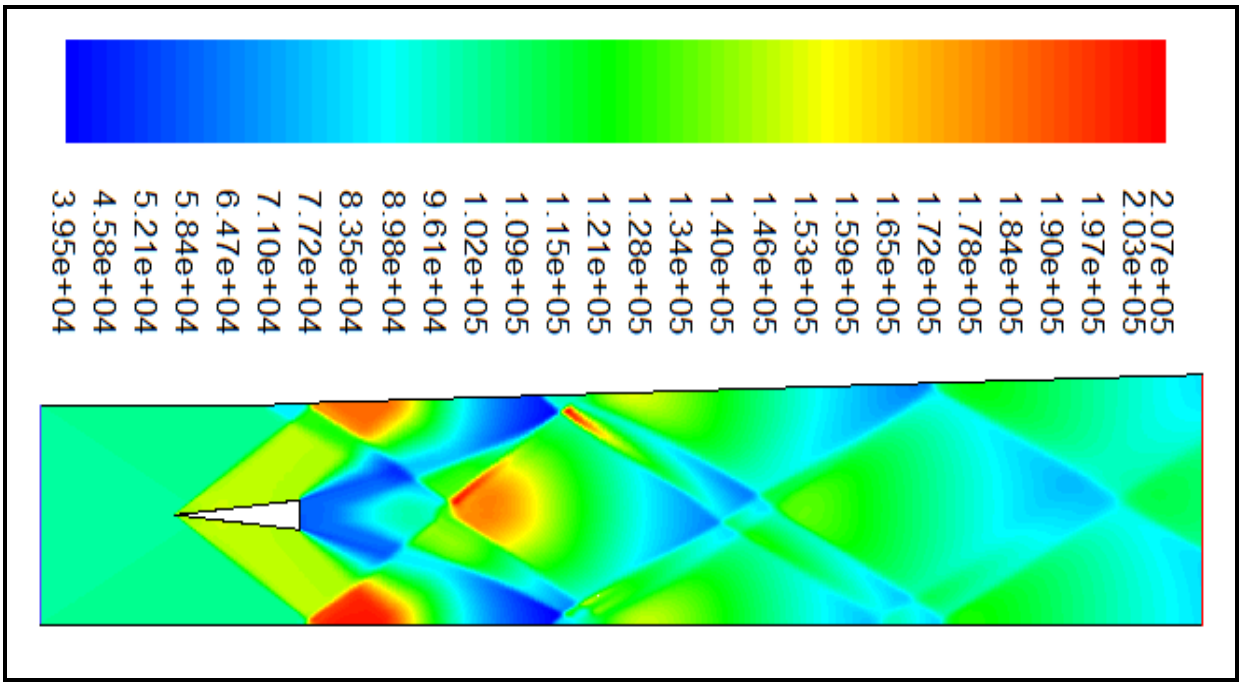

Figure 60: Static Pressure (Pascal) Contours for 2-D Cold Flow with Fuel Injection Simulation

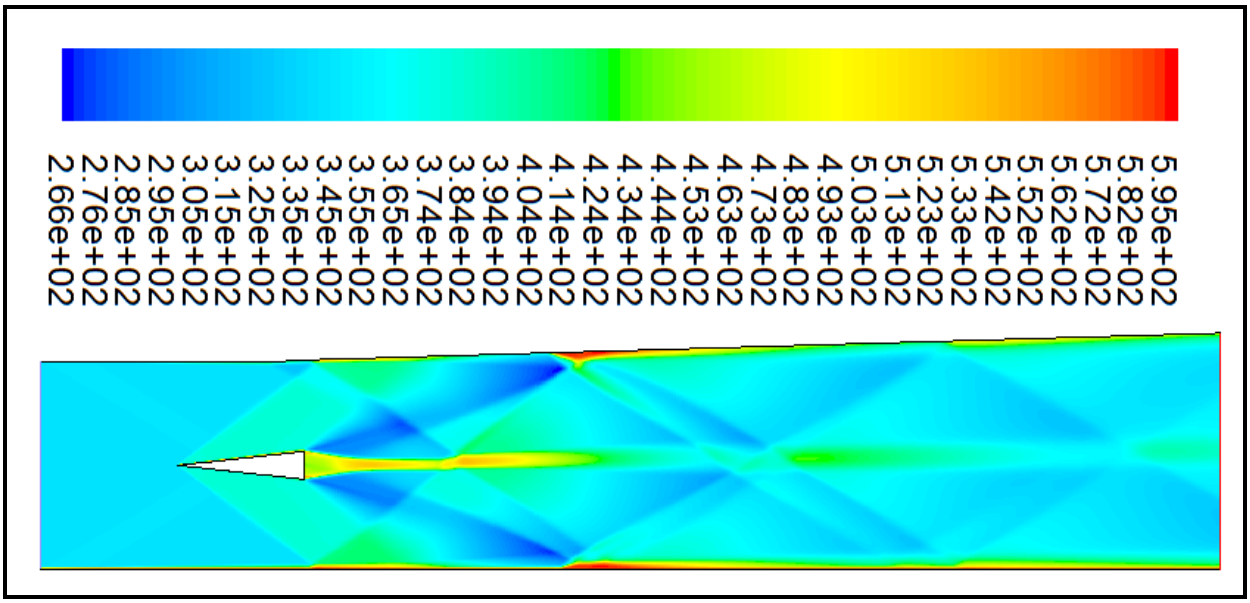

Figure 61: Static Temperature (Kelvin) Contours for 2-D Cold Flow with Fuel Injection Simulation

Figure 62 and 63 show the comparison of the 2-D CFD results obtained for static pressure distribution along the bottom wall and centerline of the DLR scramjet combustor with 3-D CFD results and experimental data.

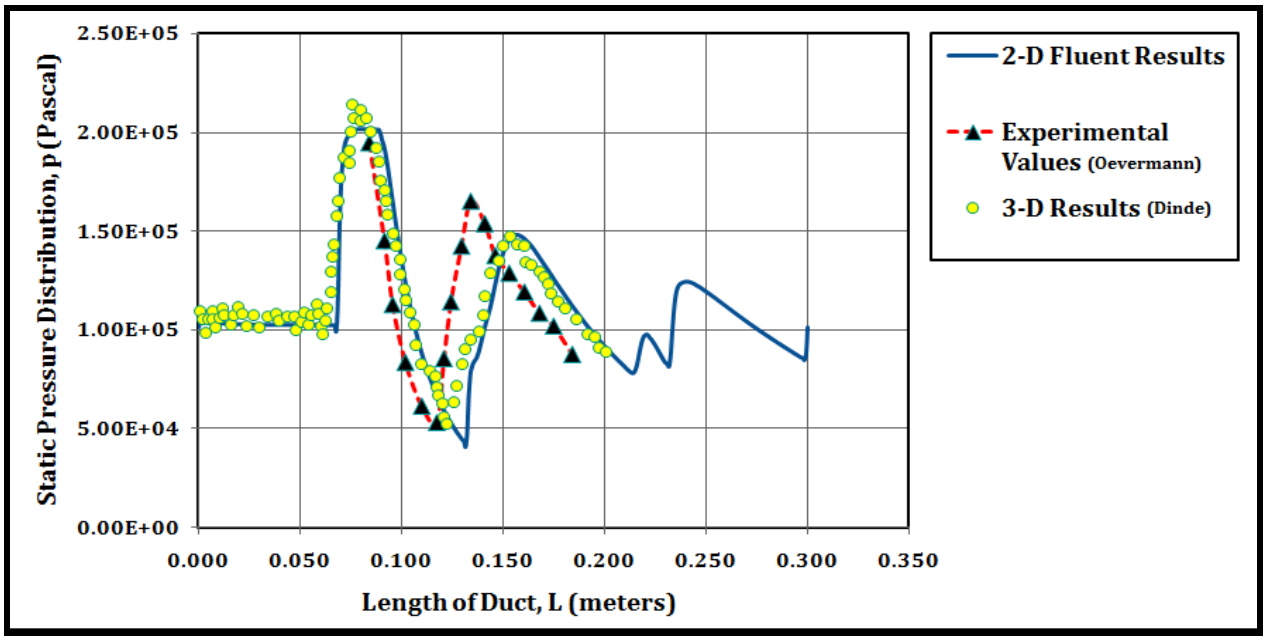

Figure 62: Comparison of Static pressure distribution along the bottom wall

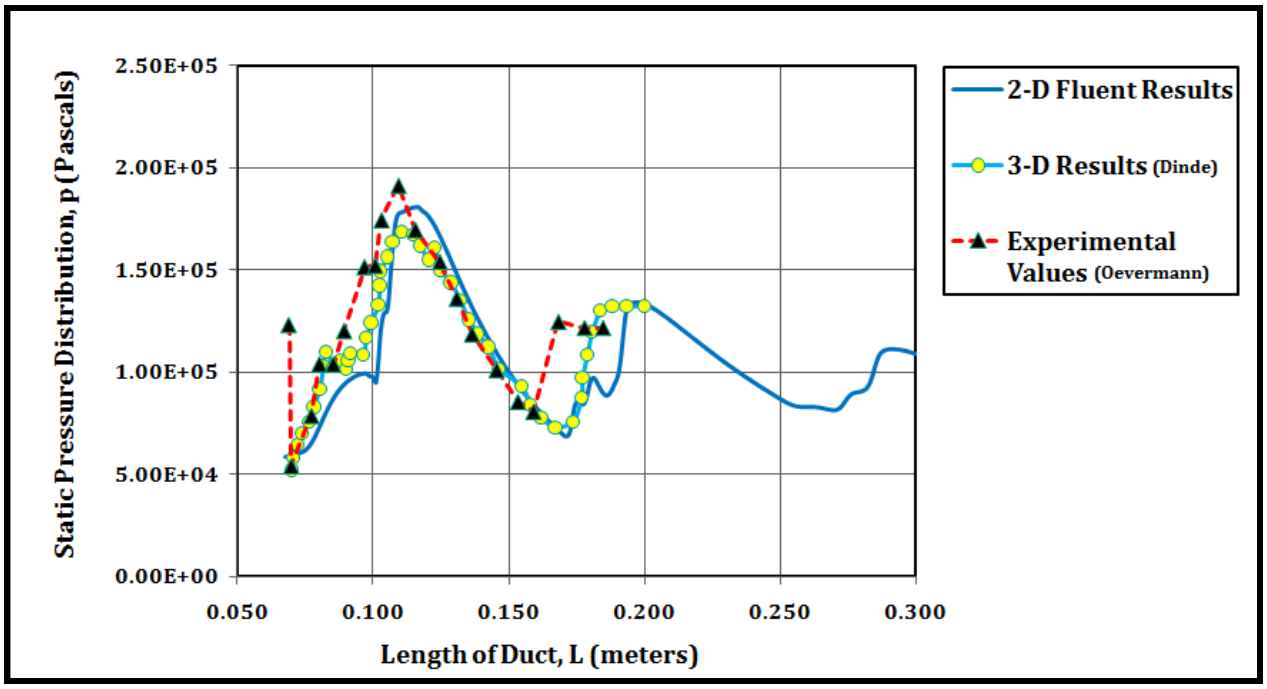

Figure 63: Comparison of Static pressure distribution along the centerline

There is a close agreement between the 2-D and 3-D computational results in static pressure initially in the duct, as seen in Fig. 62 and 63, but a detailed comparison to experimental data reveals a lack of agreement with the peaks and the streamwise location of the peaks in 2-D computational simulations. The 3-D simulations capture the peaks more closely.

- **Cold Flow with Fuel Injection and Combustion:**

The Figures 64-66, as shown below, are 2-D contours plots for Mach number, static pressure and static temperature, respectively, as obtained from FLUENT for cold flow with fuel injection and combustion simulation.

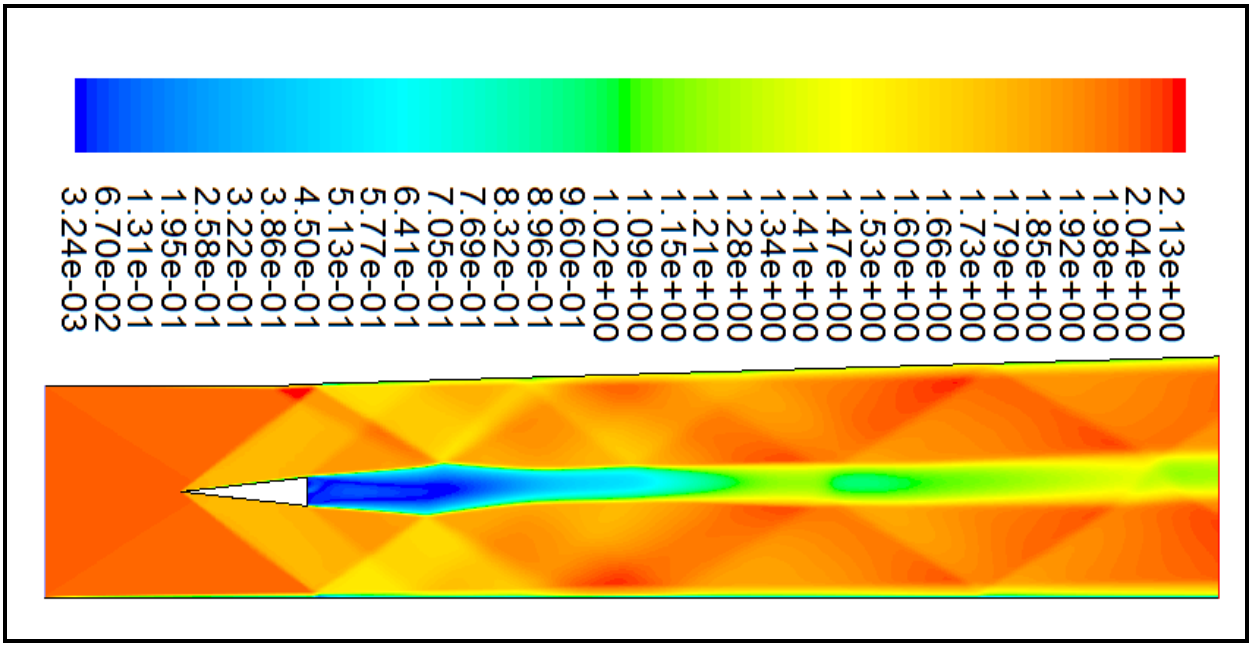

Figure 64: Mach number Contours for 2-D Cold Flow with Fuel Injection and Combustion Simulation

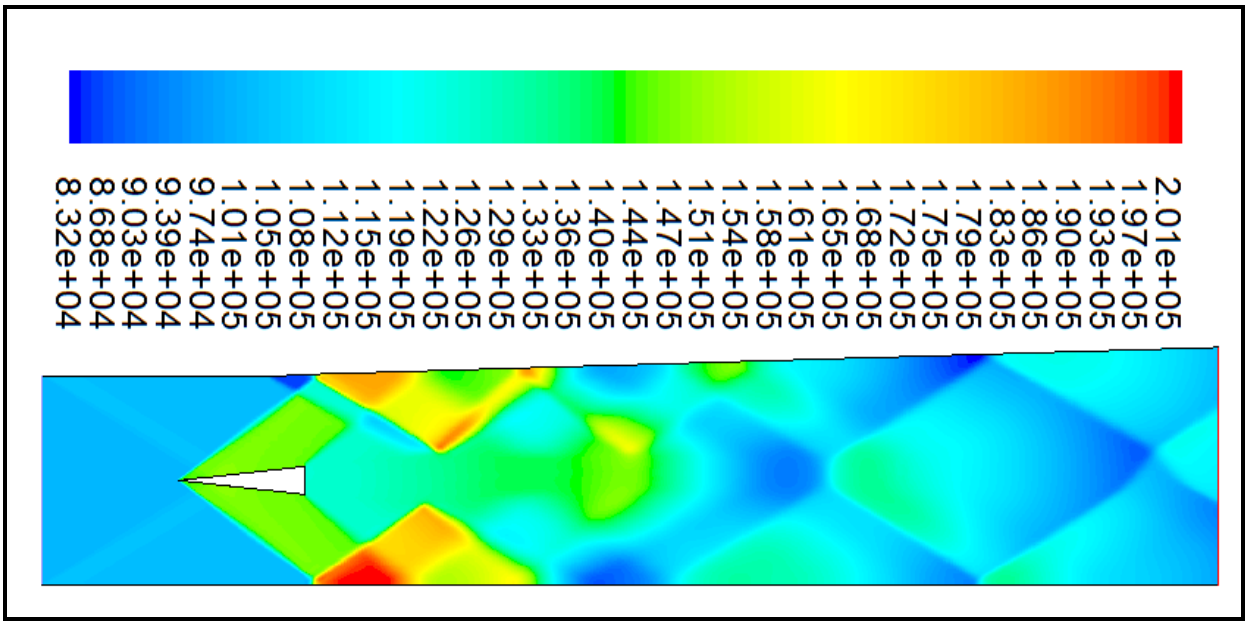

Figure 65: Static Pressure (Pascal) Contours for 2-D Cold Flow with Fuel Injection and Combustion Simulation

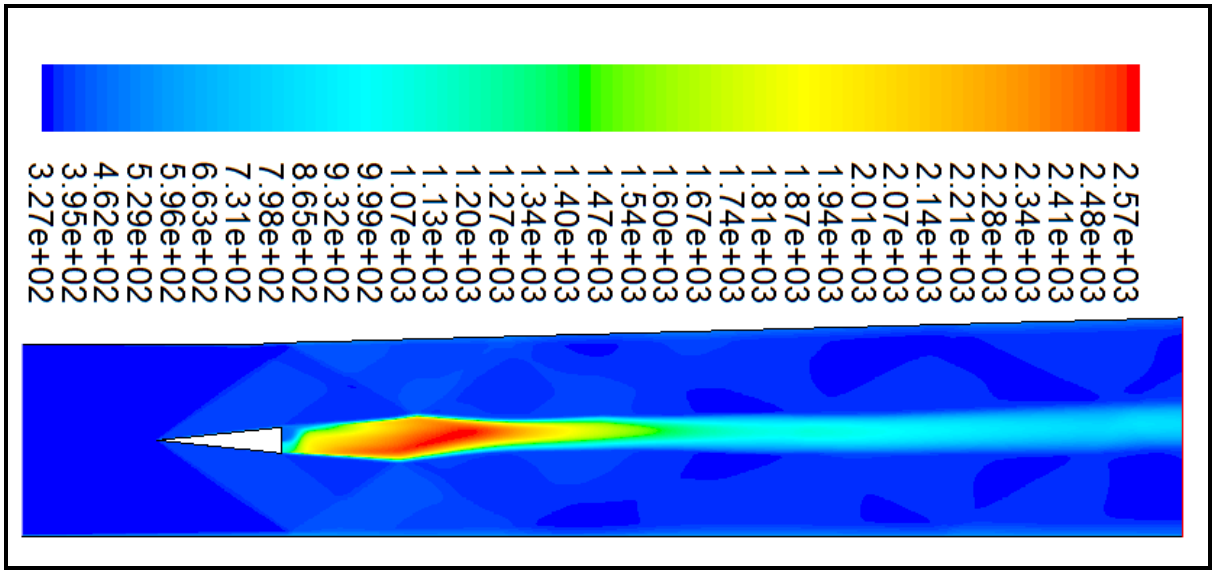

Figure 66: Static Temperature (Kelvin) Contours for 2-D Cold Flow with Fuel Injection and Combustion Simulation

From the above given 2-D FLUENT contours for Mach number, static pressure and static temperature (as shown in Figures 64-66), following flow phenomena can be observed: (1) due to the presence of combustion, the recirculation zone behind the wedge becomes larger as compared to the one in cold flow with fuel injection case. This enlarged recirculation zone acts as a flame holder for the hydrogen diffusion flame. (2) It can be seen from the above contours that combustion affects the flow field significantly. (3) The inlet temperature of approximately 350 K is insignificant in causing an auto-ignition of hydrogen-air mixture. The oblique shock generated from the tip of the wedge gets reflected from the upper and lower combustor walls and hits the wake, thereby causing a rise in temperature sufficient enough to auto-ignite hydrogen-air mixtures. This effect can be seen in static temperature contours (Figure 66) as deep red color zone within the wake region where temperatures reach around 2500 K. (4) The Prandtl-Meyer expansion fans as seen in cold flow case no more exist and the recompression shocks originating at the corners of the wedge have become much weaker than in cold flow with fuel injection case. (5) The shear layers origination at the base of the wedge become more

pronounced as continuous combustion occurs within them. (6) The presence of a subsonic recirculation zone can be seen in the Mach number contours (Figure 64) as a deep blue colored region.

Figure 67 shows the axial velocity distribution along the centerline of the DLR combustor with fuel injection and combustion. The 2-D simulation result closely agrees with the 3-D result in predicting the flow evolution with combustion, in DLR configuration, along with capturing the experimental trend. Both computational simulations indicate a reverse flow whereas the experimental result does not show a recirculation zone.

The reacting flowfield within the DLR combustor is dictated by the presence of centerline strut generated oblique shocks, expansion waves and their reflections from the walls. Moreover, these shocks interact with the shear layer (containing fuel-air mixture) produced due to the presence of a wedge shaped strut at the combustor centerline, thus enhancing the growth of the two-dimensional eddy structures (rollers) of the mixing layer. Therefore, the quasi-one dimensional model due to the inadequacy of simulating oblique waves and shear dominated viscous flow, severely fails to predict the trend followed by the experimental result along the centerline of the combustor. On the other hand, 1-D model is able to match the overall flow velocity achieved within the combustor downstream of the wedge at approximately six times the wedge chord length.

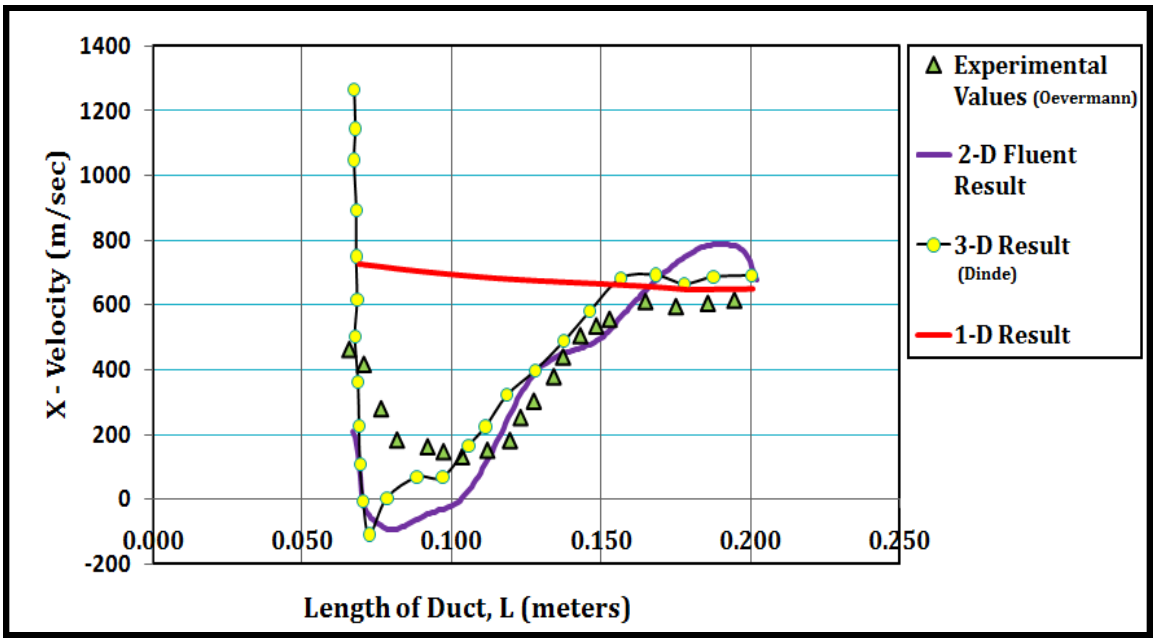

Figure 67: Comparison of Centerline Axial Velocity distribution

6 Conclusions and Future Research Scope

In the present research work, 1-D simulations based on the quasi-one dimensional equations of fluid motion plus an ignition delay model and 2-D numerical simulations based on Reynolds-Averaged Navier-Stokes (RANS) equations have been performed for NASA's SCHOLAR and DLR Supersonic Combustor. Comparisons have been drawn between the published 3-D computational and experimental results and quasi-one-dimensional and 2-D simulations. Based on the comparisons following conclusions have been drawn:

- For NASA's SCHOLAR supersonic combustor, the quasi-one dimensional model even in the absense of oblique wave model, has clearly captured the static pressure trend and the pressure peak along the combustor length in fuel-on case. This is attributed to the fact that, flowfield within the combustor resulting from a wall injection, consists of just a single three-dimensional bow shock instead of multiple oblique shock and expansions wave reflections.
- For DLR supersonic combustor, quasi-one dimensional model severely fails to predict the trend followed by the experimental result along the centerline of the combustor. This is due to the inadequacy of the 1-D model to simulate the oblique shocks, expansion waves and their multiple reflections from the combustor wall along with shear dominated viscous flow with recirculation. However, the 1-D model on the other hand is able to match the overall flow velocity achieved within the combustor downstream of the wedge at a distance of six times the wedge cord length.

Thus, the results identify the strengths and weaknesses of 1-D simulation in performing the scramjet propulsion system performance estimates that may be employed during the conceptual design phase of hypersonic vehicle.

Recommendation for future work includes:

- Develop a module based on the system of quasi-one dimensional equations as given by Shapiro [3] to perform 1-D simulation of the isolator.
- Develop a module which can perform compression system design and stream thrust analysis based on minimum total pressure loss.
- Develop a module for designing exhaust nozzle based on two-dimensional method of characteristics.
- Finally integrate the compression, isolator and nozzle module with the present combustor model for performing one-dimensional simulation of the tip-to-tail scramjet propulsion system.

7 References

1. Oevermann, M., *Numerical investigation of turbulent hydrogen combustion in a scramjet using flamelet modeling.* Aerospace science and technology, 2000. **4**(7): p. 463-480.
2. Doolan, C.J., Boyce, Russell R., *A quasi-one-dimensional mixing and combustion code for trajectory optimisation and design studies*, in *15th AIAA International Space Planes and Hypersonic Systems and Technologies Conference*. 2008, Curran Associates: Dayton, U.S.
3. Shapiro, A.H., *The Dynamics and Thermodynamics of Compressible Fluid Flow by Ascher H. Shapiro (Volume 1)*. 1983: Ronald Press.
4. Bonanos, A.M., *Scramjet Operability Range Studies of an Integrated Aerodynamic-Ramp-Injector/Plasma-Torch Igniter with Hydrogen and Hydrocarbon Fuels*. 2005: Blacksburg, VA.
5. Berglund, M., Wikstrom, N., and Fureby, C., *Numerical Simulation of Scramjet Combustion*. 2005.
6. Andreadis, D. (2004) *Scramjet Engines Enabling the Seamless Integration of Air and Space Operations*.
7. Efsic, E., *Supersonic Combustion Ramjet Propulsion Engines*. 2002.
8. Powell, O.A., Edwards, J.T., Norris, R.B., Numbers, K.E. and Pearce, J.A., *Development of Hydrocarbon-Fueled Scramjet Engines: Hypersonic Technology (HyTech) Program.* Journal of Propulsion and Power, 2001. **Vol. 17**(6).
9. Freeman, D.C., Reubush, D.E., McClinton, C.R., Rausch, V.L. and Crawford, J.L., *The NASA Hyper-X Program*, in *48th International Astronautical Congress*. 1997: Turin, Italy.
10. Warwick, G., *Hyper Reality*, in *Aviation Week & Space Technology*. 2008.
11. http://en.wikipedia.org/wiki/Boeing_X-51, *Boeing X-51A*. 2010, Wikipedia.
12. Barber, T.A., Maicke, B.A. and Majdalani, J., *Current State of High Speed Propulsion: Gaps, Obstacles, and Technological Challenges in Hypersonic Applications*, in *45th AIAA/ASME/SAE/ASEE Joint Propulsion Conference & Exhibit*. 2009: Denver, Colorado.
13. Drummond, P., Bouchez, M. and McClinton, C.R., *Overview of NATO Background On Scramjet Technology*. 2007.
14. Andreadis, D. (2004) *Scramjets Integrate Air and Space*.

15. Milligan, R.T., *Dual Mode Scramjet: A Computational Investigation On Combustor Design and Operation*. 2009, Wright State University: Dayton, OH.
16. Heiser, W.H., Pratt, D.T. , *Hypersonic Airbreathing Propulsion*. 1994: AIAA Educational Series.
17. Lin, P., Rao, G.V.R. and O'Connor, G.M., *Numerical Investigation on Shock Wave/Boundary-Layer Interations In a Constant Area Diffuser at Mach 3*, in *22nd AIAA Fluid Dynamics, Plasma Dynamics & Lasers Conference*. 1991: Honolulu, Hawaii.
18. Lin, K.C., Tam, C.J., Jackson, K.R., Eklund, D.R. and Jackson, T.A., *Characterization of Shock Train Structures Inside Constant-Area Isolators of Model Scramjet Combustors*, in *44th AIAA Aerospace Sciences Meeting and Exhibit*. 2006: Reno, NV.
19. Waltrup, P.J., and Billig, F.S., *"Prediction of Precombustion Wall Pressure Distributions in Scramjet Engines"*. Journal of Spacecraft and Rockets, 1973. **Vol. 10**(No. 9): p. 620-622.
20. Curran, E.T., Murthy, S.N.B. and Zarchan, P, *"Scramjet Propulsion"*. Progress in Astronautics and Aeronautics, copyright 2000 by AIAA, Inc. Vol. 189. 2001: AIAA.
21. Drummond, J.P., Diskin, G.S. and Cutler, A.D., *Fuel-Air Mixing and Combustion in Scramjet*. 2007: Hampton, VA.
22. Deepu, M., Gokhale, S.S. and Jayaraj, S., *Recent Advances in Experimental and Numerical Analysis of Scramjet Combustor Flow Fields.* IE(I) Journal - AS, 2007. **88**.
23. Billig, F.S., *Propulsion Systems From Takeoff to High speed Flight.* Progress in Astronautics and Aeronautics, AIAA. **137**.
24. Tishkoff, J.M., Drummond, J.P. and Edwards, T., *Future Directions of Supersonic Combustion Research - Air Force/NASA workshop on Supersonic Combustion*, in *35th, Aerospace Sciences Meeting and Exhibit,*. 1997: Reno, NV.
25. Bouchez, M., Saunier, E., Peres, P. and Lansalot, J., *Advanced Carbon/Carbon Injection Strut for Actual Scramjet.* AIAA, 1996.
26. Hunt, J.L.a.M., C.R., *Scramjet Engine/Airframe Integration Methodology*, in *AGARD Conference*. 1997: Palaiseau, France.
27. *Astronomy and Astrophysics Advisory Committee Research Facilities*, in *Astronomy and Astrophysics Advisory Committee (AAAC) Annual Report*. 2002-2003.

28. Rogers, R.C., Capriotti, D.P. and Guy, R.W., *Experimental Supersonic Combustion Research at NASA Langley*, in *20th AIAA Advanced Measurement and Ground Testing Technology Conference*. 1998: Albuquerque, NM.
29. Lorenz, P. *AEDC reaches major milestone with hypersonic engine testing*. 2009.
30. Stallings, D.W., Williams, W. D., Felderma, E. J., Beck, W. H. and K. Hannemann (2003) *Free-Piston Shock Tunnel Test Technique Development: An AEDC/DLR Cooperative Program*. Final AEDC Technical Report (TR).
31. MacLean, M., Dufrene, A.,Wadhams, T. and Holden, M., *Numerical and Experimental Characterization of High Enthalpy Flow in an Expansion Tunnel Facility.* AIAA, 2010.
32. Danehy, P.M., Gord, J. R., Grisch, F., Klimenko, D. and Clauss, W. , *CARS Temperature and Species Measurements For Air Vehicle Propulsion Systems*, in *Recent Developments in Non-Intrusive Measurement Technology for Military Application on Model-and Full-Scale Vehicles*. 2005, NATO Research and Technology Organization (RTO): Budapest, Hungary.
33. Dupoirieux, F., *Optical Diagnostics Used at Onera to Characterize Turbulent Reactive Flows and to Validate Aero- and Rocket Engine Combustor Modeling.* Aerospace Lab, The ONERA Journal, 2009(1).
34. Grisch, F., and Orain, M., *Role of Planar Laser-Induced Fluorescence in Combustion Research.* Aerospace Lab, The ONERA Journal, 2009(1).
35. Gruber, M., Carter, C., Ryan, M., Rieker, G.B., Jeffries, J.B., Hanson, R.K, Jiwen, L. and Mathur, T., *Laser-Based Measurements of OH, Temperature, and Water Vapor Concentration in a Hydrocarbon-Fueled Scramjet*, in *44th AIAA/ASME/SAE/ASEE Joint Propulsion Conference & Exhibit*. 2008: Hartford, CT.
36. Tempel, T., *Investigation of Supersonic Mixing Using Laser-Induced Breakdown Spectroscopy*. 2004.
37. Mayinger, F., *Modern Electronics in Imageprocessing and in Physical Modeling - A New Challenge for Optical Techniques.* A Chair for Thermodynamics, Technical University Munich, Munich, Germany.
38. *Raman scattering*. 2010; Available from: http://en.wikipedia.org/wiki/Raman_scattering.

39. Shah, Y.R., Prajapati, P.M. and Sen, D.J., *Knowing How Each Atom Moves in Real-Time During Chemical Reactions.* Journal of Chemical and Pharmaceutical Research, 2010. **2**(1): p. 147-154.
40. *Coherent anti-Stokes Raman spectroscopy*. Chemical Sciences: A Manual for CSIR-UGC National Eligibility Test for Lectureship and JRF 2010.
41. Crua, C., *Combustion Processes in a Diesel Engine*. 2002, University of Brighton.
42. Zheltikov, A.M., *Coherent anti-Stokes Raman scattering: from proof-of-the-principle experiments to femtosecond CARS and higher order wave-mixing generalizations.* Journal of Raman Spectroscopy, 2000. **31**(8-9): p. 653-667.
43. Tolles, W.M., Nibler, J.W., McDonald, J.R. and Harvey, A.B., *A Review of the Theory and Application of Coherent Anti-Stokes Raman Spectroscopy (CARS).* Applied Spectroscopy, 1977. **31**(4): p. 253-339.
44. Kiefer, W.a.L., D.A., *Non-Linear Raman Spectroscopy and Its Chemical Applications*. NATO Advanced Study Institutes Series. 1982: D. Reidel Publishing Company.
45. Grisch, F., *Molecular Diagnostics for the Study of Hypersonic Flows*, in *RTO AVT Course on "Measurement Techniques for High Enthalpy and Plasma Flows"*. 1999, RTO EN-8: Rhode-Saint-Genese, Belgium.
46. Rosencher, E., *Optical Diagnostics of Flows: An Introduction.* Aerospace Lab, The ONERA Journal, 2009(1).
47. Yokomae, T., *Planar Laser-Induced Fluorescence (PLIF) of H2 – O2 Combustion*. 2003, The University of Texas at Arlington.
48. *Planar Laser-Induced Fluorescence Poster*, Dantec Dynamics.
49. *Laser Doppler Velocimetry*, Dantec Dynamics.
50. *Particle Image Velocimetry Poster*, Dantec Dynamics.
51. Schetz, J.A., and Billing, F.S., *Penetration of Gaseous Jets Injected into a Supersonic Stream.* Journal of Spacecraft and Rockets, 1966. **3**: p. 1658.
52. Mao, M., Wriggins, R., and McClinton, C.R., *"Numerical Simulation of Transverse Fuel Injection"*. NASP CR 1089, 1990.
53. Gutmark, E., Schadow, K.C., Parr, T.P., Parr, D.M., and Wilson, K.J., *"Combustion Enhancement by Axial Vortices"*. Journal of Propulsion and Power, 1989. **5**(5).

54. Bayley, D., and Hartfield, R.J., *Experimental Investigation of Angled Injection in a Compressible Flow, AIAA-95-2414.* 1995.
55. Seiner, J.M., Dash, S.M., and Kenzakowski, D.C., *"Historical Survey on Enhanced Mixing in Scramjet Engines".* Journal of Propulsion and Power, 2001. **17**(6).
56. Lu, F.K., and Dickman, D.A., *"Topology of Supersonic Jet Interaction Flowfields at High Pressure Ratios"*, in *International Symposium on Flow Visualization*. 2008: Nice, France.
57. Schadow, K.C., Wilson, K.J., Lee, M.J., and Gutmark, E., *"Enhancement of Mixing in Ducted Rockets with Elliptic Gas-Generator Nozzles".* AIAA Paper 84-1260, 1984.
58. Tomioka, S., Jacobsen, L.S., and Schetz, J.A, *"Sonic Injection from Diamond-Shaped Orifices into a Supersonic Crossflow".* Journal of Propulsion and Power, 2003. **19**(1).
59. Hirano, K., Matsuo, A., Kouchi, T., Izumikawa, M., and Tomioka, S., *"New Injector Geometry for Penetrations Enhancement of Perpendicular Jet into Supersonic Flow"*, in *43rd AIAA/ASME/SAE/ASEE Joint Propulsion Conference & Exhibit*. 2007: Cincinnati, OH.
60. Kobayashi, K., Carter, C.D., and Hsu, K, *"Flowfield Studies of a Diamond-Shaped Fuel Injector in a Supersonic Flow".* Journal of Propulsion and Power, 2007. **23**(6).
61. Dimotakis, P.E., *"Turbulent Free Shear Layer Mixing and Combustion"*, in *High Speed Flight Propulsion Systems*, S.N.B. Murthy, and Curran, E.T., Editor. 1991, Progress in Astronautics and Aeronautics, AIAA: Washington, DC. p. 265-340.
62. Doster, J.C., *Hypermixer Pylon Fuel Injection for Scramjet Combustors*. 2008, Air Force Institute of Technology: Wright-Patterson Air Force Base, Ohio.
63. Stouffer, S.D., Baker, N.R., Capriotti, D.P., and Northam, G.B., *"Effects of Compression and Expansion Ramp Fuel Injector Configurations on Scramjet Combustion and Heat Transfer" AIAA paper 93-0609.* 1993.
64. Gallimore, S.D., *A Study of Plasma Ignition Enhancement for Aeroramp Injectors in Supersonic Combustion Applications"*. 2001, Virginia Polytechnic Institute and State University.
65. Parent, B., and Sislian, J.P., *"Turbulent Hypervelocity Fuel-Air Mixing by Cantilevered Ramp Injectors.* AIAA paper-2001-1888.
66. Sislian, J.P., and Schumacher, J., *"A Comparative Study of Hypersonic Fuel-Air Mixing Enhancement by Ramp and Cantilevered Ramp Injectors".* AIAA paper-99-4873, 1999.

67. Desikan, S.L.N., and Kurian, J., *"Strut-Based Gaseous Injection into a Supersonic Stream"*. Journal of Propulsion and Power, 2006. **22**(2).
68. Gruenig, C., Avrashkov, V., and Mayinger, F., *"Fuel Injection into a Supersonic Airflow by Means of Pylons"*. Journal of Propulsion and Power, 2000. **16**(1).
69. Schetz, J.A., Cox-Stouffer, S., and Fuller, R., *"Intergrated CFD and Experimental Studies of Complex Injectors in Supersonic Flows"*. AIAA paper-98-2780, 1998.
70. Jacobsen, L.S., Schetz, J.A., and Ng, W.F., *"The Flowfield Near a Multiport Injector Array in a Supersonic Flow"*. AIAA paper-98-3126, 1998.
71. Fuller, R., Nejad, A., and Schetz, J.A, *"Vortex Fuel Interaction for Enhanced Mixing in Supersonic Flow"*. AIAA paper-96-2661, 1996.
72. Jacobsen, L.S., Gallimore, S.D., Schetz, J.A., O'Brien, W.F., and Goss, L.P., *"An Improved Aerodynamic Ramp Injector In Supersonic Flow"*, in *39th Aerospace Sciences Meeting & Exhibit*. 2001: Reno, Nevada.
73. Weinberg, F.J., *"Old Flames and New"*. Inaugral Lectures, Imperial College, London, 1968.
74. Harrison, A.J., and Weinberg, F.J. *"Flame Stabilization by Plasma Jets"*. in *Proceedings of the Royal Society of London. Series A, Mathematical and Physical Sciences*. 1971.
75. Kimura, I., Aoki, H., and Kato, M., *"The Use of a Plasma Jet for Flame Stabilization and Promotion of Combustion In Supersonic Air Flows"*. Journal of Combustion and Flame, 1980. **42**: p. 297-305.
76. Warris, A., and Weinberg, F., *" Ignition and Flame Stabilization by Plasma Jets In Fast Gas Streams"*. Twentieth Symposium (International) on Combustion, The Combustion Institute, 1984: p. 1825-1831.
77. Kato, R., and Kimura, I., *Numerical Simulation of Flame-Stabilization and Combustion Promotion by Plasma Jets in Supersonic Air Streams.* Proceedings of 26th International Symposium on Combustion, 1996: p. 2941-2947.
78. Ben-Yakar, A., and Hanson, R.K., *"Cavity Flame-Holders for Ignition and Flame Stabilization in Scramjets: An Overview"*. Journal of Propulsion and Power, July-August 2001. **17**(4).
79. Epstein, M.J., and Kutshenreuter, P.H., *"Fuel Injection System for Scramjet Engines"*, U.S. Patent, Editor. 1994, General Electric Company, Cincinnati, Ohio: USA.

80. Abdel-Salam, T.M., Tiwari, S.N., and Mohieldin, T.O., *Study of Supersonic Combustion Characteristcs in a Scramjet Combustor*, in *16th AIAA Computational Fluid Dynamics Conference*. 2003: Orlando, FL.
81. Birzer, C., and Doolan, C.J., *Quasi-One-Dimensional Modeling of Hydrogen Fuelled Scramjet Combustors* Journal of Propulsion and Power, 2009. **25**(6).
82. Van Wylen, F.J., and Sonntag, R.E., *Fundamentals of Classical Thermodynamics*. 1985: John Wiley and Sons, Inc.
83. Anderson, J.D., *Fundamentals of Aerodynamics*. 2001: McGraw-Hill.
84. Baurle, R.A., *"Modeling of High Speed Reacting Flows: Established Practices and Future Challenges"*, in *42nd AIAA Aerospace Sciences Meeting and Exhibit*. 2004: Reno, Nevada.
85. *"Fluent 6.3 Documentation"*. 2006, Ansys, Inc.: Lebanon, NH.
86. Hsu, K., and Jemcov, A., *Numerical Investigation of Detonation in Premixed Hydrogen-Air Mixture Assesment of Simplified Chemical Mechanisms.* AIAA 2000-2478, 2000.
87. Dinde, P., Rajasekaran A. and Babu, V., *3D numerical simulation of the supersonic combustion of hydrogen.* The aeronautical journal, 2006.
88. Rodriguez, C.G., and Cutler, A.D., *Computational simulation of a supersonic-combustion benchmark experiment*, in *41st AIAA/ASME/SAE/ASEE Joint Propulsion Conference & Exhibit*. 2005: Tuscon, AZ.
89. d' Inca, R., and Bouchez, M. *Chapter 8: Use of SCHOLAR Supersonic Combustion Data*.
90. Rodriguez, C.G., and Cutler, A.D., *Numerical Analysis of the SCHOLAR Supersonic Combustor*, in *NASA/CR-2003-212689*. 2003.